

**Università degli Studi di Salerno**  
**Facoltà di Scienze Matematiche Fisiche e Naturali**



**DOTTORATO DI RICERCA IN CHIMICA**  
**XIII Ciclo – Nuova serie**

“Tesi di dottorato in:  
**Polymeric films with co-crystalline and  
nanoporous crystalline phases:  
orientations, chirality and possible  
applications in photonic crystals”**

**Tutor**

Dott.ssa Paola Rizzo

**Co-tutor**

Prof. Vincenzo Venditto

**Coordinatore**

Prof. Gaetano Guerra

**PhD student**

Graziella Ianniello

**Matr. 8880700113**

**Anno Accademico 2012-2015**



|   |    |
|---|----|
| <b>Introduction</b>   |    |
| Polymeric films with co-crystalline and nanoporous crystalline phases   | 5  |
| <i>References</i>   | 12 |
| <b>Chapter 1 Disordered nanoporous crystalline modifications and co-crystalline phase of syndiotactic polystyrene including carvacrol guest molecules</b> |    |
| <b>1.1 Introduction</b>   | 14 |
| <b>1.2 Guest removal from intercalate forms</b>   | 17 |
| <b>1.2.1 Guest removal from the triclinic <math>\delta</math> clathrate form with DBF</b>   | 19 |
| <b>1.2.2 Guest sorption from the disordered crystalline form obtained by guest (DBFTMB) removal from their clathrate and intercalate forms</b>            | 21 |
| <b>1.3 sPS\ carvacrol co-crystalline film</b>   | 26 |
| <b>1.3.1 FTIR method to discriminate carvacrol molecules in co-crystalline and amorphous polymer phases</b>   | 28 |
| <b>1.3.2 Partition of carvacrol molecules between amorphous and crystalline phases of <math>\delta</math>-form films</b>                                  | 31 |
| <b>1.4 Conclusion</b>   | 38 |
| <i>References</i>   | 40 |
| <b>Chapter 2 Orientations in polymeric films</b>  |    |
| <b>2.1 Introduction</b>   | 43 |
| <i>References</i>   | 46 |
| <b>2.2 Poly(2,6-dimethyl-1,4-phenylene ether) (PPO)</b>   | 48 |
| <b>2.2.1 Uniplanar orientations by <math>\alpha</math>-pinene-induced cocrystallization on amorphous films.</b>   | 48 |
| <b>2.2.2 Uniplanar orientations by decalin- and</b>   |    |

|   |     |
|---|-----|
| tetralin-induced cocrystallization of amorphous films.  | 54  |
| <b>2.2.3</b> Guest exchange in PPO cocrystalline films with two different uniplanar orientations.                   | 56  |
| <b>2.2.4</b> Uniplanar orientations by limonene induced cocrystallization of amorphous films                        | 60  |
| <b>2.2.5</b> Guest exchange in PPO/ limonene cocrystalline films with tetralin                                      | 64  |
| <b>2.2.6</b> A preliminary model of PPO nanoporous structure  | 67  |
| <b>2.2.7</b> Conclusion   | 70  |
| <i>References</i>   | 71  |
| <b>2.3 Poly(L-lactide) (PLLA)</b>   | 73  |
| <b>2.3.1</b> PLLA uniplanar orientation of $\epsilon$ form  | 73  |
| <b>2.3.2</b> Guest exchange in $\epsilon$ PLLA co-crystalline phase   | 82  |
| <b>2.3.3</b> Effects of guest removal from $\epsilon$ form  | 87  |
| <b>2.3.4</b> Conclusion   | 88  |
| <i>References</i>   |     |
| <b>2.4 Correlation between shrinkage and orientation in sPS films</b>   | 89  |
| <b>2.4.1</b> Syndiotactic polystyrene sPS   | 89  |
| <b>2.4.2</b> The shrinkage  | 90  |
| <b>2.4.3</b> Oriented $\alpha$ form   | 91  |
| <b>2.4.4</b> Amorphous sPS film   | 94  |
| <b>2.4.5</b> PP-sPS-PP film multilayer  | 100 |
| <b>2.4.6</b> Conclusion   | 104 |
| <i>References</i>   | 105 |
| <b>Chapter 3 Melt-extruded films of a commercial polymer with intense chiral optical response of achiral guests</b> |     |
| <b>3.1</b> Introduction   | 108 |
| <b>3.2</b> Induction of chirality in melt-extruded s-PS films of different thickness by cocrystallization           |     |

|  |     |
|--|-----|
| with a nonracemic guest  | 110 |
| <b>3.3</b> Chiral optical polymer films with achiral chromophores.                                       | 114 |
| <b>3.4</b> Considerations relative to g-value variations with film thickness.                            | 120 |
| <b>3.5</b> Conclusion  | 123 |
| <i>References</i>  | 124 |
| <b>Chapter 4 Photonic Crystals (PhC)</b>   |     |
| <b>4.1</b> Introduction  | 127 |
| <b>4.2</b> Cellulose Acetate (CA) and Poly(2,6-dimethyl-1,4-phenyleneether)(PPO) Photonic Crystals (PhC) | 129 |
| <b>4.3</b> Thin films  | 133 |
| <b>4.3.1</b> Comparison of FT-IR and IRRAS analysis of PPO thin films                                    | 133 |
| <b>4.3.2</b> Desorption of CCl <sub>4</sub>  | 141 |
| <b>4.3.3</b> Refractive indexes  | 144 |
| <b>4.4</b> Conclusion  | 148 |
| <i>References</i>  | 149 |
| <b>Summary</b>   | 151 |
| <b>Chapter 5 Experimental section</b>  |     |
| <b>5.1</b> Materials and Sample preparation  | 155 |
| <b>5.1.1</b> sPS   | 155 |
| <b>5.1.2</b> PPO   | 156 |
| <b>5.1.3</b> PLLA  | 157 |
| <b>5.2</b> Techniques  | 157 |
| <b>5.2.1</b> X-ray diffraction analysis  | 157 |
| <b>5.2.2</b> IR Infrared spectra   | 159 |
| <b>5.2.3</b> TGA measurements  | 162 |
| <i>References</i>  | 162 |

## List of Abbreviations

AN: Acetonitrile

CA: Cellulose Acetate

$\text{CCl}_4$ : Carbon tetrachloride

CD: Circular Dichroism

$\text{CH}_2\text{Cl}_2$ : Diclorometano

CPO: Cyclopentanone

DBF: Dibenzofuran

DBR: Distributed Bragg Reflector

DCE 1,2-dichloroethane

dis<sub>i</sub>: disordered modification from the intercalate phase

dis<sub>t</sub>: disordered modification obtained from the triclinic clathrate phase

DMF: Dimethylformamide

DMN: Dimethylnaphthalene

DNB: 1,4-dinitrobenzene

DOL: Dioxolane

g: Degree of circular polarization

GBL:  $\gamma$ -butyrolactone

NA: paranitroaniline

PhC: Photonic Crystal

PLLA: Poly (L-lactide)

PPO: Poly (2,6-dimethyl-1,4-phenylene)oxide

sPS: Syndiotactic Polystyrene

THF: Tetrahydrofuran

TMB: 1,3,5-trimethylbenzene

VCD: Vibrational Circular Dichroism

XRD: X-ray Diffraction

## *Introduction*

### **Polymeric films with co-crystalline and nanoporous crystalline phases**

Polymers can crystallize in different crystalline forms; polymorphism is the term to indicate this ability. It is known that processing and physical properties of polymer-based materials are strongly affected by the occurrence of “polymorphism”<sup>1</sup> and “metamorphism” (i.e., the occurrence of “disordered” crystalline phases, characterized by a degree of structural organization that is intermediate between those identifying crystalline and amorphous phases)<sup>2a</sup>

My PhD thesis is focused on the study and on the characterization of polymer films with co-crystalline and nanoporous crystalline phases. Many polymers are able to form co-crystals i.e. molecules of low molecular weight (guest) trapped in the crystalline polymer lattice (host). Over the past two decades it has been observed that some polymers, with co-crystalline phases, such as syndiotactic polystyrene (sPS) and poly (2,6-dimethyl-1,4-phenylene oxide) (PPO) after guest removal can form nanoporous crystalline phases, able to absorb suitable guest molecules also at low activity.

During this work, I have studied the possible molecular orientations that may be induced by solvents during co-crystallization process in polymeric films, (chapter 2); the development of chiro optical response, after co-crystallization with temporary chiral guest (chapter 3) and the possibility to realize photonic crystals by using polymers able to form nanoporous crystalline forms (chapter 4).

In detail, in chapter 1 the procedure to obtain disordered nanoporous crystalline phases in sPS films and their possible application is reported. This disordered nanoporous crystalline phase rapidly absorb low molecular mass molecules, also from very dilute aqueous solutions.

It is known in literature that nanoporous  $\delta$  form of sPS is also able to absorb ethylene<sup>2b</sup> and carbon dioxide<sup>2c-d</sup>, that have negatively effects for vegetable. Active packaging by

nanoporous-crystalline films, based on the removal of molecules generated by the vegetables being detrimental for their preservation <sup>2e</sup>, could be complemented by the slow-release of antimicrobial molecules, which could be included as guest of the film crystalline cavities. Therefore the preparation of s-PS co-crystalline films that include guests with antimicrobial activity, in particular the carvacrol guest has been studied and reported in chapter 1. The kinetics of release, in variable concentrations of carvacrol in films with different thickness, has been analyzed. It was observed that the location of antimicrobial molecules mainly in the crystalline phase assure a decrease of desorption diffusivity and hence a long-term antimicrobial release.

In chapter 2, the study of the possible molecular orientations that can be developed in polymer films able to form co-crystalline phases, are reported. This phenomenon has been observed only for sPS films until now. In particular, in my thesis has been shown that also other polymers, such as poly (2, 6-dimethyl-1, 4-phenylene oxide) (PPO) and poly (L-lactide) (PLLA), able to form co-crystalline phases, can develop orientations during the co-crystallization process with solvents. These orientations can be useful to the structural studies on PPO and PLLA co-crystalline forms.

We have also investigated on the shrinkage behavior developed in syndiotactic polystyrene (sPS) films after co-crystallization procedures leading to co-crystalline phases. High shrinkage values have been measured on sPS  $\delta$  co-crystalline phase showing a crystalline phase orientation. In order to minimize this effect, novel procedures have been developed.

Another aspect of my work is focused on the study of chiro optical response of a racemic polymer crystallized with a temporary chiral guest, as reported in chapter 3. In particular, I evaluated the degree of circular polarization of different thickness sPS films, and of the achiral guests, such as azulene and 4-nitroaniline, included in the polymer crystalline phase after guest exchange procedure. These studies have been

useful to investigate on the nature of this phenomenon.

Finally, in chapter 4, a method to realize a photonic crystal (PhC) with polymeric materials is reported. A PhC is an object composed by two or more materials with different refractive index and an alternated periodicity. The main advantage to use polymers rather than inorganic materials is the ease and the speed to obtain thin films by spin coating and the low cost of materials.

In order to realize a photonic crystal, by using thin layers of PPO presenting nanoporous crystalline phase, it has been necessary to characterize amorphous as well as crystalline phases for this purpose. Techniques such as IRRAS and ellipsometry have been used (as reported in section 4.3 of chapter 4).

*Characteristics of polymeric films presenting co-crystalline or nanoporous crystalline phases:*

*Syndiotactic polystyrene (sPS), Poly(2,6-dimethyl-1,4-phenylene ether) (PPO), Poly (L-lactide) (PLLA)*

***Syndiotactic polystyrene (sPS)*** exhibits a complex polymorphic behavior<sup>3,4</sup>, which can be described in terms of two crystalline forms,  $\alpha$ <sup>5</sup> and  $\beta$ <sup>6</sup>, containing planar zigzag chains and three forms,  $\gamma$ <sup>7</sup>,  $\delta$ <sup>8</sup> and  $\varepsilon$ <sup>9</sup>, containing  $s(2/1)2$  helical chains (helical repetition of two structural units in one turn, the structural unit being formed by two monomeric units). Both  $\beta$  and  $\alpha$  forms can exist in different modifications having different degrees of structural order, so that two limit-disordered modifications ( $\beta'$  and  $\alpha'$ ) and two limit-ordered modifications ( $\beta''$  and  $\alpha''$ ).<sup>10</sup>

$\delta$ <sup>8</sup> and  $\varepsilon$ <sup>9</sup> forms are nanoporous-crystalline, i.e. exhibit low-density packing of the polymer chains with some empty space regularly distributed in the crystalline phase and available for sorption of suitable guest molecules.<sup>11</sup>

Moreover, it is well known that s-PS can form co crystalline phases (clathrate<sup>3</sup> and intercalate<sup>4</sup>) with several low

molecular-mass molecules where the polymer always assumes its  $s(2/1)2$  helical conformation. Melt-crystallization procedures lead only to the trans-planar  $\alpha$ <sup>5</sup> and  $\beta$ <sup>6</sup> phases. On the other hand, solution crystallization and solvent-induced crystallization generally lead to the formation of helical cocrystalline and  $\gamma$  phases, although the thermodynamically favored trans-planar  $\beta$  phase is also obtained by solution casting at high temperatures as well as by annealing above 150 °C of cocrystalline and  $\gamma$  samples in the presence of solvents.<sup>12</sup> The nanoporous  $\delta$  and  $\varepsilon$  forms are obtained by guest removal from cocrystalline phases.<sup>12</sup>

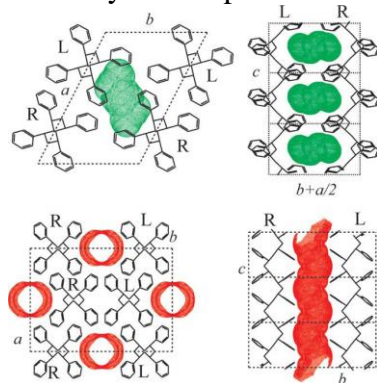


**Fig.1** Top and lateral views of the crystalline structures of the two nanoporous crystalline forms of s-PS. For the  $\delta$  (upper figures) and  $\varepsilon$  (lower figures) forms, the porosity is distributed as cavities and channels, respectively.<sup>4</sup>

Materials presenting the nanoporous  $\delta$  crystalline phase have been deeply studied for their promising applications in chemical separations (mainly air/water purification) in sensorics or possible application as films for packaging, of particular economic relevance is the ability of the nanoporous  $\delta$  form to absorb ethylene<sup>2b</sup> and carbon dioxide<sup>2c-d</sup>, they are the molecules generated by the vegetables and detrimental for their preservation<sup>2e</sup>. This ability could increase the shelf-life of vegetable. Films presenting s-PS/ active-guest co-crystals have been proposed as advanced materials, mainly for optical applications (e.g., as fluorescent, photoreactive)<sup>12</sup>

**Poly(2,6-dimethyl-1,4- phenylene ether) (PPO)** is a polymer that exhibits nanoporous-crystalline phases, as s-PS.<sup>13</sup> In most cases, his guest solubility is not only definitely higher than for the high free volume amorphous PPO phase but also higher than for the s-PS nanoporous crystalline forms.<sup>13</sup> Recently it was found that there is nearly a continuum of crystalline phases between two limit structures exhibiting highest and lowest  $2\theta$  values. The  $d$  values obtained with the different solvents clearly show that the solvent plays a fundamental role in determining the periodicity of the final crystalline phase.<sup>13</sup>

Moreover, since the end of the sixties of the last century, it is well known that PPO can co-crystallize with many guest molecules.<sup>14</sup> In fig.1.2 the X-ray diffraction pattern of clathrate structure PPO/ $\alpha$ -pinene, reported in literature,<sup>14b</sup> is reported.

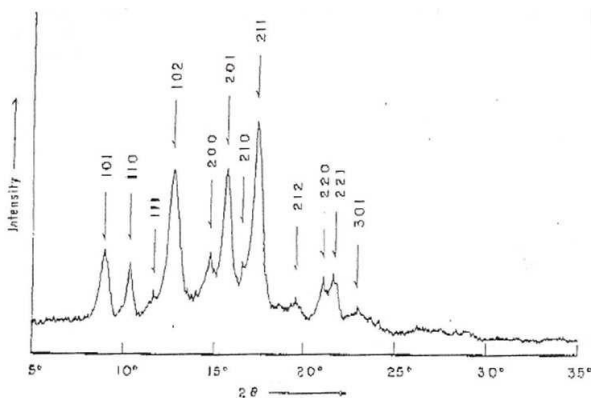


**Fig. 2** X-ray diffraction pattern of chlatrate structure PPO/ $\alpha$ -pinene taken from Horikiri S., Journal of polymer Science **1972**,(10), 1167-70

The only crystalline structure defined for PPO is the co-crystalline structure with  $\alpha$ -pinene,<sup>14c</sup> whose unit-cell has been defined many years ago by electron diffraction of single crystals<sup>14d</sup>. Recently this structure has been refined. It was observed that the chiral guest is able to induce its chirality to the crystalline structure. The packing model of the co-

crystalline form of PPO with (1S)-(-)- $\alpha$ -pinene in a tetragonal unit cell ( $a=b=1.19$  nm and  $c=1.71$  nm) and according to the  $P4_3$  space group is shown in Figure 1.3.<sup>14c</sup>

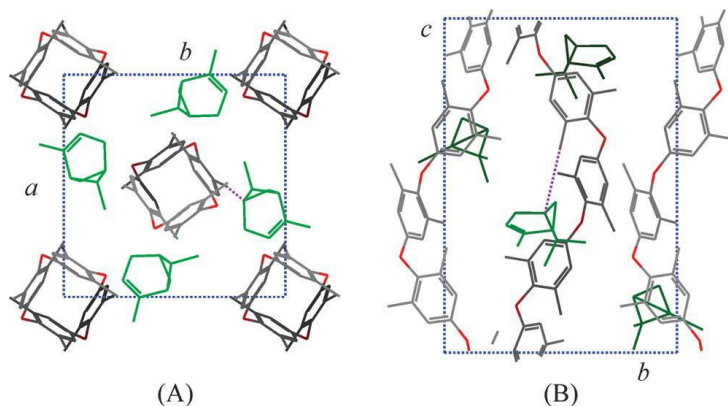


**Fig. 3** Packing model of the co-crystalline form of PPO with (1S)-(-)- $\alpha$ -pinene in the unit cell  $a= b = 1.19$  nm and  $c = 1.71$  nm, and the  $P4_3$  space group (A) Projection along  $c$ ; (B) projection along  $a$ . None bonded distances are all longer than 0.36 nm.

Major applications of PPO are for automotive, business machine, and electrical industries.

Moreover PPO is an attractive material for the preparation of membranes due to its resistant against a number of chemical agents, including aqueous solutions of strong acids and bases.

**Poly (L-lactide) (PLLA)** has different crystalline forms ( $\alpha$ ,  $\beta$  and  $\gamma$ ).<sup>15</sup>

The  $\alpha$  form of PLLA grows upon melt or cold crystallization, as well as from solution. The  $\alpha$  form has two antiparallel chains in a left-handed  $10_3$  helical conformation (or distorted  $10_3$  helix) packed in an orthorhombic (or pseudo-orthorhombic) unit cell with  $a = 1.066$  nm,  $b = 0.616$  nm,  $c = 2.888$ <sup>16-17</sup>. The  $\beta$  form<sup>18-19</sup> (orthorhombic<sup>18</sup> or trigonal<sup>19</sup>) is known to take a  $3_1$  helical conformation<sup>20</sup> the  $\gamma$  form is obtained via epitaxial crystallization on hexamethylbenzene substrate. It is characterized by two antiparallel helices with

3<sub>1</sub> conformations packed in an orthorhombic unit cell with  $a = 0.995$  nm,  $b = 0.625$  nm,  $c = 0.880$  nm<sup>15</sup>

In addition to these crystalline forms, is known a metastable crystalline form called  $\alpha'$ , and it was observed that the formation of  $\alpha'$  does not depend on the polymer molecular mass but from the crystallization temperature.<sup>16,17</sup> Two different crystal modification,  $\alpha'$  and  $\alpha$ , are obtained at low and high crystallization temperature respectively<sup>21</sup>

The  $\alpha'$  form has a 10<sub>3</sub> helix conformation and orthorhombic (or pseudoorthorhombic) unit cell, like the  $\alpha$  form, but the molecular packing within the unit cell of  $\alpha'$  is looser and more disordered than in the  $\alpha$  form, due to the larger lattice dimension and weaker interchain interaction.<sup>21</sup>

Moreover, during heating the  $\alpha'$  crystals transform into  $\alpha$  modification: the change of crystal structure from  $\alpha'$  to  $\alpha$  is a solid–solid transition that mainly involves slight rearrangements of the molecular packing within the unit cell to the more energy-favorable state, corresponding to a reduction of lattice dimensions.<sup>21</sup>

In addition in literature is reported that PLLA, treated with CO<sub>2</sub> at different temperatures and pressures, can develop different  $\alpha$ ,  $\alpha'$  and  $\alpha''$  forms. The  $\alpha''$  form is expected to be nanoporous.<sup>22</sup>

Also PLLA is able to form co-crystals, as sPS and the PPO.

It is known from literature that solvents such as CPO (cyclopentanone), DMF (dimethyl formamide), THF (tetrahydrofuran), DOL (dioxolane), GBL ( $\gamma$ -butyrolactone) are able to induce co crystalline  $\epsilon$  form.<sup>23</sup>

The  $\epsilon$  co-crystalline structure including *N,N*-dimethylformamide (DMF) has been recently described in literature, in this model the PLLA chains show a 10<sub>7</sub> helical conformation and are packed in the orthorhombic lattice with  $a=1.5$ - $1.6$  nm,  $b=1.2$ - $1.3$  nm and  $c=2.8$ - $2.9$  nm.<sup>23</sup>

PLLA is a biodegradable and biocompatible polyester that can be produced by renewable resources. Being non-toxic to human body, PLLA is used in biomedical applications, like surgical sutures, bone fixation devices, or controlled drug

delivery. The mechanical and thermal properties of this semicrystalline polymer greatly depend on the crystal structure and morphology.<sup>21</sup>

### **References**

1. a) Tashiro, K.; Tadokoro, H. In *Encyclopedia of Polymer Science and Engineering. Supplement* **1989**; p 187 b) Corradini, P; Guerra, G. *Adv. Polym. Sci.* **1992**, 100, 183
2. a)Auriemma, F.; De Rosa, C.; Corradini, P. *Adv. Polym. Sci.* **2005**, 181, 1–74. b) A. R. Alburnia, T. Minucci, G. Guerra, J. *Mater. Chem.* **2008**, 18, 1046. c) Larobina D., Sanguigno L., Venditto V., Guerra G., Mensitieri G., *Polymer* **2004**, 45, 429.
- d) Annunziata L., Alburnia A. R., Venditto V., Guerra G., *Macromolecules* ,**2006**, 39, 9166 e) P. Rizzo;C. Daniel; A. De Girolamo Del Mauro; G. Guerra **2006** SA2006A22 Università di Salerno ID:1517898 Brevetto
3. Guerra, Vitagliano, De Rosa, Petraccone, Corradini *Macromolecules* **1990**, 23, 1539
4. Guerra, G., Daniel, C., Rizzo, P., Tarallo, O.: *J.Polym.Sci.Polym.Phys.* **2012**, 50, 305
- 5 De Rosa, C., Guerra, G., Petraccone, V., Corradini, P.: *Polym. J.* **1991**, 23, 1435
6. De Rosa, C., Rapacciuolo, M., Guerra, G., Petraccone, B., Corradini, P. *Polymer*, **1992**, 33, 1423
7. Rizzo, P., Alburnia, A. R., Guerra, G. **2005**, 46, 9549
8. De Rosa, C., Guerra, G., Petraccone, V., Pirozzi, B, *Macromolecules* **1997**, 30, 4147
9. Rizzo, P., Daniel, C., De Girolamo Del Mauro, A., Guerra, G. *Chem. Mater.*, **2007**, 19, 3864
10. Rizzo P., Lamberti M., Alburnia A.R., Ruiz De Ballestreros O. Guerra G. *Macromolecules* **2002**, 35, 5854
11. Manfredi C., Del Nobile M.A., Mensitieri G., Guerra, G., Rapacciuolo, M. *J. Polym. Sci., Part B: Polym. Phys.* **1997**, 35,133
- 12.AlexandraR. Alburnia, Loredana AnnunziataGaetano Guerr a *Macromolecules* **2008**, 41,2683

- 13.** a) Daniel, C.; Longo, S.; Vitillo, J. G.; Fasano, G.; Guerra, G. *Chem. Mater.* **2011**, *23*, 3195. b) Galizia, M.; Daniel, C.; Fasano, G.; Guerra, G.; Mensitieri, G. *Macromolecules* **2012**, *45*, 3604. c) Daniel, C.; Longo, S.; Cardea, S.; Vitillo, J. G.; Guerra, G. *RSC Advances* **2012**, *2*, 12011. d) Daniel, C.; Zhovner, D.; Guerra, G. *Macromolecules* **2013**, *46*, 449.
- 14.** a) Factor, A.; Heinsohn, G. E.; Vogt, L. H., Jr. *Polym. Lett.* **1969**, *7*, 205. b) Horikiri, S. *J. Polym. Sci. A2* **1972**, *10*, 1167. c) Tarallo, O.; Petraccone, V.; Daniel, C.; Fasano, G.; Rizzo, P.; Guerra, G. *J. Mater. Chem.* **2012**, *22*, 11672. d) Barrales-Rienda, M.; Fatou, J. M. *Kolloid Z. Z. Polym.* **1971**, *244*, 317. e) Hurek, J.; Turska, E. *Acta Polym.* **1984**, *35*, 201.
- 15.** Di Lorenzo M. L., Cocca M., Malinconico M. *Thermochimica Acta* **2011**, *522*, 110
- 16.** Pan P., Kai W., Zhu B, Dong T., Inoue Y. *Macromolecules* **2007**, *40*, 6898
- 17.** Pan P., Zhu B, Kai W., Dong T., Inoue Y *Journal of applied Polymer Science*, **2008**, *107*, 54
- 18.** Di Lorenzo ML. *Eur Polym J* **2005**; *41*, 569.
- 19.** Kawai T, Rahman N, Matsuba G, Nishida K, Kanaya T, Nakano M, *Macromolecules* **2007**, *40*, 9463.
- 20.** Sawai D., Takahashi K., Sasashige A., Kanamoto T. *Macromolecules* **2003**, *36*, 3601-3605
- 21.** Cocca M., Di Lorenzo M.L., Malinconico M., Frezza V. *European Polymer Journal* **2011**, *47*, 1073
- 22.** Marubayashi H., Akaishi S., Akasaka S., Asai S., Sumita M., *Macromolecules* **2008**, *41*, 9192
- 23.** Marubayashi H., Asai S., Sumita M., *Macromolecules* **2012**, *45*, 1384

# Chapter 1

## Disordered nanoporous crystalline modifications and co-crystalline phase of Syndiotactic polystyrene including carvacrol guest molecules

### 1.1 Introduction

Different classes of co-crystalline forms have been described for s-PS, all exhibiting as a common feature the  $s(2/1)_2$  helical polymer conformation, with a repetition period of nearly 0.78 nm<sup>1,2</sup>; monoclinic  $\delta$ -clathrates<sup>1,3</sup>, triclinic  $\delta$ -clathrates<sup>4,5</sup>, intercalates (also named  $\delta$ -intercalates)<sup>6,7</sup> and  $\epsilon$ -clathrates<sup>8,9</sup>.

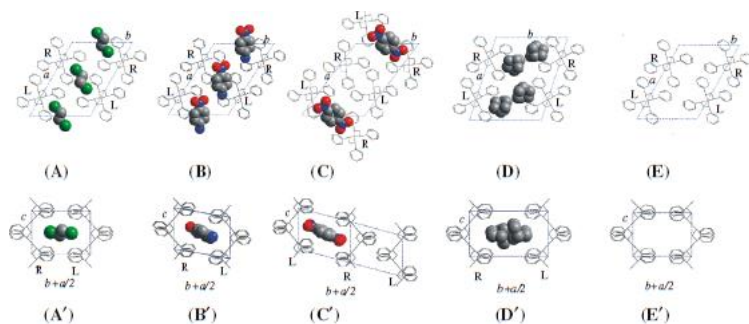


**Fig. 1.1** Schematic projections along the chain (up) and perpendicular to the chain (down) of s-PS co-crystalline forms: A, A' monoclinic  $\delta$ -clathrate form with 1,2-dichloroethane<sup>10</sup>, B, B' triclinic  $\delta$ -clathrate form with p-nitroaniline<sup>4</sup>, C, C' triclinic  $\delta$ -clathrate form with 1,4-dinitrobenzene<sup>5</sup>, D, D' intercalate form with norbornadiene<sup>11</sup>, and E, E' monoclinic  $\delta$ -nanoporous phase<sup>12</sup>

Monoclinic  $\delta$ -clathrates (Fig. 1.1A–A')<sup>10</sup>, triclinic  $\delta$ -clathrates (Fig. 1.1B–B')<sup>4,5</sup>, intercalates (Fig. 1.1D–D')<sup>11</sup> as well as the nanoporous  $\delta$  form (Fig. 1.1E)<sup>12</sup>, are all characterized by  $ac$  layers of close-packed alternated enantiomorphous helices as a common structural feature. The distance between such layers ( $d_{010}$ ) as well as between the guest molecules can change largely, mainly depending on the class of the co-crystalline form but also on the molecular volume of the guest molecules. In particular, monoclinic  $\delta$ -

clathrates are obtained with guests whose molecular volumes are significantly lower than  $0.12 \text{ nm}^3$ . As the bulkiness of the guest increases, there is typically an increase of the spacing ( $d_{010} = b \sin \gamma$ ) between the *ac* layers (in the range  $1.06\text{--}1.2 \text{ nm}$ )<sup>1,3,13</sup>. Because in most cases a single guest molecule is present in each cavity, the maximum molar ratio between guest molecules and styrenic units is 1/4. On the other hand, triclinic  $\delta$ -clathrates are generally obtained with guests whose molecular volumes are higher than  $0.12 \text{ nm}^3$ .<sup>4,5</sup> Guests having a volume close to  $0.12 \text{ nm}^3$ , like *p*-nitro-aniline (NA,  $V_{\text{mol}} \sim 0.122 \text{ nm}^3$ ), can be accommodated only by shifting the dense *ac* layers along the chain axis, keeping the  $d_{010}$  value almost equal to that of the  $\delta$  form, and thus leading to a triclinic unit cell (Fig. 1.1B–B')<sup>4</sup>. Also, in this case the maximum molar ratio between guest molecules and styrenic units is 1/4. For triclinic  $\delta$ -clathrates obtained with guests having a higher molecular volume, e.g. 1,4 dinitrobenzene (DNB) ( $V_{\text{mol}} \sim 0.134 \text{ nm}^3$ ) or dibenzofuran (DBF) ( $V_{\text{mol}} \sim 0.159 \text{ nm}^3$ ), the close packing of the polymer chains in the *ac* layers is partially lost and one half of the cavities initially present in the  $\delta$  phase are lost allowing the volume of the other half to increase and becoming suitable to host bulky guest molecules (Fig. 1.1C–C')<sup>5</sup>. This of course halves the maximum guest/monomer-unit molar ratio that then becomes 1/8.

A further class of *s*-PS  $\delta$  co-crystals, defined as  $\delta$ -intercalates (or simply intercalates)<sup>6,7</sup>, is characterized by the same layers of alternated enantiomorphous *s*(2/1)2 polymer helices (Fig.1.1A, B, D), but the spacing between the *ac* layers ( $d_{010}$ ), for all the known *s*-PS intercalates, is larger than  $1.4 \text{ nm}$  and values as high as  $1.75 \text{ nm}$  have been observed<sup>13</sup>. In fact, in these co-crystals the guest molecules are not isolated into host cavities but are contiguous inside layers intercalated with the dense polymer *ac* layers. Of course, these intercalate structures present higher guest content with respect to the clathrate structures.

Therefore disordered crystalline modifications formed by *s*(2/1)2 helices of syndiotactic polystyrene (*s*-PS) can be

prepared by the removal of bulky guest molecules from intercalate as well as from triclinic  $\delta$  clathrate forms. As a consequence, the obtained disordered crystalline modifications of s-PS can be fully considered disordered nanoporous-crystalline modifications.

Moreover the semicrystalline s-PS samples exhibiting the nanoporous  $\delta$ <sup>12,14</sup> and  $\epsilon$ <sup>15,16</sup> crystalline phases can rapidly and selectively absorb volatile organic compounds as well as gas molecules, even when present at very low concentrations. This active packaging by nanoporous-crystalline films, based on the removal of molecules generated by the vegetables being detrimental for their preservation, could be complemented by the slow-release of antimicrobial molecules. The film not only is able to absorb ethylene<sup>17</sup> and carbon dioxide, but also could be complemented by the slow-release of antimicrobial molecules, which could be included as guest of the film crystalline cavities.

In fact, it is well established that the release of many low molecular-mass guest molecules is slower from the s-PS nanoporous-crystalline host phases than for the corresponding amorphous phases.<sup>17,18</sup> In addition, guest diffusivity can be further reduced by suitable selection of the uniplanar orientation<sup>19,20</sup> of the host crystalline phase. In particular, in most cases the guest diffusivity is minimized for the  $\delta$ -form films exhibiting their dense *ac* layers of closely packed alternated enantiomorphous helices, green ribbons in Fig. 1.2 (A), parallel to the film plane. This orientation brings the *a* and *c* axes parallel to the film plane and has been defined as *a//c//* uniplanar orientation.<sup>17,18,21,22</sup>

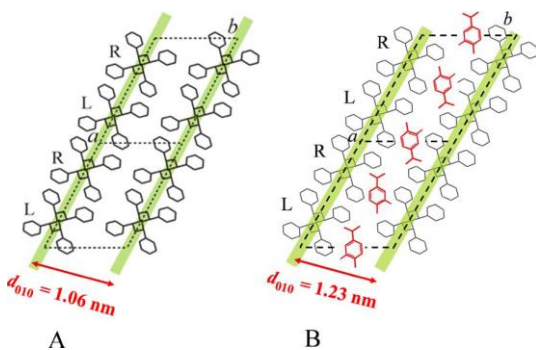


**Fig 1.2** Schematic projections along the chain axis (*c* axis) showing the crystal structure of: (A) monoclinic nanoporous  $\delta$ -form; (B) monoclinic *d* clathrate form with carvacrol. High density *ac* layers of closely packed enantiomorphous helices have been pointed out by green ribbons. [Color figure can be viewed in the online issue, which is available at <http://wileyonlinelibrary.com>.]

## 1.2 Guest removal from intercalate forms

In Fig.1.3, X-ray diffraction patterns of s-PS films exhibiting  $a//c//$  uniplanar orientation of intercalate phases including 1,4-dimethyl-naphthalene (DMN)<sup>13</sup> (A) and 1,3,5-trimethylbenzene (TMB)<sup>13</sup> (B) are shown. The formation of intercalate structures is clearly shown by the shift of the 010 diffraction peak of the  $\delta$  form samples ( $2\theta_{\text{CuK}\alpha} = 8.4^\circ$ )<sup>12</sup> down to  $2\theta_{\text{CuK}\alpha} = 5.8^\circ$ , and down to  $2\theta_{\text{CuK}\alpha} = 6.0^\circ$  for the intercalate structures including DMN (A) and TMB (B), respectively.

After extraction of the bulky guests from the intercalates by using acetonitrile (AN), a shift of the 010 diffraction peaks from  $2\theta_{\text{CuK}\alpha} = 5.8^\circ$  (Fig.1.3A), or from  $2\theta_{\text{CuK}\alpha} = 6.0^\circ$

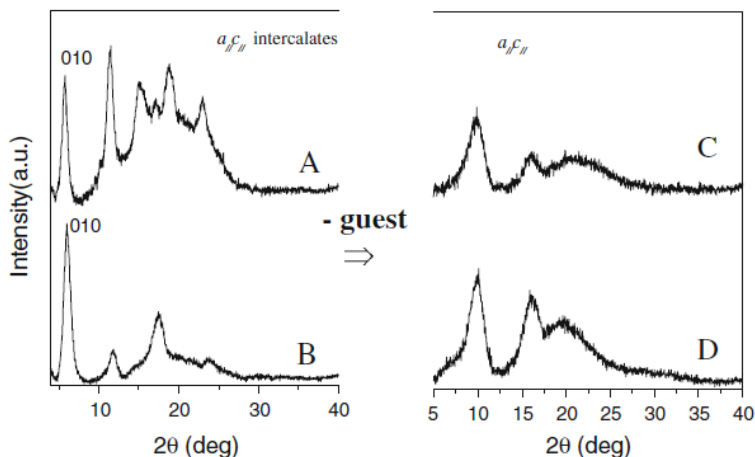


**Fig. 1. 3** X-ray diffraction patterns of s-PS films exhibiting  $a_{//c_{//}}$  uniplanar orientation of: A intercalate phase with DMN, B intercalate phase with TMB, C disordered crystalline modification obtained by DMN removal, and D disordered crystalline modification obtained by TMB removal

(Fig. 1.3B), to a higher  $2\theta$  value of  $2\theta_{CuK\alpha} = 9.8^\circ$  is apparent (Fig. 1.3C–D); moreover, a decrease of crystallinity is clearly observed. For instance, the degree of crystallinity, as evaluated on powdered samples, changes from  $\chi_c = 38\%$  for s-PS films including TMB to  $\chi_c = 26\%$  for the same films after TMB removal.

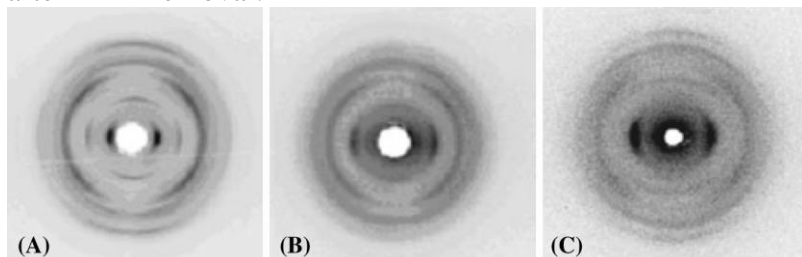


**Fig. 1. 4** X-ray diffraction patterns of s-PS films exhibiting the  $a_{//c_{//}}$  uniplanar orientation of the intercalate phase with TMB, before (A) and after (B) TMB removal. The photographic pattern of a  $\delta$  form film exhibiting the  $a_{//c_{//}}$  uniplanar orientation is also reported for comparison (C)

In Fig. 1.4 the EDGE photographic X-ray diffraction patterns, i.e. the pattern taken by having the X-ray beam parallel to the

film surface (and by placing the film sample parallel to the axis of the cylindrical camera), for films including TMB before (A) and after (B) guest removal are reported. The EDGE photographic pattern of the  $\delta$  form film exhibiting the  $a//c//$  uniplanar orientation, obtained as described in Ref. 19, is also included for comparison (Fig. 1.4C).

It is worth noting that for sPS films exhibiting the  $a//c//$  uniplanar orientation, after extraction of bulky guests from the intercalates, a decrease of uniplanar orientation is observed. In particular, the degree of uniplanar orientation of the 010 crystallographic planes ( $f_{010}$ ), with respect to the film plane, formalized by using Hermans' orientation function according to Experimental section (Chapter 5 section 5.2.1 equation 1), is  $f_{010} = 0.8$  for the s-PS film including TMB (Fig. 1.4A) and  $f_{010} = 0.65$  after TMB removal (Fig. 1. 3B).

In summary, the guest extraction from the considered intercalates of sPS films can lead to a disordered crystalline modification characterized by a broad diffraction peak at  $2\theta_{CuK\alpha} \sim 9.8^\circ$  and presenting a lower degree of crystallinity as well as a lower degree of uniplanar orientation with respect to the starting intercalate samples.

### **1.2.1 Guest removal from the triclinic $\delta$ clathrate form with DBF**

The X-ray diffraction pattern of an unoriented s-PS film presenting the s-PS/styrene<sup>23</sup> monoclinic  $\delta$  clathrate form is reported in Fig. 1. 4A.

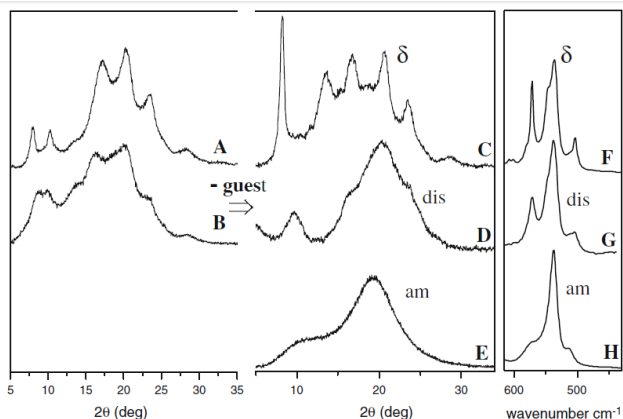


**Fig.1.5** X-ray diffraction patterns of unoriented s-PS samples: A monoclinic  $\delta$  co-crystalline phase with styrene, B triclinic  $\delta$ -clathrate phase with DBF, C sample A after styrene removal by supercritical  $\text{CO}_2$  (monoclinic nanoporous-crystalline  $\delta$  form), D sample B after DBF removal by acetonitrile (disordered nanoporous-crystalline modification), and E fully amorphous film. FTIR spectra (F–H), in range  $600\text{--}500\text{ cm}^{-1}$ , of the s-PS samples whose X-ray diffraction patterns are shown in (C–E)

Styrene was removed by supercritical carbon dioxide, leading to a highly crystalline nanoporous  $\delta$  phase (Fig. 1.5C,  $\chi_c \sim 40\%$ ). Analogous highly crystalline  $\delta$  form samples can be obtained by styrene removal by other volatile guests such as acetone or acetonitrile. Guest desorption processes from the s-PS co-crystalline form, leading to the nanoporous  $\delta$  phase, have been thoroughly described elsewhere<sup>6,20</sup>.

The achievement of the nanoporous  $\delta$  form by removal of guests from  $\delta$  co-crystalline forms is rather common but it is not general. In fact, different behaviors can be observed when  $\delta$  removing bulky guest molecules from triclinic  $\delta$ -clathrate forms. For instance, the X-ray diffraction pattern of a s-PS film, including the triclinic  $\delta$ -clathrate form with DBF, is shown in Fig. 1.5B. The DBF clathrate was prepared by immersion of a  $\delta$  form film in a saturated solution of DBF in acetone<sup>5</sup>. The  $\delta$  spacing (1.06 and 0.91 nm) of the two diffraction peaks at lower angles ( $2\theta = 8.4^\circ$  and  $9.7^\circ$ , Fig. 1.4B) clearly indicates the occurrence of this s-PS/DBF triclinic clathrate form<sup>5</sup>. The X-ray diffraction pattern of the s-PS film

of Fig. 1.5B, after complete guest removal by AN, only shows two broad peaks centered at  $2\theta_{\text{CuK}\alpha} \sim 9.6^\circ$  and  $20.3^\circ$  and two shoulders at  $16.6^\circ$  and  $23.6^\circ$  and (Fig. 1.5D).

Moreover, the crystallinity index, going from the co-crystalline (Fig. 1.5B) to the disordered empty crystalline form (Fig. 1.5D), is reduced from  $\chi_c \sim 27\%$  down to  $\chi_c \sim 17\%$ . For the sake of comparison, the X-ray diffraction pattern of a fully amorphous s-PS sample (obtained by quenching s-PS samples from the melt) is also shown in Fig. 1.5E.

A substantial reduction of crystallinity as a consequence of DBF removal is clearly confirmed by the FTIR spectra reported in Fig. 1.4F–H for the spectral range  $600\text{--}500\text{ cm}^{-1}$ .

In fact, the  $572$  and  $501\text{ cm}^{-1}$  absorbance peaks, corresponding to vibrational modes of the  $s(2/1)_2$  helices of the crystalline phases<sup>24,25</sup>, present intensities for the sample of Fig. 1.5G that are lower than for the  $\delta$  form sample (Fig. 1.5F) and higher than for the fully amorphous sample (Fig. 1.5H).

It is worth noting that similar or more crystalline samples, presenting in their X-ray diffraction patterns two broad peaks centered at  $2\theta_{\text{CuK}\alpha} \sim 9.6^\circ$  and  $20.3^\circ$ , analogous to those shown in Fig. 1.5D, can be obtained by crystallization of amorphous samples by using eco-friendly solvents such as ethylacetate<sup>26</sup>.

### **1.2.2 Guest sorption from the disordered crystalline form obtained by guest (DBF-TMB) removal from their clathrate and intercalate forms**

The choice of an organic pollutant (1,2-dichloroethane, DCE) was motivated by its presence in contaminated aquifers and by its resistance to remediation techniques based on reactive barriers containing  $\text{Fe}^0$ <sup>27,28</sup>. Moreover, additional information comes from its conformational equilibrium<sup>29, 30, 31, 32, 22</sup>,

essentially only the trans conformation is included in the crystalline clathrate phase, while both trans and gauche conformers are included in the amorphous phase. Quantitative evaluations of vibrational peaks associated with these conformers allow the evaluation of the amounts of DCE

confined as a guest in the clathrate phase or simply absorbed in the amorphous phase.

The sorption of DCE from aqueous dilute solutions (50 ppm) are compared for s-PS films of similar thickness exhibiting a disordered crystalline modification, obtained by DBF ( $dis_i$ ) as well as TMB ( $dis_i$ ) removal from their co-crystalline forms, and for s-PS films showing the nanoporous  $\delta$  as well as the dense  $\gamma$  forms.

The FTIR spectra in the range 1400–1140  $cm^{-1}$  of unoriented films showing different crystalline phases, after DCE equilibrium sorption from 50 ppm aqueous solutions, are shown in Fig. 1.6.

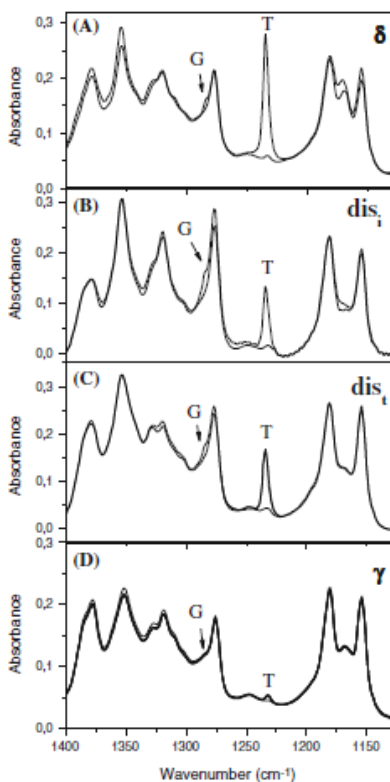


**Fig. 1.6** FTIR spectra of sPS films in the range 1,400–1,140  $cm^{-1}$  showing the A nanoporous  $\delta$  phase, B disordered nanoporous crystalline modification obtained from the intercalate phase ( $dis_i$ ), C disordered nanoporous crystalline modification obtained from triclinic clathrate phase

(dis<sub>t</sub>), and D dense  $\delta$  phase, before (thin line) and after (thick line) DCE equilibrium sorption from 50 ppm aqueous solutions

As already discussed in previous reports, the DCE uptake, which can be easily quantified by the absorbance of the trans (T) DCE peak at around  $1234\text{ cm}^{-1}$ , is nearly negligible for the  $\gamma$  form sample (Fig. 1.6D) while it is high (nearly 5 wt%) for the  $\delta$  form sample (Fig. 1.6A). The DCE uptake in the sample presenting the disordered crystalline modifications of Fig.1.5D and Fig.1.3D is intermediate (Fig. 1.6B, C), nearly 2.7 wt% as revealed from thermogravimetric measurements (TGA) (Fig. 1.7), lying between that of the  $\delta$  form and that of the  $\gamma$  form samples, and it is similar to those recently reported for the s-PS films exhibiting the  $\varepsilon$  nanoporous crystalline form<sup>22</sup>.

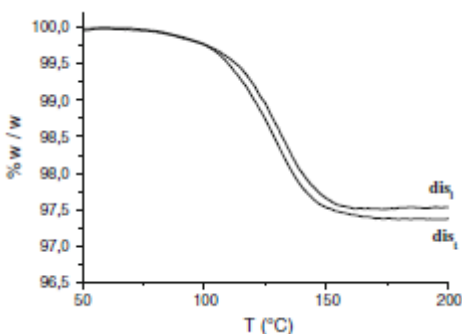


**Fig.1.7** TGA measurements of sPS films in the disordered nanoporous-crystalline modification, obtained from the intercalate phase (dis<sub>i</sub>) and from the triclinic clathrate phase (dis<sub>t</sub>), after DCE equilibrium sorption from 50 ppm aqueous solutions

Furthermore, the DCE absorbance peaks are characterized by features similar to those of DCE molecules in the nanoporous  $\delta$  form samples (Fig. 1.6A), i.e. by a very low intensity of the gauche (G) DCE peak located at  $1285\text{ cm}^{-1}$  and by the location of the trans (T) peak at  $1234\text{ cm}^{-1}$  rather than at  $1232\text{ cm}^{-1}$  as for liquid DCE or for DCE simply absorbed in the amorphous phases of s-PS<sup>22</sup>.

Both features clearly indicate that the DCE molecules are essentially absorbed only as guest of a co-crystalline phase

rather than dissolved in the amorphous phase. Hence, these disordered crystalline modifications can be better defined as disordered nanoporous-crystalline modifications.

In this respect, it is worth adding that the mesomorphic helical modification, as obtained by thermal treatments in the temperature range 90–120 °C<sup>33,34</sup>, presents a negligible DCE uptake comparable with those of the  $\gamma$  form samples.

Additional information relative to the sorption of DCE in the disordered crystalline phase has been obtained for axially oriented films. In particular, X-ray diffraction patterns of a uni-axially stretched film showing a disordered crystalline structure, as obtained by dibenzofuran removal by acetonitrile, before and after equilibrium DCE uptake from 50 ppm aqueous solutions, are compared in Fig. 7A, B, respectively.

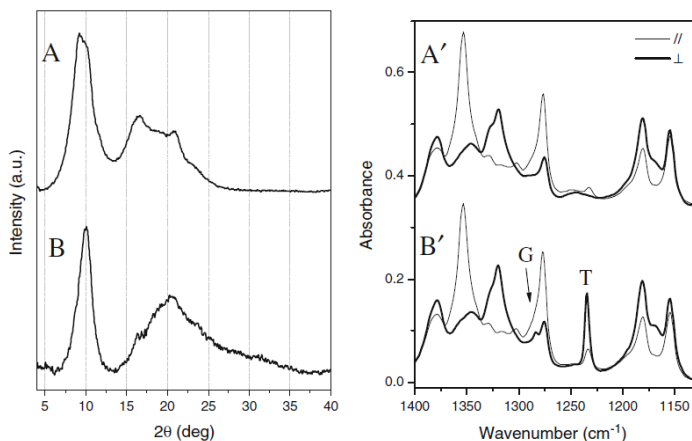


**Fig. 1.8** X-ray diffraction patterns of an axially oriented s-PS film exhibiting the disordered crystalline phase before (A) and after DCE equilibrium sorption from a 50 ppm aqueous solution (B). FTIR spectra, in the range 1400–1140 cm<sup>-1</sup>, taken with the polarization plane parallel (thin line) and perpendicular (thick line) to the stretching direction of films

The intense peak at  $d = 0.92$  nm ( $2\theta \sim 9.6^\circ$ ) indicates the presence of the disordered crystalline phase. Moreover, the decrease of the intensity of this peak and the appearance of a peak at  $d = 0.88$  nm ( $2\theta \sim 10^\circ$ ) suggests formation of the s-PS/DCE clathrate phase<sup>10</sup>.

Even more informative are the polarized FTIR spectra of the films of Fig. 1.8A, B, taken with the polarization plane parallel (thin line) and perpendicular (thick line) to the film stretching direction, which are shown in Fig. 1.8A', B', before and after equilibrium DCE uptake from 50 ppm aqueous solutions, for the spectral range 1400–1140  $\text{cm}^{-1}$ . In fact, not only the peaks corresponding to the vibrational modes of the  $s(2/1)2$  helices of the crystalline phase (like those at 1277 and 1354  $\text{cm}^{-1}$ )<sup>25</sup> are highly dichroic (indicating a high degree of axial orientation,  $f_c = 0.96$ ), but the DCE peak of the trans conformer (T) is also highly dichroic. In particular, based on the dichroism of this peak, it is possible to evaluate the angle between the transition moment vector of the corresponding vibrational mode with respect to the chain axis of the host crystalline phase ( $\alpha = 76.5^\circ$ ), which is indistinguishable from that of DCE molecules being the guest of highly crystalline  $\delta$  form films<sup>31</sup>.

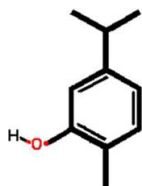
Hence, the results of Fig. 7 clearly indicate that the host–guest co-crystalline phases obtained by sorption of DCE molecules (also from dilute aqueous solutions) in the  $\delta$  form or in the disordered nanoporous-crystalline form are essentially indistinguishable.

So disordered crystalline modifications formed by  $s(2/1)2$  helices of syndiotactic polystyrene (s-PS) can be prepared by the removal of bulky guest molecules from intercalate as well as from triclinic  $\delta$  clathrate forms. The X-ray diffraction pattern of the disordered crystalline modification is characterized from  $2\theta_{\text{CuK}\alpha} < 12^\circ$  by only a broad diffraction peak whose maximum is located in the  $2\theta_{\text{CuK}\alpha}$  range between  $8.7^\circ$  and  $9.8^\circ$ . Films presenting disordered crystalline modifications have been used for the removal of an organic pollutant from dilute aqueous solutions. The sorption behaviors of the disordered crystalline modifications are compared with that of the nanoporous-crystalline  $\delta$  form as well as of the dense  $\gamma$  form. The disordered crystalline modifications of s-PS presents pollutant (1,2-dichloroethylene) uptake comparable to those of the

nanoporous  $\delta$  and  $\epsilon$  forms and much higher than those obtained for the dense  $\gamma$  form. Moreover, FTIR data relative to sorption of 1,2-dichloroethane show that the guest sorption occurs essentially only in the crystalline phase. As a consequence, the obtained disordered crystalline modifications of s-PS can be fully considered disordered nanoporous-crystalline modifications.

### 1.3. sPS\ carvacrol co-crystalline film

Antimicrobials are widely used for food protection, and are also often provided as additives to food packaging.<sup>35,36</sup> A wide variety of essential oils and many of their components, mainly mono- and sesquiterpenes, have been shown to have antimicrobial activity.<sup>37,38</sup> In particular, many studies describe the antimicrobial activity of carvacrol,<sup>39,40</sup> a well known phenolic monoterpene (Scheme 1) constituent of essential oils produced by various aromatic plants such as oregano, thyme, and marjoram.



**SCHEME 1.1** A schematic representation of carvacrol molecular structure.

X-ray diffraction patterns, as taken by an automatic powder diffractometer, of an axially oriented  $\delta$ -form s-PS film before and after immersion in a 40 wt % carvacrol/chloroform solution (followed by complete chloroform removal) are shown in Figure 1.9 (A,A').

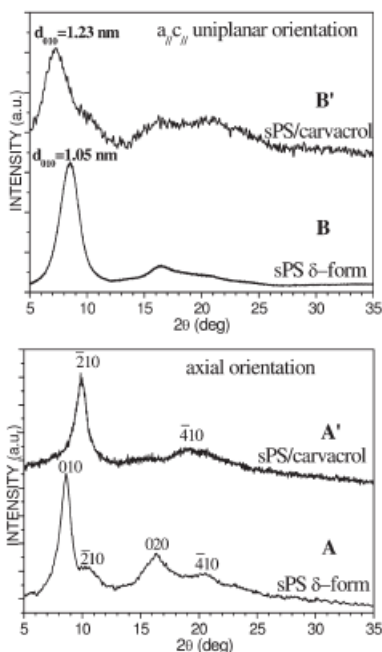


**Fig. 1.9** X-ray diffraction patterns, as taken by an automatic powder diffractometer, of s-PS films exhibiting: (A,B) the  $\delta$  nanoporous-crystalline form with (A) axial orientation and (B)  $a_{//}c_{//}$  uniplanar orientation; (A',B') the sPS/carvacrol  $\delta$ -clathrate form, with (A') axial orientation and (B')  $a_{//}c_{//}$  uniplanar orientation.

The formation of a s-PS/carvacrol co-crystalline form is

clearly shown by the large increase of the intensity of the  $\bar{2}10$  reflection at  $2\theta \sim 10^\circ$  and by the nearly complete disappearance of the intense 010 reflection, typical of the nanoporous  $\delta$ -form.<sup>1,12,13</sup> It is worth adding that, for the s-PS/carvacrol co-crystalline form, this phenomenon of increase and decrease of

intensities of the  $\bar{2}10$  and 010 reflections, respectively, is more pronounced than generally observed for other  $\delta$  clathrates.<sup>1,12,13</sup>

Weak 010 reflections can be easily studied by using films exhibiting the  $a_{//}c_{//}$  uniplanar orientation, because their X-ray diffraction patterns, as taken by an automatic powder diffractometer, maximize the intensity of the 0k0 reflections,

that is, the reflection planes parallel to the *ac* plane.<sup>19-41</sup> X-ray patterns, by an automatic powder diffractometer, of a  $\delta$ -form s-PS film with  $a//c//$  uniplanar orientation ( $f_{010}=0.85$ ),<sup>41</sup> before and after immersion in a 40 wt % carvacrol/chloroform solution (followed by complete chloroform removal) are shown in Figure 1.9 (B,B'). As usual, the starting nanoporous-crystalline film shows essentially only the 010 and 020 reflections [Fig. 1.9(B)].<sup>19-41</sup> The pattern of this film after carvacrol sorption (amplified of 10 times, due to the weakness of the 0*k*0 reflections) clearly shows that the 010 reflection of the s-PS/carvacrol co-crystalline form is located at  $2\theta \sim 7.2^\circ$ , corresponding to a Bragg distance  $d_{010}=1.23$  nm. A comparison with the data of  $\delta$  clathrates, presenting the  $d_{010}$  values included between 1.02 nm for s-PS/azobenzene and 1.16 nm for s-PS/indene  $\delta$  clathrates (Table 1 of ref. 5), show that the s-PS/carvacrol  $\delta$  clathrate presents the largest distance between the *ac* layers of closely packed alternated enantiomorphous helices. As discussed in detail in ref. 5,  $d_{010} > 1.1$  nm clearly indicates the formation of a monoclinic (rather than of a triclinic)  $\delta$  clathrate form.<sup>5</sup> A schematic projection along the polymer chain axes of the crystal structure of the monoclinic  $\delta$  clathrate form with carvacrol is shown in Figure 1.2 (B). As generally occurs for monoclinic  $\delta$  clathrates of s-PS, only one isolated guest molecule is enclosed per host crystalline cavity, with a preferential orientation of the guest molecular plane perpendicular to the polymer chain axes.<sup>1,12,13,14</sup>

### 1.3.1 FTIR Method to discriminate carvacrol molecules in co-crystalline and amorphous polymer phases

s-PS films exhibiting the  $\delta$  clathrate form with carvacrol have also been characterized by FTIR measurements. Particularly informative is the spectral region  $3650\text{--}2800$   $\text{cm}^{-1}$ , shown in Figure 1.10. In fact, the broad O-H stretching band of liquid carvacrol, in the range  $3630\text{--}3100$   $\text{cm}^{-1}$  (thick dashed line) is located in a spectral region where the absorbance of the polymer host (dotted line) is negligible. The spectrum of a  $\delta$

clathrate film with a carvacrol content close to 40 wt % [obtained by immersion in a 20 wt % carvacrol acetone solution, whose X-ray diffraction pattern is similar to that one of Fig. 1.9 (B')] presents an intense narrow peak located at  $3532\text{ cm}^{-1}$  (thin full line in Fig. 1.10).

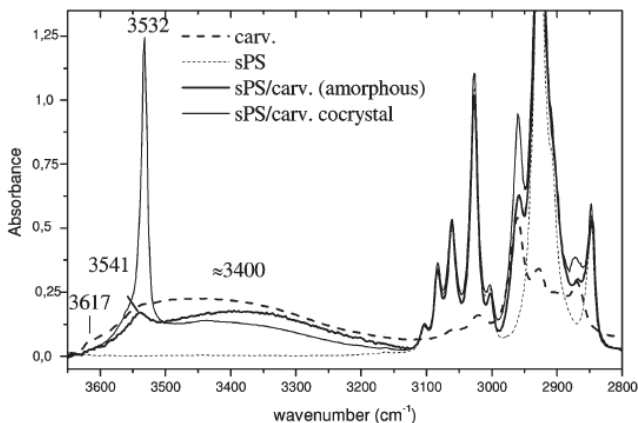


**Fig.1.10** FTIR spectra of s-PS films presenting: (thin dotted line) nanoporous  $\delta$ -form; (thin full line)  $\delta$  clathrate form with carvacrol and (thick full line)  $\lambda$ -form. The FTIR spectrum of liquid carvacrol is shown as a thick dashed line.

This clearly indicates the presence of OH groups of carvacrol molecules isolated in apolar environment, as expected for isolated guests of  $\delta$  clathrate forms. In this respect, particularly useful is a comparison with a s-PS  $\gamma$ -form film,<sup>42-43</sup> that is, a film presenting a dense crystalline phase, where guest molecules (as generally occurs for semicrystalline polymers) can be only located in the amorphous phase. This film containing roughly 20 wt % of carvacrol presents on the broad OH stretching band only a weak peak located at  $3541\text{ cm}^{-1}$ . This indicates that most carvacrol molecules, being dissolved in amorphous s-PS phases, are not isolated.

Also highly informative are the polarized FTIR spectra of axially oriented s-PS films, before and after carvacrol uptake, which are represented in Figure 1.11(A,B).

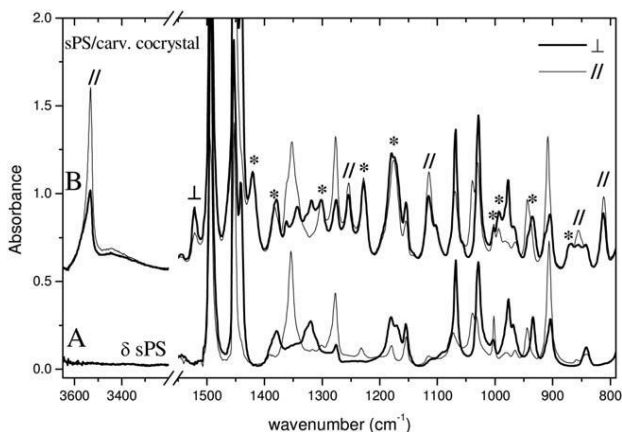


**Fig. 1.11** Polarized FTIR spectra, in the wavenumber ranges 3650–3200 and 1550–800  $\text{cm}^{-1}$ , taken with polarization plane parallel (thin lines) and perpendicular (thick lines) to the draw direction, for axially oriented s-PS films presenting different crystalline forms: (A) nanoporous  $\delta$ -form; (B)  $\delta$ -clathrate form with carvacrol (~10 wt %). Symbols (//) and ( $\perp$ ), label dichroic guest peaks, whose transition moment vectors are preferentially parallel and perpendicular to the stretching direction (and hence to the chain axis,  $c$ , of the co-crystalline phase), respectively. Symbol (\*) labels guest peaks, exhibiting poor linear dichroism.

The absorbance peaks of the  $s(2/1)2$  helical polymer chains,<sup>44-25</sup> like for example those at 1354 and 1277  $\text{cm}^{-1}$

[Fig. 1.11(A)], are highly dichroic and a high degree of axial orientation ( $f_{c,IR} \sim 0.95$ ) can be evaluated. The FTIR spectrum of the s-PS/carvacrol co-crystalline film [Fig. 1.11(B)], with a carvacrol content roughly equal to 10 wt %, shows dichroism also for the guest peaks labeled by (//) and ( $\perp$ ), that is, peaks that present higher sorption of light with polarization parallel and perpendicular with respect to the film stretching direction, respectively. As for the guest OH stretching band, it is worth noting that the broad band nearly centered at 3400  $\text{cm}^{-1}$  is not dichroic whereas the OH stretching peak of isolated carvacrol molecules at 3532  $\text{cm}^{-1}$  exhibits a high dichroism ( $R=A_{//}/A_{\perp}=2.3$ ). This clearly confirms the hypothesis that the isolated OH groups belong to molecules being isolated guests of axially oriented  $\delta$ -clathrate phases whereas the hydrogen-

bonded OH groups belong to molecules dissolved in the essentially unoriented amorphous phase.

The use of the O-H stretching region of FTIR spectra to discriminate between guest molecules of the crystalline phase and molecules dissolved in the amorphous phase, is shown here for the first time for nanoporous-crystalline polymers.

It is worth adding that preliminary analyses have shown that this method is applicable to many other substituted phenols, like for example, thymol (2-isopropyl-5-methylphenol) and methylparaben (Benzoic acid, 4-hydroxy-, methyl ester) as well as to alcohols like ethanol and menthol.

### **1.3.2 Partition of carvacrol molecules between amorphous and crystalline phases of $\delta$ -form films**

The carvacrol content in s-PS films and its partition between amorphous and nanoporous-crystalline  $\delta$  phases have been investigated, mainly by FTIR analyses. In particular, we show results relative to films exhibiting a partial filling of the crystalline cavities, as obtained by carvacrol sorption from diluted solutions, as well as to films exhibiting a complete filling of the crystalline cavities, as obtained by carvacrol sorption from concentrated solutions. The FTIR spectra in the wavenumber range 3650–3150  $\text{cm}^{-1}$  of a  $\delta$ -form s-PS film with a 5- $\mu\text{m}$  thickness, after equilibrium sorption (18 hours) from a 5 wt % carvacrol solution in acetone are compared in Figure 1.12, for different desorption times.

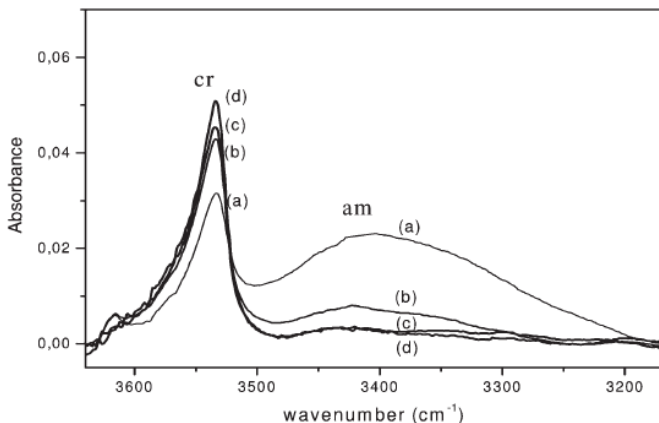


**Fig 1.12** FTIR transmission spectra in the wavenumber range 3650–3150  $\text{cm}^{-1}$  of a  $\delta$ -form s-PS film, after equilibrium sorption from a 5 wt % carvacrol solution in acetone, as collected at various desorption times: (a) 1 hour; (b) 24 hours; (c) 155 hours; (d) 395 hours.

The variation of the absorbances of the O-H stretching carvacrol peaks at  $3532\text{ cm}^{-1}$  (labeled as cr) and at  $3400\text{ cm}^{-1}$  (labeled as am), as normalized with respect to a s-PS reference peak ( $1601\text{ cm}^{-1}$ ), are compared in Figure 1.12; and they are associated with carvacrol molecules isolated guest of the crystalline phase and dissolved in the amorphous phase, respectively.

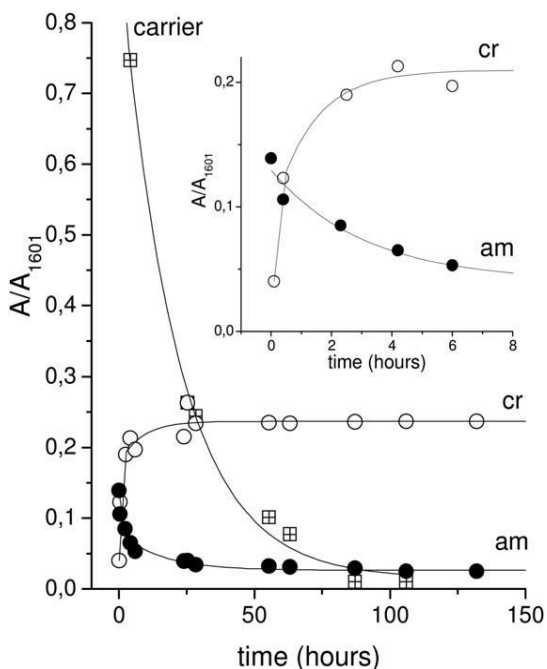


**Fig. 1.13** Absorbances, normalized with respect to the  $1601\text{ cm}^{-1}$  s-PS peak, of the carvacrol peaks at  $3532\text{ cm}^{-1}$  associated with the fraction hosted in the crystalline phase (cr) and at  $3400\text{ cm}^{-1}$  associated with the fraction dissolved in the amorphous phase (am) as well as of an intense solvent carrier peak (of acetone at  $1716\text{ cm}^{-1}$ ), versus desorption time at room temperature. The inset enlarges the observed behavior for the first few hours of desorption.

Figure 1.13 also shows the solvent carrier (acetone) desorption by the decrease of the absorbance of the intense carbonyl peak at  $1716\text{ cm}^{-1}$ . It is apparent that the complete desorption of the carrier molecules occurs at room temperature after nearly 90 hours.

For the first hours of desorption (inset in Fig. 1.13), a large increase in the absorbance of the peak associated with isolated carvacrol molecules (cr) and a corresponding decrease of the absorbance of the broad peak associated with aggregated carvacrol molecules (am) are clearly apparent.

After nearly 20 hours of desorption, both  $A(\text{cr})$  and  $A(\text{am})$  become constant and their ratio  $A(\text{cr})/A(\text{am})$  becomes nearly equal to 10. These data can be easily rationalized by assuming

that, with the carrier desorption, the crystalline cavities, initially occupied by the carrier molecules, are progressively filled by the carvacrol molecules, which mostly move from the amorphous toward the crystalline phase. After the preparation procedure described in Figure 1.13, the overall carvacrol content in the film, as determined by TGA measurements, is of 2.1 wt %.

The carvacrol desorption at 35 °C of a film, like that one of Figure 1.12(D) with most molecules being guest of the s-PS crystalline phase, based on the reduction of the absorbance of the 3532  $\text{cm}^{-1}$  FTIR peak, is shown in Figure 1.14.

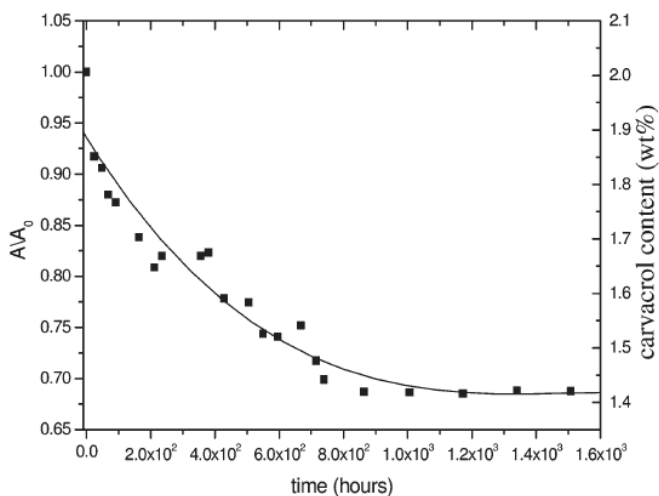


**Fig. 1.14** Carvacrol desorption at 35 °C from a s-PS film with a carvacrol content of 2.1 wt % with most molecules being guest of the s-PS crystalline phase.

A simple approximate calculation, based on the degree of crystallinity (35%) and on the styrene/cavity ratio of the nanoporous crystalline  $\delta$ -form (4/1) allows establishing that <15% of the crystalline cavities are filled by carvacrol molecules while the other crystalline cavities remain empty. This can be an advantage for packaging films, because a fraction of the crystalline cavities are used for natural antimicrobial release while the other crystalline cavities

remain active for removal of molecules (ethylene and carbon dioxide) generated by vegetables being detrimental for their preservation. The FTIR spectra of a s-PS  $\delta$ -form film (with a thickness of 62  $\mu\text{m}$  thick and exhibiting a//c// uniplanar orientation), after immersion in a 40 wt % carvacrol/chloroform solution for 6 hours are shown in Figure 1.15, for different desorption times (up to 104 hours). Differently from the case of sorption from diluted solutions (Fig. 1.13), continuous carvacrols desorption from both crystalline and amorphous phase is apparent.

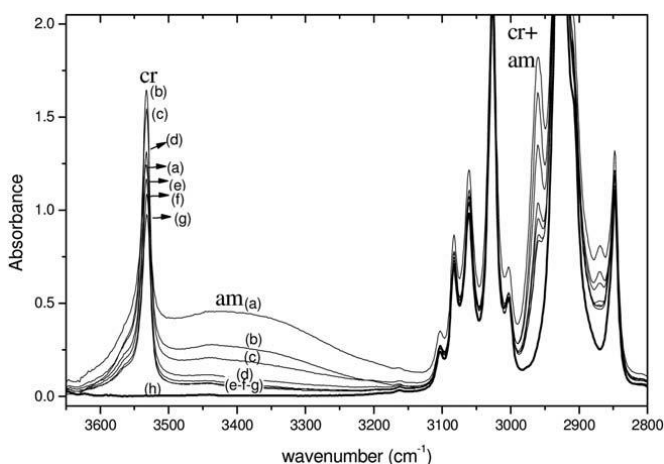


**Fig. 1.15** FTIR transmission spectra in the wavenumber range 3650–2800  $\text{cm}^{-1}$  of a s-PS/carvacrol co-crystalline film, with an initial carvacrol content close to 40 wt %, as collected at various desorption times (up to 104 hours): (a) t50; (b) 2 days; (c) 20 days; (d) 45 days; (e) 63 days; (f) 157 days; (g) 595 days. FTIR spectra s-PS films nanoporous  $\delta$ -form is also reported (h).

A quantitative evaluation of the guest desorption is shown in Figure 1.16, where the absorbance reduction for several vibrational peaks ( $A/A_0$ , where  $A_0$  is the peak absorbance in the spectrum of the freshly prepared co-crystalline film) are reported versus the desorption time.

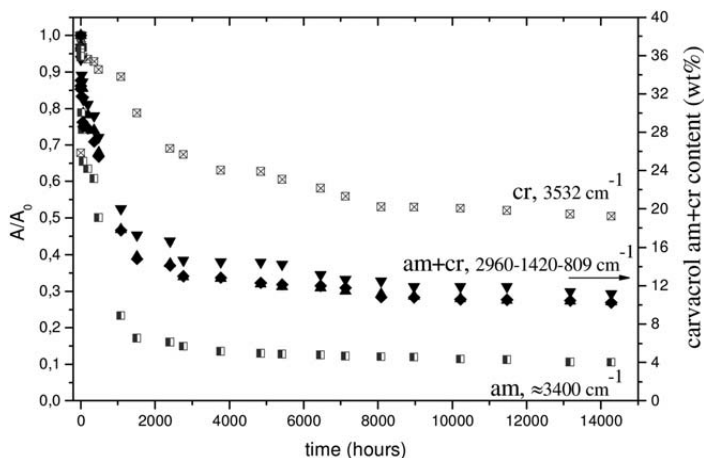


**Fig. 1.16** Reduced absorbance of carvacrol infrared bands of guest molecules only in the crystalline ( $3532\text{ cm}^{-1}$ ) or only in the amorphous ( $3400\text{ cm}^{-1}$ ) or in both phases ( $2960$ ,  $1420$ , and  $809\text{ cm}^{-1}$ ), versus desorption time. On the right scale, the overall carvacrol content in the film, as determined by thermogravimetry

It is clearly apparent that the reduction of the intensity of the broad band at  $3400\text{ cm}^{-1}$ , (labeled as am), due to carvacrol molecules in the polymer amorphous phase, is much faster than for the peak at  $3532\text{ cm}^{-1}$ , (labeled as cr), due to carvacrol molecules in the polymer co-crystalline phase. The reduction of the intensity with time of the  $2960$  (labeled as cr+am),  $1420$ , and  $809\text{ cm}^{-1}$  peaks, due to carvacrol molecules in both polymer phases, is intermediate.

Thermogravimetric scans indicate that the residual carvacrol content in the film is of  $10.5\text{ wt\%}$ . Based on this kind of TGA calibration, the overall carvacrol content in the film is shown in the right scale of Figure 1.16, indicating that the initial overall carvacrol content is close to  $40\text{ wt\%}$ . The ratio  $A(\text{cr})/A(\text{am})$ , after long-term desorption (more than  $104$  hours), is close to  $5$ , indicating that nearly  $80\%$  of carvacrol is in the crystalline phase.

The results of Figure 1.16 are also reported as classical Fick's plots in Figure 1.17, with  $(A_0 - A_t)/A_0$  versus the square root of desorption time (s) divided by film thickness (cm) ( $\sqrt{t/L}$ ).

For the sake of comparison, the desorption kinetics of carvacrol being dissolved in the amorphous phase of a  $\gamma$ -form film (maximum carvacrol uptake of nearly 20 wt %, FTIR spectrum in Fig. 1.10), is also shown in Figure 1.17.

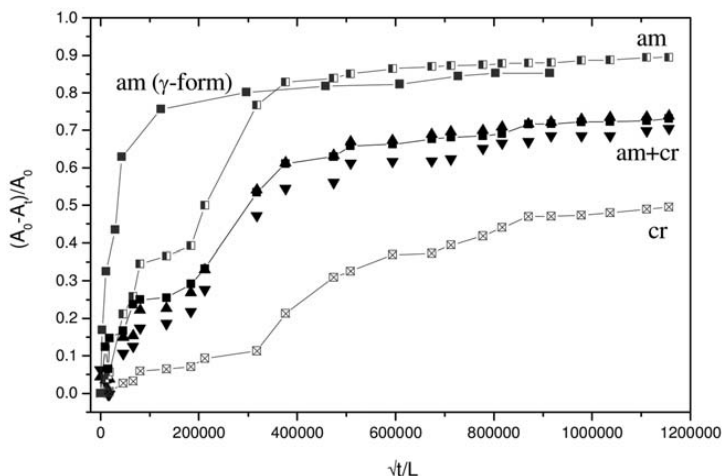


**Fig. 1.17** Carvacrol desorption isotherms, presenting the FTIR absorbance variations  $(A_0 - A_t)/A_0$  versus the square root of desorption time divided by film thickness  $(\sqrt{t}/L)$ . For comparison, the desorption of carvacrol from the amorphous phase of a  $\gamma$ -form s-PS film is also reported (black squares).

The curves of Figure 1.17 confirm that the slowest carvacrol desorption occurs from the crystalline phase ( $D_{\text{crys}} \sim 4.3 \times 10^{-14} \text{ cm}^2 \text{ s}^{-1}$ ) while a definitely faster desorption occurs from the amorphous phase ( $D_{\text{am},\delta} \sim 3.7 \times 10^{-12} \text{ cm}^2 \text{ s}^{-1}$ ).

The plot also indicates that a much faster desorption occurs from the amorphous phase of the semicrystalline film exhibiting the dense  $\lambda$  phase ( $D_{\text{am},\gamma} \sim 3.2 \times 10^{-11} \text{ cm}^2 \text{ s}^{-1}$ ). The slower carvacrol desorption from the amorphous phase of the  $\delta$ -form film is possibly due to the equilibrium between carvacrol molecules hosted by the amorphous and nanoporous-crystalline phases, which has been clearly shown by the data of Figure 1.13.

So a monoclinic  $\delta$ -clathrate form of syndiotactic polystyrene (s-PS) with carvacrol (a relevant natural phenolic antimicrobial) has been prepared and characterized by X-ray

diffraction. Very informative are Fourier transform infrared spectra, in particular their OH stretching region that shows a narrow peak and a broad band, corresponding to carvacrol molecules being isolated guest of the co-crystalline phase or dissolved in the amorphous phase, respectively. Analogous spectral features allow discriminating, for many different s-PS guests, between molecules being in crystalline or in amorphous phases. s-PS co-crystalline films with carvacrol molecules being prevailing (more than 90%) guest of the cocrystalline phase have been prepared, even for high carvacrol content (up to 10–11 wt %). The location of most antimicrobial molecules in the crystalline phase assures a decrease of desorption diffusivity of two to three orders and hence longterm antimicrobial release.

## 1.4 Conclusion

In section 1.2 we talk about the disordered nanoporous crystalline modification and we show that the guest removal from s-PS intercalates or triclinic  $\delta$ -clathrates can lead to disordered crystalline modifications, still exhibiting  $s(2/1)2$  helices. In particular, the X-ray diffraction pattern of the disordered crystalline modification is characterized, from  $2\theta_{\text{CuK}\alpha} < 12^\circ$ , by only a broad diffraction peak whose maximum is located in the  $2\theta_{\text{CuK}\alpha}$  range between  $8.7^\circ$  and  $9.8^\circ$ . The sorption of an organic pollutant (1,2-dichloroethane) from dilute solutions in water, for films presenting these disordered crystalline structures, has been compared with those of analogous films exhibiting the nanoporous  $\delta$  and the dense  $\gamma$  crystalline phases. The equilibrium DCE uptake from these films is roughly 60 % with respect to that of highly crystalline  $\delta$  form films and much higher than for  $\gamma$  form films. FTIR spectra have shown that, as previously established for the nanoporous  $\delta$  phase, for the disordered crystalline modification, the DCE molecules are absorbed essentially only as guest of a co-crystalline phase, rather than dissolved in the amorphous phase.

In summary, the reported results show that these disordered crystalline modifications of s-PS can be considered to be formed of small bundles of  $s(2/1)_2$  helices, which can recrystallize as a consequence of sorption of suitable guest molecules, eventually leading to  $\delta$  co-crystalline phases. This makes the sorption behavior of the disordered crystalline phase high and comparable to that of the nanoporous  $\delta$  phase, rather than being negligible as for the dense  $\gamma$  phase. As a consequence, these disordered crystalline forms of s-PS can be considered as nanoporous-crystalline.

Moreover in section 1.3 we study the co-crystalline phase of sPS including antimicrobial guest.

A co-crystalline form of s-PS with carvacrol (a relevant natural antimicrobial molecule) has been prepared by carvacrol sorption, from solutions in suitable carrier solvents, in films exhibiting the nanoporous-crystalline  $\delta$  phase. For s-PS/carcacrol co-crystalline samples, FTIR spectra are very informative and in particular their OH stretching region. In fact, this spectral region shows a narrow peak and a broad band corresponding to carvacrol molecules being isolated guest of the co-crystalline phase or simply dissolved in the corresponding amorphous phase, respectively. This interpretation has been confirmed by polarized FTIR spectra of axially oriented films. It is worth adding that this phenomenon, which allows discriminating between guest molecules being present in crystalline and amorphous phases, is shown here for the first time for polymeric co-crystalline phases and occurs for many other guests exhibiting hydroxy groups. FTIR analyses have allowed investigating the carvacrol content in s-PS films and its partition between amorphous and nanoporous-crystalline  $\delta$  phases. In particular, analyses of carvacrol sorption from diluted solutions (5 wt %) show that the crystalline cavities, initially occupied by carrier molecules, are progressively filled by carvacrol molecules moving from the amorphous phase. After carrier desorption for a guest content of nearly 2 wt %, more than 90% of the guest molecules are in the crystalline phase, which constitutes

<40 wt % of the film sample. For these films, <15% of the crystalline cavities is filled by carvacrol molecules while the other crystalline cavities remain empty. Analyses of carvacrol sorption from concentrated solutions (40 wt %) show that very large carvacrol uptake is possible (up to 40 wt %), occurring in both crystalline and amorphous phase. The analysis also shows that desorption from the amorphous phase is much faster than desorption from the crystalline phase. The apparent carvacrol diffusivity at room temperature from the co-crystalline phase is nearly  $10^2$  times lower than from the corresponding amorphous phase and nearly  $10^3$  times lower than from the amorphous phase of s-PS films exhibiting a dense crystalline phase ( $\gamma$  form). In summary, we have described the preparation of s-PS films with antimicrobial molecules, being prevalingly present as guest of the crystalline phase. This assures slow antimicrobial release and hence long-term antimicrobial properties. These s-PS films, mainly for low guest content (possibly <1 wt %) can be useful for packaging of fruits and vegetables, due to the combination of ethylene and carbon dioxide removal from the empty cavities of the  $\delta$  nanoporous crystalline phase and the slow release of a scented natural antimicrobial guest from the filled cavities of the same crystalline phase.

### ***Refernces***

1. Chatani, Y., Inagaki, Y., Shimane, Y., Ijitsu, T., Yukimori, H., Shikuma, H.: *Polymer* **1993**,*34*, 1620
2. Alburnia, A.R., D'Aniello, C., Guerra, G. *Cryst. Eng. Commun.* **2010**,*12*, 3942
3. Tarallo, O., Schiavone, M.M., Petraccone, V. *Eur. Polymer J.* **2010**, *46*, 456
- 4 . Tarallo, O., Petraccone, V., Daniel, C., Guerra, G. *Cryst. Eng. Commun.* **2009**,*11*, 2381
5. Tarallo, O., Petraccone, V., Alburnia, A.R., Daniel, C., Guerra, G. *Macromolecules* **2010**,*43*, 8549
6. Rastogi, S., Goossens, J.G.P., Lemstra, P.J. *Macromolecules* **1998**, *31*, 2983

7. Alburnia, A.R., Rizzo, P., Coppola, M., De Pascale, M., Guerra, G. *Polymer* , **2012**, *53*, 2727
8. Tarallo, O., Schiavone, M.M., Petraccone, V., Daniel, C., Rizzo, P., Guerra, G. *Macromolecules* **2010**, *43*, 1455
9. Alburnia, A.R., D’Aniello, C., Guerra, G. *Cryst. Eng. Commun.* **2010**, *12*, 3942
10. De Rosa, C., Rizzo, P., Ruiz de Ballesteros, O., Petraccone, B., Guerra, G. *Polymer* **1999**, *40*, 2103
11. Petraccone, V., Tarallo, O., Venditto, V., Guerra, G. **2003**, *8*, 6965
12. De Rosa, C., Guerra, G., Petraccone, V., Pirozzi, B. *Macromolecules* **1997**, *30*, 4147
13. Tarallo, O., Petraccone, V., Venditto, V., Guerra, G. *Polymer* **2006**, *47*, 2402
14. Gowd E. B., Shibayama N., Tashiro K., *Macromolecules* **2006**, *39*, 8412–8418
15. Rizzo P., Daniel C., De Girolamo Del Mauro A., Guerra G., *Chem. Mater.* **2007**, *19*, 3864
16. V. Petraccone, O. Ruiz de Ballesteros, O. Tarallo, P. Rizzo, G. Guerra, *Chem. Mater.* **2008**, *20*, 3663
17. Alburnia A. R., Minucci T., Guerra G., *J. Mater. Chem.* **2008**, *18*, 1046.
18. Annunziata L., Alburnia A. R., Venditto V., Guerra G., *Macromolecules* **2006**, *39*, 9166.
19. Rizzo P., Lamberti M., Alburnia A. R., Ruiz de Ballesteros O., Guerra G., *Macromolecules* **2002**, *35*, 5854
20. Alburnia A. R., Rizzo P., Guerra G., *Macromolecules* **2011**, *44*, 5671.
21. Milano G., Guerra G., Muller-Plathe F., *Chem. Mater.* **2002**, *14*, 2977.
22. Alburnia A. R., Rizzo P., Guerra G., *Polymer* **2013**, *54*, 1671
23. Loffredo, F., Pranzo, A., Venditto, V., Longo, P., Guerra, G. *Macromol. Chem. Phys.* **2003**, *204*, 859
24. Alburnia, A.R., Rizzo, P., Guerra, G., Torres, F.J., Civalleri, B., Zicovich-Wilson, C.M. *Macromolecules* **2007** *40*, 3895
25. Torres, F.J., Civalleri, B., Meyer, A., Musto, P., Alburnia, A.R., Rizzo, P., Guerra, G. *J. Phys. Chem. B* **2009**, *113*, 5059
26. Alburnia, A. R., Bianchi, R., Di Maio, L., Galimberti, M., Guerra, G., Pantani, R., Senatore, S. Disordered nanoporous crystalline form of syndiotactic polystyrene, production method and

- articles; from PCT Int. Appl. (2012), WO 2012089805 A1 20120705
27. Jeen, S.W., Jambor, J.L., Blowes, D.W., Gillham, R.W.: *Environ. Sci. Tech.* **2007**, 41, 1989
28. Di Molfetta, A., Sethi, R. *Environ. Geol* **2006**, 50, 361
29. Guerra, G., Manfredi, C., Musto, P., Tavone, S. *Macromolecules* **1998**, 31, 1329
30. Musto, P., Manzari, M., Guerra, G. *Macromolecules* **1999** 32, 2770
31. Alburnia, A.R., Di Masi, S., Rizzo, P., Milano, G., Musto, P., Guerra, G. *Macromolecules* **2003**, 36, 8695
32. Musto, P., Rizzo, P., Guerra, G. *Macromolecules* **2005**, 38, 6079
33. Manfredi, C., De Rosa, C., Guerra, G., Rapacciuolo, M., Auriemma, F., Corradini, P. *Macromol. Chem. Phys.* **1995**, 196, 2795
34. Gowd, E.B., Tashiro, K., Ramesh, C. *Prog. Polym. Sci.* **2009**, 34, 280
35. Benavente-Garcia O., Castillo J., Marin F. R., Ortuno A., Del Rio J.A., *J. Agric. Food* **1997**, 45, 4505.
36. Persico P., Ambrogi V., Carfagna C., Cerruti P., Ferrocino I., Mauriello G., *Polym. Eng. Sci.* **2009**, 49, 1447.
37. Griffin S. G., Wyllie S. G., Markham J. L., Leach D. N., *Flavour Fragr. J.* **1999**, 14, 322
38. Muriel-Galet V., Cerisuelo J. R., Lopez-Carballo G., Aucejo S., Gavara R., Hernandez-Munoz P., *Food Control* **2013**, 30, 137.
39. Ben Arfa A., Preziosi-Belloy L., Chalier P., Gontard N., *J. Agric. Food Chem.* **2007**, 55, 2155
40. J. Pasqual Cerisuelo, J. Alonso, S. Aucejo, R. Gavara, P. Hernandez-Munoz, *J. Membr. Sci.* **2012**, 423, 247
41. Alburnia A. R., Rizzo P., Tarallo O., Petraccone V., Guerra G., *Macromolecules* **2008**, 41, 8632
42. Immirzi A., de Candia F., Iannelli P., Zambelli A., Vittoria V., *Makromol. Chem. Rapid Commun.* **1988**, 9, 761
43. Rizzo P., Alburnia A. R., Guerra G., *Polymer* **2005**, 46, 9549.
44. Alburnia A. R., Musto P., Guerra G., *Polymer* **2006**, 47, 234.

## Chapter 2

### Orientations in polymeric films

#### 2.1 Introduction

Orientation is a phenomenon of great technical and theoretical importance nearly for all materials and many examples could be reported to illustrate how the orientation affects the properties of materials. For polymeric materials, the effects of orientation on properties are more relevant: for instance, the extent to which is possible to increase stiffness and strength find no parallel with other materials.<sup>1</sup>

Orientation is particularly relevant for functional polymeric materials, mainly when the functionality is associated with crystalline phases, as for conductive<sup>2</sup> or ferroelectric<sup>3</sup> polymers. In this respect, several studies have shown that the kind and degree of orientation can be relevant for properties of co-crystalline polymer phases, whose functionality is due to 3-D ordered active guest molecules (fluorescent,<sup>4</sup> photo-reactive,<sup>5</sup> magnetic,<sup>6</sup> ferroelectric<sup>7</sup> or chiral-optical<sup>8</sup>).

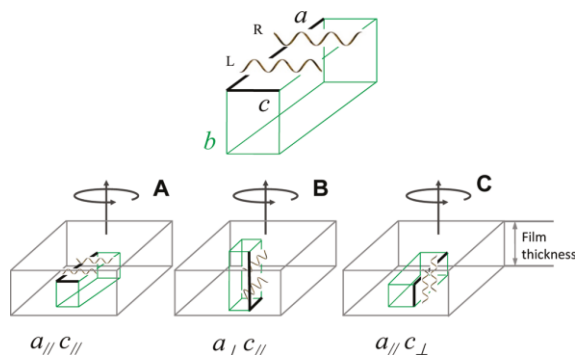
Polymer crystals, although generally much smaller than inorganic and organic crystals, present the advantage of easy orientation, also at macroscopic scale. In fact, for all semicrystalline polymers it is easy to get *axial* orientation of the crystalline phases, by imposing the alignment of the polymer chain axes (generally assumed coincident with the crystallographic *c* axis) parallel to a stretching direction. For biaxial stretching, beside the slip direction also a slip plane tends to be parallel to the film plane, thus leading to *uniplanar*<sup>9a-g</sup> or *uniplanar-axial*<sup>9h</sup> orientations. In polymers with no specific intermolecular interactions (such as hydrocarbon polymers), molecular shape and packing density play major roles in determining the slip planes. For instance, for poly(ethylene-terephthalate) (PET) the slip plane is parallel to the phenyl rings,<sup>9a-c</sup> while, for the monoclinic  $\alpha$  form of isotactic polypropylene, the primary slip plane is the highest density (0k0) plane.<sup>9d-e</sup>

Uniaxial stretching and biaxial stretching are industrially mechanical processes utilized to obtain films with good mechanical properties. Generally, the molecular chains are oriented parallel to the direction of the applied stress when molecules are exposed to a stress field and stretching is employed to improve the mechanical strength and the transparency of polymers.

The biaxial process is widely utilized because excellent balances of properties to achieve strength and stability in all directions are necessary that the orientation occurs in both longitudinal and transverse.

Recently it has been shown that polymers able to form co-crystalline structure (i.e. host polymeric crystalline structure include a low-molecular-mass guest) can develop crystalline phase orientations; for instance, as for co-crystalline s-PS films, uniplanar orientations can be achieved not only by usual thermo mechanical procedures but also by simple procedures involving co-crystallization in the presence of suitable guest molecules (solution crystallization,<sup>10</sup> solvent-induced crystallization in amorphous samples<sup>11</sup> or solvent-induced recrystallizations of  $\gamma$  and  $\alpha$  unoriented samples<sup>12</sup>). Moreover, for cocrystalline s-PS films, it has been observed the unprecedented formation of three different kinds<sup>11c, 13</sup> of uniplanar orientations.

The three uniplanar orientations of s-PS co-crystalline films correspond to the three simplest orientations of the high planar-density  $ac$  layers (i.e., layers of close-packed alternated enantiomorphous s-PS helices that characterize most s-PS co-crystalline phases as well as the nanoporous  $\delta$  phase) with respect to the film plane.<sup>14</sup> As shown in scheme 2.1 these three uniplanar orientations have been named  $a//c//$ ,  $a//c\perp$ , and  $a\perp c//$ , indicating crystalline phase orientations presenting the  $a$  and  $c$  (chain) axes parallel ( $//$ ) or perpendicular ( $\perp$ ) to the film plane.<sup>14</sup>



**Scheme 2. 1.** Schematic Presentation of the Three Uniplanar Orientations of s-PS CocrySTALLINE Films, Corresponding to the Three Simplest Orientations of the High-Planar-Density ac Layers with Respect to the Film Plane

The structural feature determining three different kinds of uniplanar orientations is the layer of close-packed alternated enantiomorphous helices<sup>13</sup> that characterizes most s-PS cocrySTALLINE phases ( $\delta$  clathrates<sup>15</sup> and  $\delta$  intercalates<sup>16</sup>). These uniplanar orientations of s-PS cocrySTALLINE phases are also maintained as a consequence of guest-exchange procedures<sup>17</sup> but also as a consequence of procedures leading to different crystalline phases.<sup>10,11c,12</sup>

Considering the knowledge and the procedures acquired by studying the co-crystal structures and orientations of s-PS, in this research we have focused the attention on polymers able to form co-crystalline phase. The main objective is to determine if co-crystalline phase of polymers can develop orientation. In particular, we have been considered in this work: poly (2,6-dimethyl-1,4-phenylene)oxide (PPO), described in section 2.2 , poly(L-lactide) (PLLA) described in section 2.3. Moreover, the influence of orientation on shrinkage, during crystallization process for sPS films will be described in section 2.4.

## References

1. a) Ward I. M. In *Structured and properties of Oriented Polymers*, Chapman & Hall, London, **1975**; Chapter 1, p. 1. b) Simmons, A.H.; Michal, C.A.; Jelinski, L.W. *Science* **1991**, *271*,84-
2. a) Frommer, J. E. ; Chance R. R. In *Encyclopedia of Polymer Science and Engineering* 2nd ed.; Wiley-Interscience: New York, **1986**; Vol. 5 p. 462.
- 3.a)Prasad P. N.; Williams D. J. In *Introduction to nonlinear optical effects in molecules and polymers*, Wiley & Sons, New York, **1990**; Chapter 7, p.132. b) Hu, Z.; Tian, M.; Nysten, B.; Jonas, A.M. *Nature Mater.* **2009**, *8*, 62.
- 4.a) Venditto, V.; Milano, G.; De Girolamo Del Mauro, A.; Guerra, G.; Mochizuki, J.; Itagaki, H. *Macromolecules* **2005**, *38*, 3696. b) Uda, Y.; Kaneko, F.; Tanigaki, N.; Kawaguchi, T. *Adv. Mater.* **2005**, *17*, 1846. c) De Girolamo Del Mauro, A.; Carotenuto, M.; Venditto, V.; Petraccone, V.; Scoponi, M.; Guerra, G. *Chem. Mater.* **2007**, *19*, 6041.d) Itagaki, H.; Sago, T.; Uematsu, M.; Yoshioka, G.; Correa, A.; Venditto, V.; Guerra, G. *Macromolecules* **2008**, *41*, 9156.
5. a) Stegmaier, P.; De Girolamo Del Mauro, A.; Venditto, V.; Guerra, G. *Adv.Mater.* **2005**, *17*, 1166. b) D'Aniello, C.; Musto, P.; Venditto, V.; Guerra G. *J. Mater. Chem.* **2007**, *17*, 531. c) Alburnia, A.R.; Rizzo, P.; Coppola, M.; De Pascale, M.; Guerra, G. *Polymer* **2012**, *53*, 2727.
6. a) Kaneko, F.; Uda , Y.; Kajiwara, A.; Tanigaki, N. *Macromol.Rapid Commun.* **2006**, *27*, 1643. b) Alburnia, A.R.; D'Aniello, C.; Guerra, G.; Gatteschi, D.; Mannini, M.; Sorace, L. *Chem. Mater.* **2009**, *21*, 4750. c) Alburnia, A.R.; D'Aniello, C.; Guerra, G. *Cryst.Eng.Comm* **2010**, *12*, 3942
7. a) Daniel, C.; Galdi, N.; Montefusco, T.; Guerra, G. *Chem.Mater.* **2007**, *19*, 3302. b) Tarallo, O.; Petraccone, V.; Daniel, C.; Guerra, G. *CrystEngComm* **2009**, *11*, 2381. c) Tarallo, O.; Schiavone, M.M.; Petraccone, V.; Daniel, C.; Rizzo, P.; Guerra, G. *Macromolecules* **2010**, *43*, 1455. d) Daniel, C.; Rufolo, C.; Bobba, F.; Scarfato, A.; Cucolo, A.; Guerra, G. *J.Mater.Chem.* **2011**, *21*, 19074.
8. a) Buono A., Immediata I., Rizzo P., G. Guerra, Detection and memory of nonracemic molecules by a racemic host polymer film, *J. Am. Chem. Soc.* **2007**,*129* 10992.
9. a) Heffelfinger C. J.; R. L. Burton R. L. *J. Polym. Sci.* 1960, *47*, 289. b) Werner, E. ; Janocha, S. ; Hopper, M.J. ; *Mackenzie*

*Encyclopedia of Polymer Science and Engineering* 2nd ed.; Wiley-Interscience: New York, **1986**; Vol. 12 p. 193. c) Gohil, R.M. *J.Appl.Polym.Sci.* **1993**, *48*, 1649. d) Uejo, H. Hoshino, S. *J.Appl.Polym.Sci.* **1970**, *14*, 317. e) Rizzo, P.; Venditto, V.; Guerra, G.; Vecchione, A. *Macromol.Symp.* **2002**, *185*, 53. f) P. Rizzo, A. R. Alburnia, G. Milano, V. Venditto, G. Guerra, G. Mensitieri, L. Di Maio *Macromolecular Symposia* 2002, 185, 65-75. g) P. Rizzo, A. R. Alburnia *Macromolecular Chemistry and Physics* 2011, 212,1419-26. h) P. Rizzo, A. R. Alburnia, G. Guerra *Macromolecules* 2011, 44, 5671-81.

**10.** a) Rizzo, P.; Lamberti, M.; Alburnia, A. R.; Ruiz de Ballesteros, O.; Guerra, G. *Macromolecules* 2002, 35, 5854. b) Rizzo, P.; Costabile, A.; Guerra, G. *Macromolecules* 2004, 37, 3071.

**11.** a) Rizzo, P.; Alburnia, A. R.; Milano, G.; Venditto, V.; Guerra, G.; Mensitieri, G.; Di Maio, L. *Macromol. Symp.* 2002, 185, 65. b) Rizzo, P.; Della Guardia, S.; Guerra, G. *Macromolecules* 2004, 37, 8043. c) Rizzo, P.; Spatola, A.; De Girolamo Del Mauro, A.; Guerra, G. *Macromolecules* 2005, 38, 10089.

**12.** a) Alburnia, A. R.; Annunziata, L.; Guerra, G. *Macromolecules* 2008, 41, 2683–2688. b) Alburnia, A. R.; Rizzo, P.; Guerra, G. *Chem. Mater.* **2009**, *21*, 3370.

**13.** Alburnia, A. R.; Rizzo, P.; Tarallo, O.; Petraccone, V.; Guerra, G. *Macromolecules* **2008**, *41*, 8632.

**14.** Alburnia, A. R.; Rizzo, P.; Guerra, G. *Chem. Mater.* **2009**, *21*, 3370

**15.** a) Chatani, Y.; Shimane, Y.; Inagaki, T.; Iijtsu, T.; Yukimori, T.; Shikuma, H. *Polymer* **1993**, *34*, 1620. b) Chatani, Y.; Inagaki, T.; Shimane, Y.; Shikuma, H. *Polymer* **1993**, *34*, 4841. c) De Rosa, C.; Rizzo, P.; Ruiz de Ballesteros, O.; Petraccone, V.; Guerra, G. *Polymer* **1999**, *40*, 2103. d) Tarallo, O.; Petraccone, V. *Macromol. Chem. Phys.* **2005**, 206, 672

**16.** a) Petraccone, V.; Tarallo, O.; Venditto, V.; Guerra, G. *Macromolecules* **2005**, 38, 6965. b) Tarallo, O.; Petraccone, V.; Venditto, V.; Guerra, G. *Polymer* **2006**, *47*, 2402. c) Malik, S.; Rochas, C.; Guenet, J. M. *Macromolecules* **2006**, 39, 1000.

**17.** a) Yoshioka, A.; Tashiro, K. *Macromolecules* **2003**, 36, 3593. b) Uda, Y.; Kaneko, F.; Kawaguchi, T. *Macromol. Rapid Commun.* **2004**, 25, 1900. c) Uda, Y.; Kaneko, F.; Kawaguchi, T. *Macromolecules* **2005**, 38, 3320.

## 2.2 Poly(2,6-dimethyl-1,4-phenylene ether) (PPO)

Poly(2,6-dimethyl-1,4-phenylene ether) (PPO) is an industrially relevant polymer with excellent thermal and mechanical properties. It has high strength, chemical resistance, stiffness, high heat distortion temperature and fracture toughness.<sup>1,2</sup>

However, it is rarely used in its pure form due to its brittleness and poor processability. It is mainly used as blend with polystyrene<sup>3</sup>. Major applications of PPO are for automotive, business machine, and electrical industries.

Moreover PPO is an attractive material for the preparation of membranes due to its resistant against a number of chemical agents, including aqueous solutions of strong acids and bases. The main interest is in the application of unmodified and modified PPO membranes to gas separations<sup>4-7</sup> to reverse osmosis,<sup>8</sup> and in a lesser extent to vapour permeation<sup>9</sup>

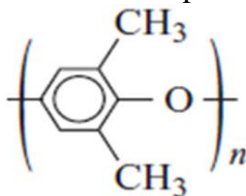


Fig. 2.2.1 Chemical structure of PPO repeating unit

### 2.2.1 Uniplanar orientations by $\alpha$ -pinene-induced cocrystallization on amorphous films.

Many co-crystalline forms of PPO with low-molecular-mass guest molecules have been described.<sup>10</sup> Particularly large crystallites are obtained for the structurally similar co-crystalline forms with  $\alpha$ -pinene,<sup>10c-e</sup> decahydronaphthalene (decalin)<sup>10d</sup> or 1,2,3,4 tetrahydronaphthalene (tetralin)<sup>10d</sup>

The X-ray diffraction pattern (Cu K $\alpha$ ) of a PPO/ $\alpha$ -pinene cocrystalline powder, prepared from the corresponding gel after  $\alpha$ -pinene desorption at room temperature, is shown in Figure 2.2.2 A and the main peaks have been labeled according to the known tetragonal unit cell.<sup>10c,e</sup> The X-ray diffraction patterns, also collected by an automatic powder

diffractometer, of amorphous PPO films after crystallization by exposure to  $\alpha$ -pinene vapor at different temperatures are shown in Figures 2.2.2 B-G. The degree of crystallinity of the oriented films of Figure 2.2.2 has been evaluated by the X-ray diffraction patterns of the corresponding powders. The films crystallized in the temperature range 130–160 °C present a higher crystallinity similar to that of the powder obtained by gel drying (Figure 2.2.2 A, in the range 50–55%) while films crystallized at 110 and 120 °C present crystallinity of 20% and 30%, respectively.<sup>11</sup>

For all these patterns, the diffraction peaks are those observed for the unoriented PPO/ $\alpha$ -pinene cocrystalline powder, although their relative intensity are heavily changed and markedly dependent on the temperature of guest-vapor treatment.<sup>11</sup>

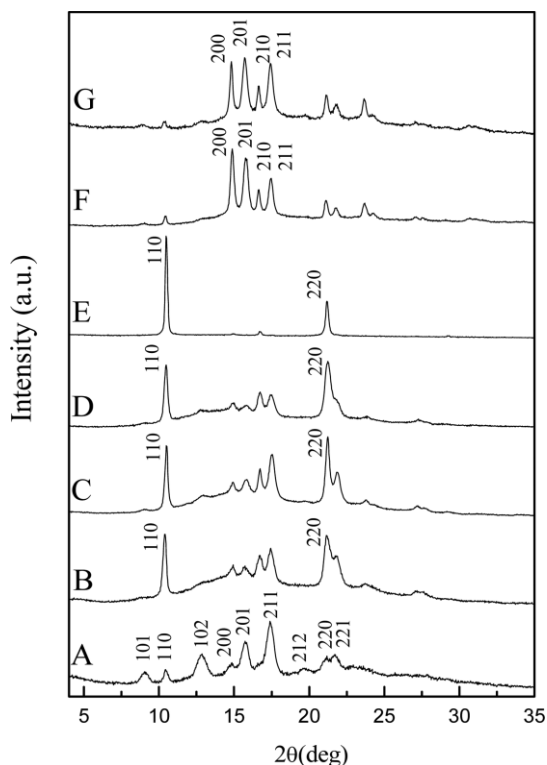


**Fig 2.2.2** X-ray diffraction, as collected by an automatic powder diffractometer, of PPO/ $\alpha$ -pinene cocrystalline samples: (A) powder; (B–G) amorphous films exposed to  $\alpha$ -pinene vapor at different temperatures: (B) 110 °C; (C) 120 °C; (D) 130 °C; (E) 140 °C; (F) 150 °C; (G) 160 °C. Close to the main diffraction peaks, the Miller indexes are indicated.

In particular, X-ray diffraction patterns of PPO/ $\alpha$ -pinene cocrystalline films obtained by vapor treatments in the temperature ranges 100–140 °C show very intense 110 and 220 reflections (Figure 2.2.2 B–E) while films treated in the temperature range 150–160 °C present an intense 200 reflection (Figure 2.2.2 F,G), which is weak for unoriented samples (Figure 2.2.2 A).

These results suggest that most crystallites in the films of Figure 2.2.2 B–E present their (110) crystal planes preferentially parallel to the film plane and most crystallites in the films of Figures 2.2.2 F,G present their (200) crystal

planes preferentially parallel to the film plane. A better understanding of the crystalline phase orientation in these films, can be achieved by X-ray diffraction patterns taken with beam perpendicular (THROUGH) or parallel (EDGE) to the film plane and collected on a photographic cylindrical camera. The THROUGH patterns of PPO/ $\alpha$ -pinene cocrystalline films of Figure 2.2.2 B–G, show only Debye rings, indicating the absence of axial orientation. The EDGE patterns of the films of Figure 2.2.2, parts E and F, reported in Figure 2.2.3, parts A and B, respectively, show the presence of arcs rather than of Debye rings, clearly indicating the presence of two different kinds of uniplanar orientations.

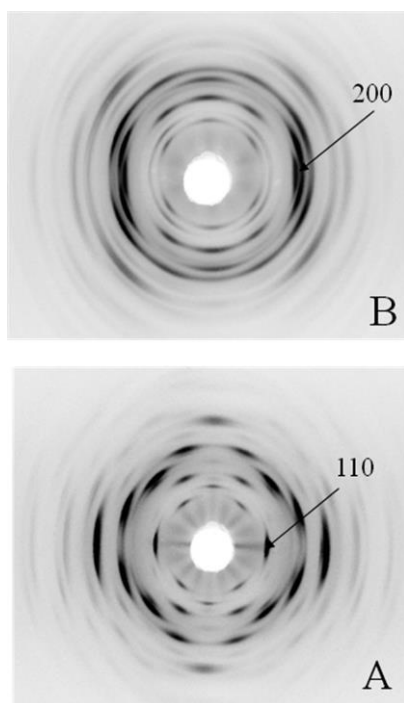


**Fig. 2.2.3.** Photographic X-ray diffraction patterns, obtained with X-ray beam parallel to the film plane (EDGE), of amorphous films crystallized by exposure to  $\alpha$ -pinene vapor, whose patterns as collected by an automatic powder diffractometer are shown in Figure 2, parts E (A) and F (B). The Miller indexes of the most intense equatorial peaks are indicated.

The relative intensities of the reflections, as collected by THROUGH and EDGE patterns, of the PPO/ $\alpha$ -pinene cocrystalline films of Figure 2.2.2, parts E and F, are reported in Table 2.2.1 (columns 4–5 and 8–9, respectively) and compared

with those of the corresponding cocrystalline powder of Figure 2.2.2A (column 3). In particular, in columns 6 and 10 of Table 1, the azimuthal angles ( $\chi_{obs}$ ) of maximum intensity observed for the different reflections in the X-ray EDGE patterns of Figure 2.2.3, parts A and B, have been compared with those calculated ( $\chi_{calc}$ ), columns 7 and 11, in the assumption of complete parallelism of the (110) and of the (200) planes with respect to the film plane. The good agreement between  $\chi_{obs}$  and  $\chi_{calc}$  clearly indicates the occurrence of 110 or of 200 uniplanar orientations for the PPO/ $\alpha$ -pinene cocrystalline films of Figure 2.2.3, parts A and B, respectively.

This information can be also obtained by the simpler consideration that the EDGE diffraction patterns of Figure 2.2.3, parts A and B, show, on their equator, intense 110 and 200 reflections, respectively, which almost disappear in the corresponding THROUGH patterns.

**Table 2.2.1.** Comparison between Relative Intensities of the Reflections of the PPO/ $\alpha$ -Pinene Co-Crystalline Form Observed in Xray Diffraction Patterns of a Powder and of Amorphous PPO Films Crystallized by  $\alpha$ -Pinene Sorption

| hkl           | powder          |           | film crystallized by guest sorption (110) uniplanar orientation |         |           |      | film crystallized by guest sorption (200) uniplanar orientation |                     |           |         |           |      |                    |                     |
|---------------|-----------------|-----------|---|---------|-----------|------|---|---------------------|-----------|---------|-----------|------|--------------------|---------------------|
|               | $2\theta_{obs}$ | $I_{obs}$ | $I_{obs}$   | THROUGH | $I_{obs}$ | EDGE | $\chi_{obs}$ (deg)  | $\chi_{calc}$ (deg) | $I_{obs}$ | THROUGH | $I_{obs}$ | EDGE | $\chi_{obs}$ (deg) | $\chi_{calc}$ (deg) |
| 101           | 9.0             | m         | m   | mw      | ms        |      | 53  | 54                  | m         | m       | ms        |      | 34                 | 35                  |
| 011           |                 |           |   |         |           |      |   |                     |           |         |           |      | 90                 | 90                  |
| 110           | 10.4            | m         | w   | w       | vs        |      | 0   | 0                   | vw        | m       |           |      | 43                 | 45                  |
| 1 $\bar{1}$ 0 |                 |           |   |         | ms        |      | 90  | 90                  |           |         |           |      |                    |                     |
| 111           | 11.8            | w         | —   | —       | vw        |      | 28  | 26                  | —         | w       |           |      | 53                 | 51                  |
| 1 $\bar{1}$ 1 |                 |           |   |         | vw        |      | 90  | 90                  |           |         |           |      |                    |                     |
| 102           | 12.8            | s         | s   | s       | s         |      | 64  | 66                  | vs        | s       |           |      | 54                 | 54                  |
|               |                 |           |   |         |           |      |   |                     |           | s       |           |      | 90                 | 90                  |
| 200           | 14.8            | w         | w   | w       | m         |      | 43  | 45                  | w         | ms      |           |      | 0                  | 0                   |
| 201           | 15.8            | s         | w   | w       | vs        |      | 44  | 48                  | s         | vs      |           |      | 21                 | 19                  |
|               |                 |           |   |         |           |      |   |                     |           | m       |           |      | 90                 | 90                  |
| 210           | 16.7            | w         | w   | vs      | vs        |      | 22  | 18                  | —         | w       |           |      | 25                 | 27                  |
| 2 $\bar{1}$ 0 |                 |           |   | w       | w         |      | 70  | 71                  |           |         |           |      |                    |                     |
| 211           | 17.4            | vs        | s   | vs      | vs        |      | 22  | 24                  | s         | vs      |           |      | 28                 | 31                  |
| 2 $\bar{1}$ 1 |                 |           |   | vs      | vs        |      | 70  | 72                  |           | m       |           |      | 63                 | 65                  |
| 212           | 19.6            | w         | w   | mw      | mw        |      | 35  | 36                  | —         | mw      |           |      | 43                 | 41                  |
| 2 $\bar{1}$ 2 |                 |           |   | w       | w         |      | 73  | 74                  |           |         |           |      |                    |                     |
| 220           | 21.2            | m         | vs  | vs      | vs        |      | 0   | 0                   | mw        | m       |           |      | 45                 | 45                  |
| 2 $\bar{2}$ 0 |                 |           | s   | s       | s         |      | 90  | 90                  |           |         |           |      |                    |                     |
| 221           | 21.7            | m         | m   | vs      | vs        |      | 8   | 13                  | w         | m       |           |      | 47                 | 47                  |
| 2 $\bar{2}$ 1 |                 |           |   | s       | s         |      | 90  | 90                  |           |         |           |      |                    |                     |
| 301           | 23              |           | w   | w       | w         |      | 43  | 46                  |           | m       |           |      | 13                 | 18                  |
| 310           | 23.6            |           | w   | w       | w         |      | 24  | 26                  |           |         |           |      |                    |                     |
| 3 $\bar{1}$ 0 |                 |           | vw  | vw      | vw        |      | 65  | 63                  |           |         |           |      |                    |                     |

Quantitative evaluations of the degree of uniplanar orientation can be obtained on the basis of the EDGE patterns (like those of Figure 2.2.3), by using the method described in the Experimental Section (chapter 5 section 5.2.1). The maximum degrees of orientation that have been achieved for PPO/ $\alpha$ -pinene cocrystalline films, for 110 and 200 uniplanar orientations, are  $f_{110} = 0.9$  and  $f_{200} = 0.75$ , respectively.

It is worth adding that the kind and the degree of uniplanar orientation is determined by initial cocrystallization conditions and is not altered by subsequent thermal annealing procedures.

These high degrees of uniplanar orientation, simply generated by guest-induced cocrystallization without any mechanical process, are quantitatively similar to those obtained for s-PS cocrystalline films.<sup>12,13</sup> Hence, this phenomenon is observed for polymers able to form cocrystalline phases while, to our knowledge, it has never been observed for usual polymer crystalline phases.

### **2.2.2 Uniplanar orientations by decalin- and tetralin-induced cocrystallization of amorphous films.**

The X ray diffraction patterns PPO/decalin or PPO/tetralin cocrystalline powders (Figure 2.2.4, parts A and A', respectively) are very similar to those of the PPO/ $\alpha$ -pinene cocrystalline powder of Figure 2.2.2 A.<sup>11</sup>

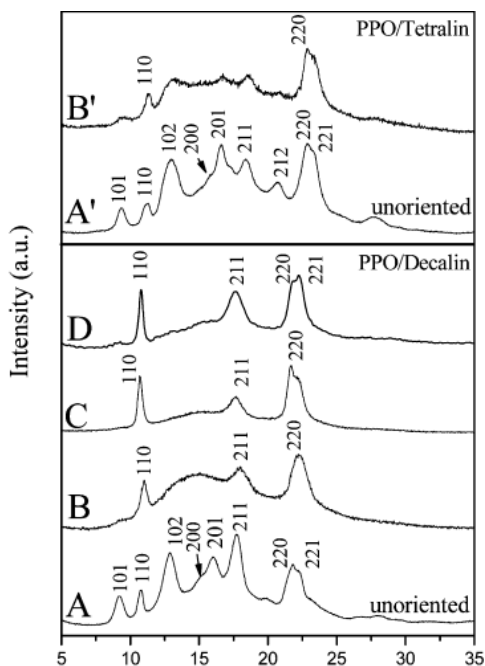


**Fig 2.2.4.** X-ray diffraction patterns, as collected by an automatic powder diffractometer, of PPO/decalin (A–D) and PPO/tetralin (A’–B’) cocrystalline samples: (A, A’) powders; (B–D) amorphous films exposed to decalin vapor for 24 h at 80 °C (B), 100 °C (C) and 150 °C (D); (B’) amorphous film immersed in pure tetralin at room temperature for 1 h. Close to the main diffraction peaks, the Miller indexes are indicated.

As a consequence, the reflections have been indexed by assuming analogous tetragonal crystalline structures with  $a = b = 1.17$  nm and  $c = 1.71$  nm for the cocrystalline form of PPO with decalin and  $a = b = 1.12$  nm and  $c = 1.71$  nm for the cocrystalline form of PPO with tetralin. The X-ray diffraction patterns (collected by an automatic powder diffractometer) of amorphous PPO films, as crystallized by exposure to decalin vapor at 80 °C (B), at 100 °C (C), or at 150 °C (D) or by immersion in liquid tetralin at room temperature (B’), are also shown in Figures 2.2.4

For these patterns, the diffraction peaks are those observed for the unoriented PPO/decalin or PPO/tetralin cocrystalline powders (Figure 2.2.4, parts A and A’) but their relative

intensities are heavily changed, clearly indicating the occurrence of uniplanar orientations with (110) planes preferentially parallel to the film plane. Differently from PPO/ $\alpha$ -pinene cocrystalline films (Figure 2.2.2), for all the examined crystallization conditions, only the 110 uniplanar orientation is observed.<sup>11</sup>

### 2.2.3 Guest exchange in PPO cocrystalline films with two different uniplanar orientations.

The relevance of crystalline phase orientations in polymer films is also related to their possible stability as a consequence of crystal phase transitions. The two different kinds of uniplanar orientations, as obtained by  $\alpha$ -pinene induced cocrystallization from amorphous PPO, can be fully maintained as a consequence of guest exchange procedures.

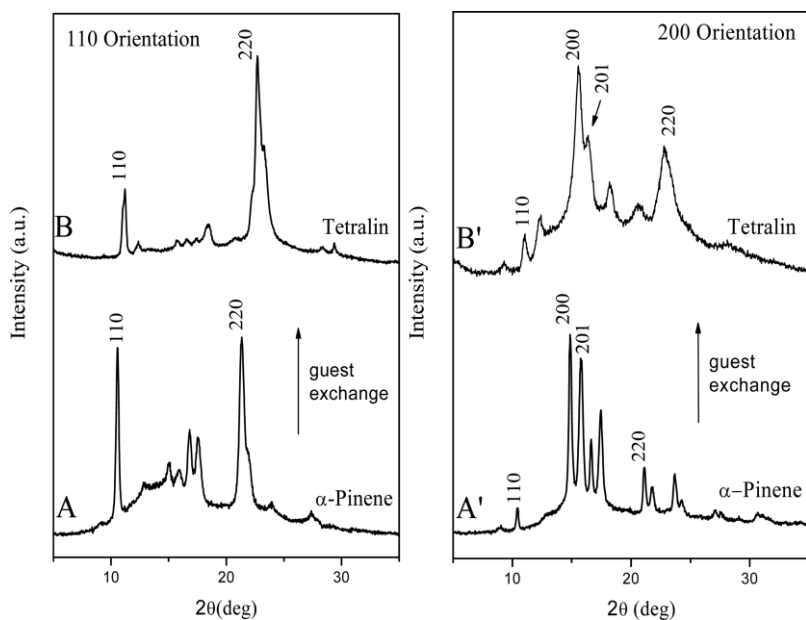


**Fig. 2.2.5.** X-ray diffraction patterns of PPO films: (A, A') exhibiting two different uniplanar orientations of the cocrystalline phase with  $\alpha$ -pinene, 110(A) or 200 (A'); (B, B') as obtained by  $\alpha$ -pinene exchange with tetralin (retention of uniplanar orientations).

This is shown, for instance, for films exhibiting large PPO/ $\alpha$ -pinene crystallites with high degree of 110 (A) and 200 (A') uniplanar orientations, whose X-ray diffraction patterns are shown in Figure 2.2.5, parts A and A', respectively. The X-ray diffraction patterns of these cocrystalline films after exposure to tetralin vapor for 25 min at 100 °C and complete  $\alpha$ -pinene replacement are shown in Figure 2.2.5, parts B and B', respectively. The patterns of Figure 2.2.5 indicate the formation of the PPO/ tetralin cocrystalline phases, as shown for instance by the shift of the 110 and 200 peaks from  $2\theta_{\text{CuK}\alpha} = 10.5$  and  $2\theta_{\text{CuK}\alpha} = 14.8$  up to  $2\theta_{\text{CuK}\alpha} = 11.2$  and  $2\theta_{\text{CuK}\alpha} = 15.8$ , respectively. The (110) and (220) diffraction peaks, which are the most intense peaks of the starting PPO/ $\alpha$ -pinene cocrystalline film (Figure 2.2.5 A), remain the most intense peaks of the derived PPO/tetralin cocrystalline film (Figure 2.2.5 B). Analogously, the (200) peak, being the most intense of the PPO/ $\alpha$ -pinene cocrystalline film (Figure 2.2.5 A'), remains the most intense of the derived PPO/ tetralin cocrystalline film (Figure 2.2.5 B'). This allows to conclude that 110 and 200 uniplanar orientations are both retained after guest exchange.

Strictly analogous considerations hold for the  $\alpha$ -pinene exchange by treatments with decalin vapor, e.g. at 100 °C for 12 h.

**Hence, simple guest exchange procedures allows the preparation of PPO/decalin and PPO/tetralin cocrystalline films with preferential 200 uniplanar orientation, which cannot be directly achieved by PPO crystallization.** Quantitative evaluations of the degrees of orientation, as obtained on the basis of EDGE patterns, indicate that the degree of orientation remains essentially unaltered as a consequence of guest exchange. For instance, films with high degree of uniplanar orientations ( $f_{110} = 0.90$  and  $f_{200} = 0.75$ ) of the PPO/ $\alpha$ -pinene cocrystalline phase, after guest exchange leading to the PPO/tetralin cocrystalline phase, maintain their high degree of orientation ( $f_{110} = 0.84$  and  $f_{200} = 0.75$ ). It is

worth adding that guest exchange procedures leading to cocrystalline phases presenting largely different X-ray diffraction patterns (and structures), like those with benzene or carbon tetrachloride,<sup>14</sup> always lead to unoriented samples. In a recent paper, it has been established that by guest removal from PPO/ $\alpha$ -pinene cocrystalline samples by supercritical CO<sub>2</sub> (scCO<sub>2</sub>) a nanoporous crystalline modification is obtained.<sup>10e</sup> This guest removal procedure, when applied to the uniplanar oriented cocrystalline films of Figure 2.2.2, leads to unoriented nanoporous-crystalline phases with a degree of crystallinity lower than 30% or to fully amorphous phases. Alternative extraction procedures by using solvents such as acetone or acetonitrile lead to analogous results. This behavior is completely different from that one observed for s-PS, for which the uniplanar orientations achieved by guest induced cocrystallization are generally maintained after guest removal procedures, which occur through solid-state crystal-to-crystal transitions and lead to oriented nanoporous-crystalline phases. The loss of orientation occurring in the preparation of nanoporous-crystalline and of most cocrystalline PPO films indicates that these crystal phase transitions can only occur by loss of crystallinity followed by crystallization from unoriented amorphous phases.

This need of amorphization-crystallization processes for the preparation of nanoporous-crystalline modification and of most cocrystalline forms from the PPO/ $\alpha$ -pinene cocrystalline form is possibly due to changes of the polymer host conformation, which can be inferred by FTIR measurements. The FTIR spectra of unoriented films exhibiting the cocrystalline phases with  $\alpha$ -pinene, tetralin, decalin and carbon tetrachloride are shown in Figure 2.2.6 A, B, C and D, respectively. The FTIR spectra of the nanoporous-crystalline and amorphous unoriented PPO films (as, e.g., derived by guest removal by scCO<sub>2</sub> and thermal treatments on cocrystalline films with  $\alpha$ -pinene) are shown in Figure 2.2.6, parts E and F, respectively. It is apparent that, crystalline

peaks of the cocrystalline forms with  $\alpha$ -pinene, tetralin, or decalin associated with vibrations of the  $4_1$  PPO helix, are located at 753, 741, 658, 641, 581, 532, 476  $\text{cm}^{-1}$  (Figure 1.8A,B,C), while the crystalline peaks of derived nanoporous-crystalline modification are located at 773, 563, 495, and 414  $\text{cm}^{-1}$  (Figure 2.2.6E), i.e., close to those observed for the cocrystalline phase with  $\text{CCl}_4$  (located at 564, 494, and 414  $\text{cm}^{-1}$  Figure 2.2.6D). Hence, both uniplanar orientations, as obtained by  $\alpha$ -pinene induced cocrystallization of amorphous PPO, are only maintained after guest exchange procedures leading to cocrystalline phases exhibiting the starting  $4_1$  polymer conformation. Crystal transitions leading to nanoporous crystalline forms or cocrystalline forms exhibiting a different polymer host conformation lead to complete loss of orientation, possibly due to the need of destruction of crystalline order for the conformational reorganization.<sup>11</sup>

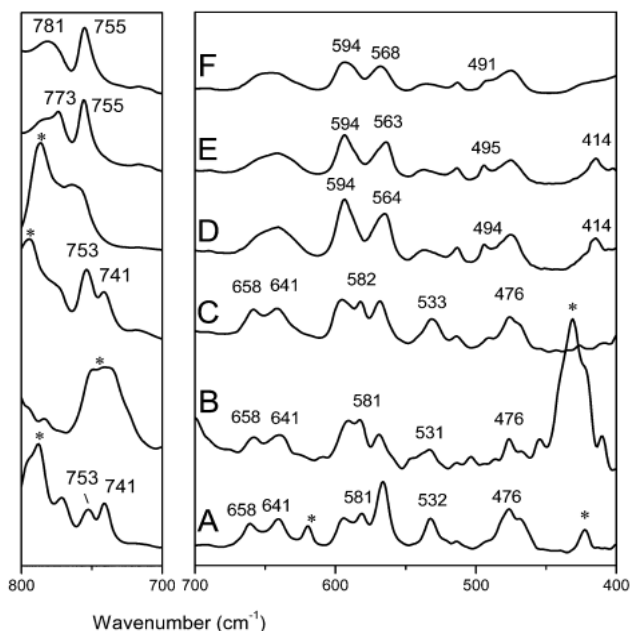


**Fig 2.2.6.** FTIR spectra in the 800–700 and 700–400  $\text{cm}^{-1}$  ranges of unoriented PPO films: (A) cocrystalline with  $\alpha$ -pinene; (B) cocrystalline with tetralin; (C) cocrystalline with decalin; (D) cocrystalline with carbon

tetrachloride; (E) nanoporous–crystalline; (F) amorphous. The  $\alpha$ -pinene, tetralin, decalin, and carbon tetrachloride peaks are indicated by a star (\*).

### 2.2.4 Uniplanar orientations by limonene induced cocrystallization of amorphous films

The limonene is an additional guest which induces crystallization in amorphous films of PPO and develops orientation. The X-ray diffraction pattern ( $\text{Cu K}\alpha$ ) of a PPO/limonene cocrystalline powder, prepared from the corresponding gel after  $\alpha$ -pinene desorption at room temperature, is shown in Figure 2.2.7 A. The X-ray diffraction patterns, also collected by an automatic powder diffractometer, of amorphous PPO films after crystallization by exposure to limonene vapour at different temperatures are shown in Figures 2.2.7 B-E

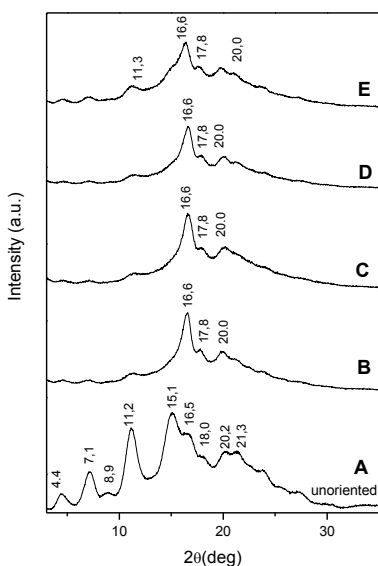


**Fig.2.2.7.** X-ray diffraction, as collected by an automatic powder diffractometer, of PPO/limonene co crystalline samples: (A) powder; (B–E) amorphous films exposed limonene vapor at different temperatures: (B) 70 °C; (C) 80 °C; (D) 120 °C; (E) 160 °C.  $2\theta$  values are indicated close to the main diffraction peaks.

In these oriented samples the most intense peak is the diffraction peak with  $2\theta = 16.6^\circ$ . A better understanding of the crystalline phase orientation in these films, can be achieved by X-ray diffraction patterns taken with beam perpendicular (THROUGH) or parallel (EDGE) to the film plane and collected on a photographic cylindrical camera. In fig.2.2.8 A the EDGE photographic X-ray diffraction patterns is reported, it is observed the equatorial reflection with  $2\theta$  value of  $16.6^\circ$ ,  $d = 5.3 \text{ \AA}$ , probably associated to the plans  $00l$ , while the less intense reflections at  $2\theta$   $4.6^\circ$ ,  $7.2^\circ$ ,  $11.3^\circ$ ,  $15.1^\circ$  along the meridional line corresponds the reflections  $hk0$ .

The THROUGH profile, in fig. 2.2.8 B, show only Debye rings, indicating the absence of axial orientation.

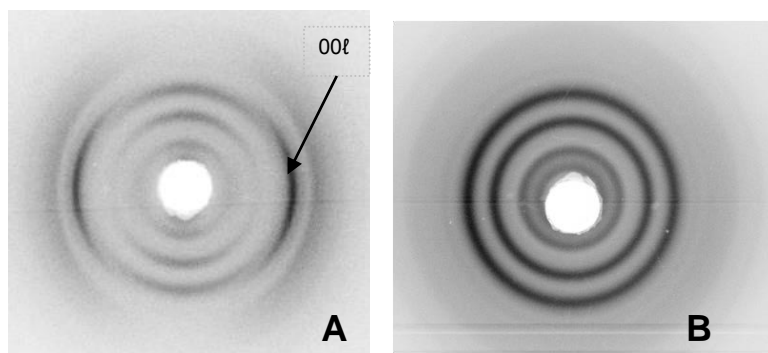


**Fig. 2.2.8** Photographic X-ray diffraction patterns of the same films of Fig.2.2.7C (A) edge, obtained with X-ray beam parallel to the film plane by using a cylindrical camera, recorded on a imaging plate and (B) trough perpendicular to the film plane.

The Edge profile (Figure 2.2.8 A) appears similar to a "tilted" fiber spectrum i.e. to a fiber spectrum mounted in such a way that the reflections  $00l$  end up on the equatorial line. The tilted procedure is commonly applied to determine the  $c$  axis of the polymer.<sup>15</sup>

The relative reflections intensities, collected by THROUGH and EDGE patterns, of the PPO/limonene co-crystalline films are reported in Tables 2.2.2 (columns  $I_{obs//}$ , EDGE and  $I_{obs\perp}$ ,

THROUGH), and compared with those of the corresponding co-crystalline powder of Figure 2.2.7 A (columns  $I_{obs}$ ).

**Table 2.2.2** Comparison between the relative intensities of the reflections of the PPO/limonene co-crystalline form observed in X-ray diffraction patterns for a powder and for an amorphous film crystallized by guest sorption at 80°C (collected with beams perpendicular ( $\perp$ ) and parallel ( $//$ ) to the film plane).

| Powder           |                       |            | (00 $\ell$ ) orientation |               |        |
|------------------|-----------------------|------------|--------------------------|---------------|--------|
| $2\theta_{obs.}$ | $d_{hkl}(\text{\AA})$ | $I_{obs.}$ | $I_{obs. \perp}$         | $I_{obs. //}$ | $\chi$ |
| 4.6              | 19.2                  | m          | m                        | m             | 90°    |
| 7.2              | 12.3                  | m          | m                        | m             | 90°    |
| 11.3             | 7.82                  | s          | m                        | m             | 90°    |
| 15.1             | 5.85                  | s          | m                        | m             | 90°    |
| 16.6             | 5.33                  | m          | -                        | s             | 0°     |
| 18.0             | 4.89                  | w          | m                        | w             |        |
| 19.8             | 4.48                  | -          | -                        | w             |        |

As previously mentioned, the PPO, beside s-PS, exhibit nanoporous-crystalline phases but is worth adding that this polymer exhibit a continuum of crystalline phases between two limit structures. In fact, powders from gels subjected to complete solvent removal present a progressive shift of the diffraction peaks to lower  $2\theta$  values, along the sequence benzene ( $2\theta$  values 7.8-13.0)  $\approx$  tetralin > methylene chloride > 1,2-dichloroethane >  $\alpha$ -pinene > trichlorobenzene > chlorodecane  $\approx$  CCl<sub>4</sub> ( $2\theta$  values 7.1-11.2) <sup>10</sup> as show in fig 2.2.9(A-I). <sup>10e</sup>

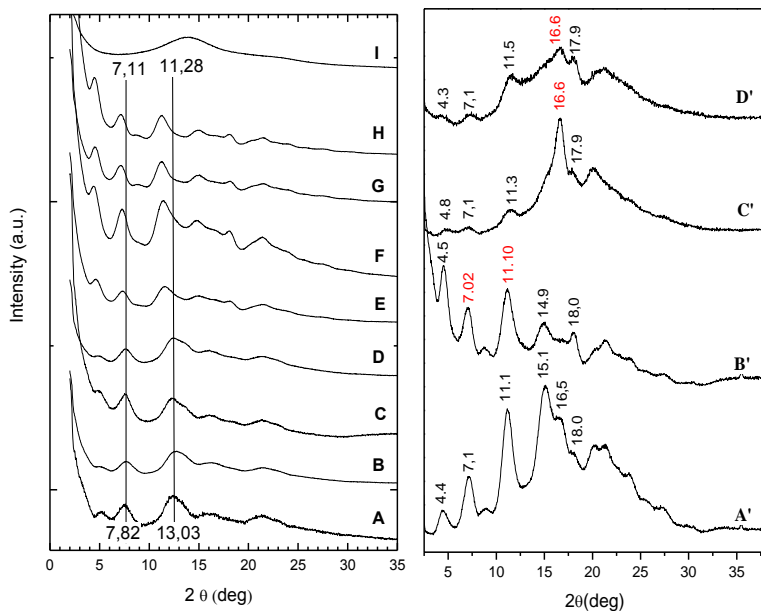


**Fig. 2.2.9** X-ray diffraction, collected by an automatic powder diffractometer, (A-I) trend of different nanoporous crystalline phase. (A) benzene; (B) tertralin; (C)  $\text{CH}_2\text{Cl}_2$ ; (D) DCE; (E)  $\alpha$  pinene; (F) TCB; (G) clorodecane; (H)  $\text{CCl}_4$ ; (I) decalin (A') powder of PPO/ limonene 25/75 wt%; (B') Powder emptied with  $\text{CO}_2$  (C') amorphous films exposed Limonene vapor at 80 °C; (D') Oriented film emptied with  $\text{CO}_2$ .  $2\theta$  values are indicated close to the main diffraction peaks

A nanoporous-crystalline phase obtained after complete limonene removal (fig 2.2.9 B') is similar to nanoporous limit structures obtained by removal of  $\text{CCl}_4$  (fig 2.2.9 H), but there is an additional shift to lower  $2\theta$  values from  $\text{CCl}_4$  ( $2\theta$  values 7.1-11.3) to limonene ( $2\theta$  values 7.0-11.1).

Particularly relevant is similarity between powder diffraction profile of PPO/Limonene (Figure 2.2.9A') and the profile of the extracted powder diffraction (Figure 2.2.9B'), this similarity suggests that PPO/limonene co-crystalline phase is structurally related to the corresponding nanoporous crystalline phase.

In particular, the shift of the value of  $2\theta$  (from  $4.4^\circ$  to  $4.5^\circ$ ,  $7.1^\circ$  to  $7.0^\circ$ , from  $15.1^\circ$  to  $14.9^\circ$ ) and the variation of the intensity appears to be related to the removal of the guest.

The obtaining of PPO oriented simple is particularly relevant in order to help the resolution of the nanoporous structure still not resolved.

Moreover, in fig 2.2.9 PPO/ limonene oriented films, before (fig 2.2.9C') and after guest removal with  $\text{CO}_2$ , (fig 2.2.9D'), are reported. It is apparent that the signal  $2\theta=16.6^\circ$  is only partially retained after guest removal.

### **2.2.5 Guest exchange in PPO/ limonene cocrystalline films with tetralin**

The relevance of crystalline phase orientations in polymer films is also related to their possible stability as a consequence of crystal phase transitions. The uniplanar orientation, obtained by limonene-induced co-crystallization from amorphous PPO, can be fully maintained as a consequence of guest exchange procedures.

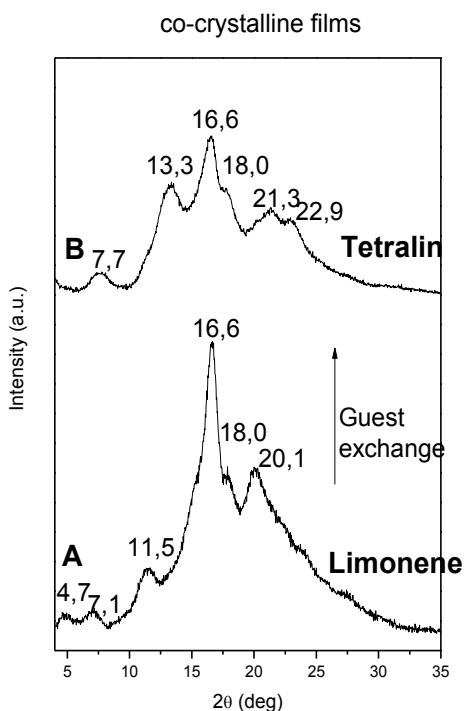


**Fig. 2.2.10.** X-ray diffraction patterns of PPO films: (A) exhibiting 00 $l$  orientations of the cocrystalline phase with limonene; (B) after exchange with tetralin;

This is shown, for instance, for films exhibiting large PPO/limonene crystallites uniplanar orientations, whose X-ray diffraction patterns are shown in Figure 2.2.10, parts A. The X-ray diffraction patterns of this cocrystalline films after exposure to tetralin vapor for 25 min at 100 °C and complete limonene replacement are shown in Figure 2.2.10, parts B. The patterns of Figure 2.2.10 indicate the formation of the PPO/ tetralin co-crystalline phases, as shown for instance by the disappearance to  $2\theta_{\text{CuK}\alpha} = 4.7$  and the shift of peaks from  $2\theta_{\text{CuK}\alpha} = 7.1$  to  $2\theta_{\text{CuK}\alpha} = 7.7$  and from  $2\theta_{\text{CuK}\alpha} = 11.5$  to,

$2\theta_{\text{CuK}\alpha} = 13.3$ . The  $00\ell$  ( $2\theta_{\text{CuK}\alpha} = 16.6$ ) diffraction peak, which is the most intense peak of the starting PPO/limonene co-crystalline film (Figure 2.2.10A), remain the most intense peak of the derived PPO/tetralin co-crystalline film (Figure 2.2.10B). This allows concluding that  $00\ell$  is retained after guest exchange.

The degree of  $00\ell$  uniplanar orientation in PPO\limonene co-crystalline film (fig 2.2.10 A) is  $f_{00\ell} = 0.4$ , after guest exchange, with tetralin (fig. 2.2.10 B), the orientation is partially retained, the degree of orientation is  $f_{00\ell} = 0.2$

Also after guest removal by supercritical  $\text{CO}_2$  (sc  $\text{CO}_2$ ) the orientation is partially retained as shown in fig 2.2.11 A–B.

Particularly relevant is the nanoporous crystalline form by tetralin (fig. 2.2.11 B), it is very similar to the nanoporous structure by benzene (fig. 2.2.11 B'), one of nanoporous limit structures of PPO.

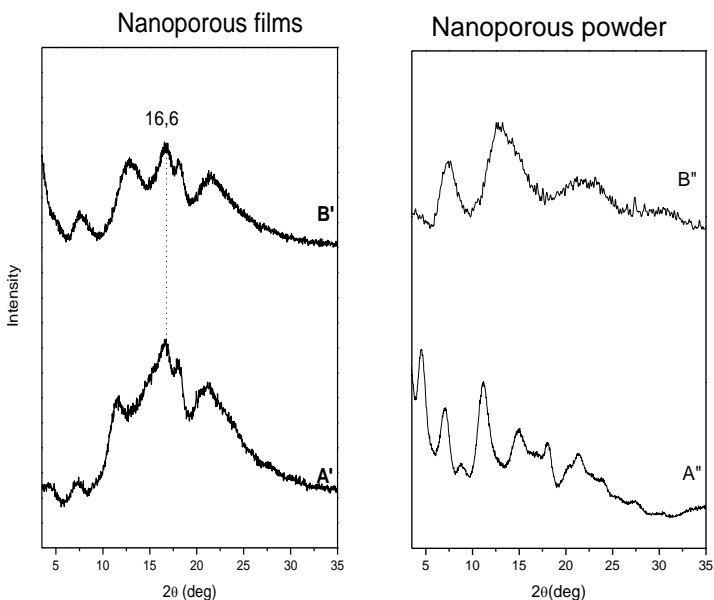


**Fig. 2.2.11** (A) oriented PPO/limonene film emptied with  $\text{CO}_2$ ; (B) oriented PPO/tetralin film emptied with  $\text{CO}_2$ ; (A') PPO/limonene powder emptied with  $\text{CO}_2$ ; (B') PPO/tetralin powder emptied with  $\text{CO}_2$

This oriented nanoporous structure may be important data to study one of the limit nanoporous structure of PPO.

### **2.2.6 A preliminary model of PPO nanoporous structure**

PPO fiber spectra are absent, the development of uniplanar orientations with limonene, in PPO films (described in section 2.2.2), can be useful to solve co-crystalline, and nanoporous crystalline structure of PPO.

In collaboration with the group of Professor De Rosa, and Professor Auriemma at University of Naples, it has been proposed a preliminary model of PPO nanoporous structure in according to the space group  $P222_1$ . Unit cell with:  $a = 19.72 \text{ \AA}$ ;  $b = 12.4 \text{ \AA}$ ;  $c = 10.6 \text{ \AA}$ ;  $\alpha = \beta = \gamma = 90^\circ$  has been proposed. By arranging in the proposed unit cell six independent polymer chains, the calculated density is  $0.92 \text{ g/cm}^3$ . A schematic representation of the chain conformation is reported in figure 2.2.12. The chain conformation has been proposed by imposing  $tc$  symmetry, that is compatible with found sequence of torsional angles ( $\theta_1, \theta_1, -\theta_1, -\theta_1$  con  $\theta_1 = 90^\circ$  deg) and  $c$  periodicity  $1.06 \text{ nm}$ .

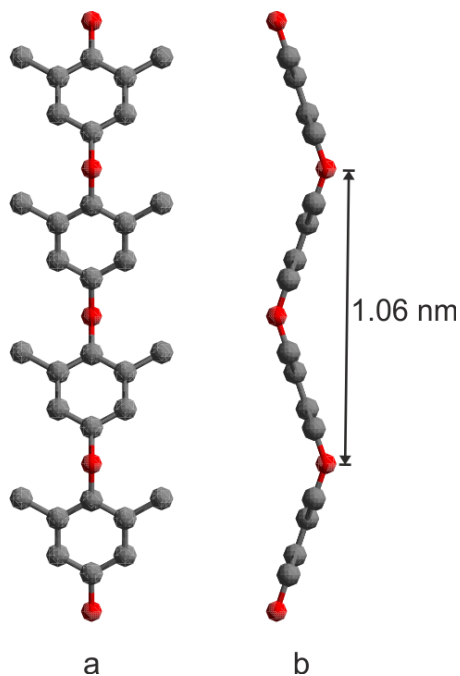


**Fig. 2.2.12** Conformation of PPO chain proposed by imposing  $tc$  symmetry, and  $c$  periodicity 1.06 nm. Projection along  $c$  axis

In figure 2.2.13 is reported the hypothetical packing model, two cells along  $b$  are shown. The guest molecules could be arranged in a cylindrical cavity with axis located at  $(0, b / 2)$  and parallel to  $c$  axis, with  $11 \times 9 \text{ \AA}$  approximate dimension, or in isolated smaller cavity (about  $7 \times 7 \text{ \AA}$ ) located at  $(a / 2, b / 2)$ .

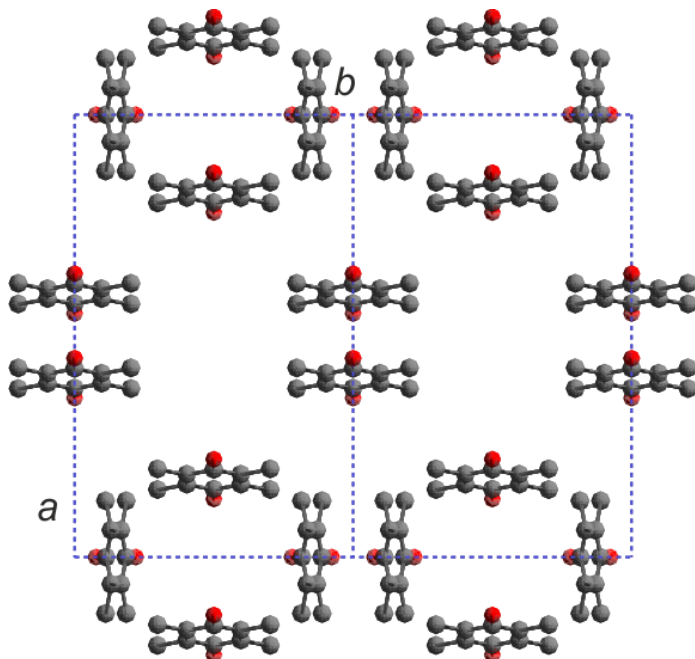


**Fig. 2.2.13** Packing model of the nanoporous PPO form in the unit cell  $a = 19.72 \text{ \AA}$ ;  $b = 12.4 \text{ \AA}$ ;  $c = 10.6 \text{ \AA}$ ;  $\alpha = \beta = \gamma = 90$  and  $P222_1$  space group. Projection along  $c$

Figure 2.2.14 shows the comparison between the calculated x-ray diffraction profile (red) according to the structural model of figure 2.2.13 vs. experimental X-ray diffraction pattern (black), after subtraction of amorphous and background contribution as shown in the insert.

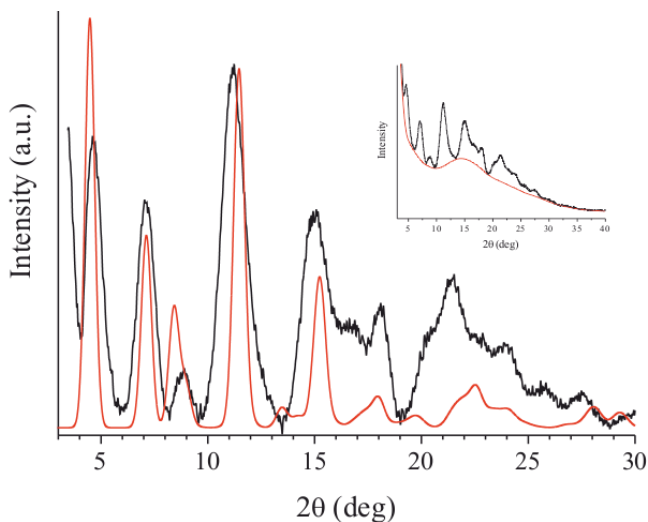


**Fig. 2.2.14** comparison between the calculated x-ray diffraction profile (red) according to the structural model of figure 1.15 vs. experimental X-ray diffraction pattern (black), after subtraction of amorphous and background contribution

### 2.2.7 Conclusion

The guest induced co-crystallization of amorphous PPO films has been investigated by x-ray diffraction and FT-IR spectroscopy. The occurrence of orientations has been described in terms of X-ray diffraction patterns as collected by standard automatic powder diffractometers, and in terms of thorough analyses of photographic patterns as collected by sending the X-ray beam perpendicular and parallel to the film plane (THROUGH and EDGE patterns).

Two different kinds of uniplanar orientations have been found for the PPO cocrystalline phase with  $\alpha$ -pinene. In particular, the cocrystalline phases obtained by  $\alpha$ -pinene vapor treatments of amorphous films in the temperature ranges 100–140 °C and 150–160 °C, present their (110) and (200) crystal planes preferentially parallel to the film plane, with high degrees of uniplanar orientations ( $f_{110} = 0.90$  and  $f_{200} = 0.75$ ), respectively. Analogous high degrees of 110 uniplanar orientations are obtained by cocrystallization of amorphous films as induced by decalin or tetralin sorption.

Guest exchange procedures allow the preparation of PPO/decalin and PPO/tetralin cocrystalline films with 200 uniplanar orientation, which are not achieved by direct PPO cocrystallization. A new 00 $\ell$  uniplanar orientation has been found with limonene. After guest exchange procedure allows the preparation of PPO/ tetralin cocrystalline films with 00 $\ell$  uniplanar orientation which is not achieved by direct PPO cocrystallization.

Moreover, it is worth noting that due to the absence of fiber spectra, the development of uniplanar orientations in PPO films could be useful to solve crystal structures of both crystalline and nanoporous-crystalline modifications, in fact it has been proposed a preliminary model of PPO nanoporous structure according to the space group P222<sub>1</sub> with an unit cell with :  $a = 19.72 \text{ \AA}$ ;  $b = 12.4 \text{ \AA}$ ;  $c = 10.6 \text{ \AA}$ ;  $\alpha = \beta = \gamma = 90$

### **References**

1. Hay A.S., *J Polym Sci Part A*, **1998**, 36, 505.
2. Wang X., Feng W., Li H., Ruckenstein E., *Polymer*, **2002**, 43, 37.
3. John Wiley & Sons: Polymer for Electricity and Electronics; Cap 2.
4. Alentiev A., Drioli E., Golemme M., Olinich O., Lapkin A., Volkow V., Yamobolski Yu., *Journal of Membrane Science*, **1998**, 138, 99.
5. Ilinitch O., M., Fenelonov V. B., Lapkin A. A., Okkel L. G., Terskikh V. V., Zamaraev K. I., *Microporous Mesoporous Materials*, **1999**, 31, 97.
6. Khulbe K.C., Matsuura T., Lamarche G., Lamarche A.-M., *Journal of Membrane Science*, **2000**, 170, 81.
7. a) Bauer C. J. M., Smid J., Olijslager J., Smolders C. A., *Journal of Membrane Science*, **1991**, 57, 307; b) Smid J., Albers J. H. M., Kusters A. P. M., *Journal of Membrane Science*, **1991**, 64, 121; c) Fu H., Jia L., Xu J., *Journal of Applied Polymer Science*, **1994**, 51, 1405; d) Polotski E. A., Polotskaya G. A., *Journal of Membrane Science*, **1998**, 140, 97.
8. a) Huang R Y. M., Kim J. J., *Journal of Applied Polymer Science*, **1984**, 29, 4017; b) Hamza A., Chowdhury G., Matsuura T., Sourirajan S., *Journal of Applied Polymer Science*, **1995**, 58, 613;

- c) Hamza A., Chowdhury G., Matsuura T., Sourirajan S., *Journal of Membrane Science*, **1997**, 129, 55.
9. Fu H., Jia L., Xu J., *Journal of Applied Polymer Science*, **1994**, 51, 1405.
10. a) Factor, A.; Heinsohn, G. E.; Vogt, L. H., Jr. *Polym. Lett.* **1969**, 7, 205. b) Barrales-Rienda, M.; Fatou, J. M. G. *Kolloid Z. Z. Polym.* **1971**, 244, 317. c) Horikiri, S. *J. Polym. Sci. A2* **1972**, 10, 1167. d) Hurek, J.; Turska, E. *Acta Polym.* **1984**, 35, 201–207. e) Tarallo, O.; Petraccone, V.; Daniel, C.; Fasano, G.; Rizzo, P.; Guerra, G. *J. Mater. Chem.* **2012**, 22, 11672.
11. Rizzo P., Ianniello G., Longo S., Guerra G. *Macromolecules* **2013**, 46, 3995
12. a) Rizzo, P.; Lamberti, M.; Albuñia, A. R.; Ruiz de Ballesteros, O.; Guerra, G. *Macromolecules* **2002**, 35, 5854. b) Rizzo, P.; Costabile, A.; Guerra, G. *Macromolecules* **2004**, 37, 3071.
13. a) Rizzo, P.; Albuñia, A. R.; Milano, G.; Venditto, V.; Guerra, G.; Mensitieri, G.; Di Maio, L. *Macromol. Symp.* **2002**, 185, 65. b) Rizzo, P.; Della Guardia, S.; Guerra, G. *Macromolecules* **2004**, 37, 8043–8049. c) Rizzo, P.; Spatola, A.; De Girolamo Del Mauro, A.; Guerra, G. *Macromolecules* **2005**, 38, 10089
14. Daniel, C.; Longo, S.; Cardea, S.; Vitillo, J. G.; Guerra, G. *RSC Advances* **2012**, 2, 12011.
15. “Fondamenti di Scienza dei polimeri” a cura di M. Guaita, F. Ciardelli, F. La Mantia, E. Pedemonte, Pacini Editori

## 2.3 Poly (L-lactide) (PLLA)

Poly (L-lactide) (PLLA) is a biodegradable and biocompatible polyester that can be produced by renewable resources. Being non-toxic to human body, PLLA is used in biomedical applications, like surgical sutures, bone fixation devices, or controlled drug delivery. Moreover, the good mechanical properties and easy of processability make PLLA a good candidate to substitute petroleum-based polymers in selected and commodity application, with the added value of biodegradability<sup>1</sup>. Nowadays, more advantageous applications of this environmentally friendly polymer are under development for car and computer parts, which bring forward the demand on improving the thermal and mechanical properties of the PLLA-based product<sup>2</sup>.

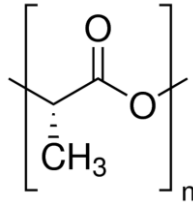


Fig. 2.3.1 Chemical structure of PLLA repeating unit

The mechanical and thermal properties of a semicrystalline polymer greatly depend on the crystal structure and morphology.

In addition, as for biodegradable polymers, their biodegradability is also influenced by the polymorphism<sup>3</sup>

### 2.3.1 PLLA uniplanar orientation of $\epsilon$ form

The PLLA is able to form co-crystals with some low-molecular-mass guest molecules. After co-crystallization procedure with solvents able to form the  $\epsilon$  co-crystalline phase, particularly, Cyclopentanone (CPO), *N,N*-dimethylformamide (DMF), tetrahydrofuran (THF), develop uniplanar orientation in PLLA co-crystalline films<sup>4</sup>.

In Figures 2.3.2, the X-ray diffraction patterns are reported, collected by an automatic powder diffractometer of amorphous PLLA films after crystallization procedures by

immersion in pure CPO at +25°C (Fig. 2.3.2 B), +2°C (Fig. 2.3.2 C), and -25°C (Fig. 2.3.2 D) for 3 days. The crystallization procedure at +25°C leads to the formation of  $\alpha$  phase (Fig. 2.3.2 B) whereas crystallization procedure at lower temperatures lead to the formation of  $\epsilon$  co-crystalline phase (Fig. 2.3.2 C and 2.3.2 D). Moreover crystallization procedures conducted at +2°C leads to films presenting unoriented  $\epsilon$  PLLA/CPO co-crystalline phase. Instead it appears that the pattern of Figure 2.3.2 D (crystallization procedures conducted at -25°C) shows diffraction peaks analogous at those observed for the PLLA/CPO co-crystalline powder, although the relative intensity are heavily changed.

In particular, the X-ray diffraction pattern of Figure 2.3.2 D shows as the most intense reflection the peak located at  $2\theta=14.1$  that can be attributed to the 020 crystallographic planes, this result strongly suggests the occurrence of (020) uniplanar orientation.

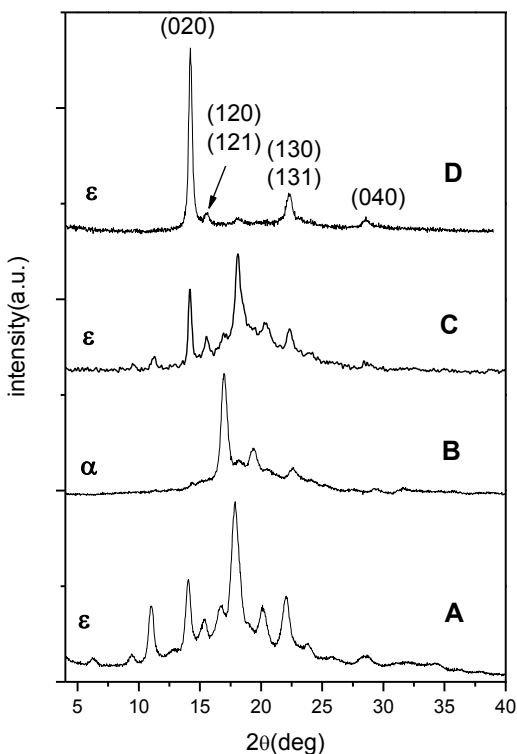


**Fig. 2.3.2.** X-ray diffraction, as collected by an automatic powder diffractometer of PLLA crystalline samples: PLLA/CPO powder (A); PLLA amorphous films immersed in CPO at +25°C (B), +2°C (C), and at -25°C (D) for 3 days. Close to the main diffraction peaks, the Miller indexes of the  $\epsilon$  PLLA co-crystalline phase are indicated.

Crystallization procedures by immersion of amorphous PLLA films in pure tetrahydrofuran (THF) and *N,N*-dimethylformamide (DMF) at -25°C for 3 days have been performed, the corresponding X-ray diffraction patterns are shown in Figures 2.3.3 A and 2.3.3 B respectively. The X ray diffraction pattern obtained by using CPO has been also reported in Figure 2.3.3 C for sake of comparison.

For all X-ray diffraction patterns the most intense reflection is located at  $2\theta=14.1$ , strongly indicating that by using low crystallization temperatures (close to  $-25^{\circ}\text{C}$ ) not only the formation of  $\epsilon$  PLLA co-crystalline phase but also a strong orientation of the (020) crystallographic planes occurs.

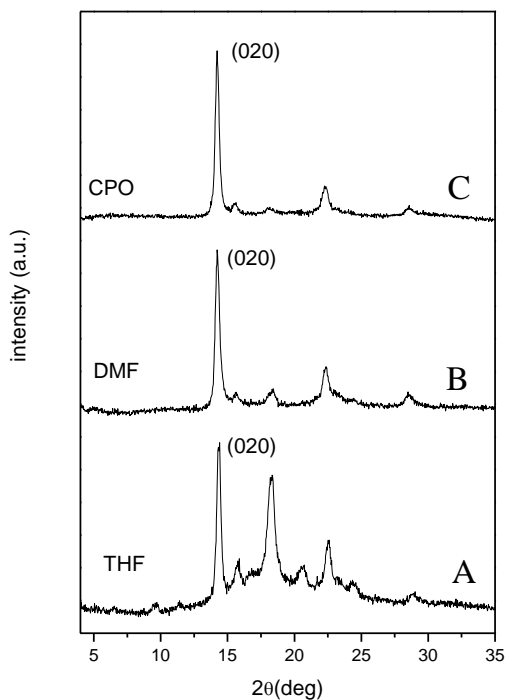


**Fig. 2.3.3.** X-ray diffraction, as collected by an automatic powder diffractometer of PLLA films presenting  $\epsilon$  PLLA co-crystalline phases with THF (A), DMF (B) and CPO (C) guest molecules.

A better understanding of the crystalline phase orientation in these films, can be achieved by X-ray diffraction patterns taken with beam perpendicular (THROUGH) or parallel (EDGE) to the film plane and collected on a photographic cylindrical camera. EDGE pattern as well as EDGE and THROUGH profiles of the film of Figure 2.3.2 D are reported in Figure 2.3.4 A and 2.3.4 B, and 2.3.4 C

respectively. The presence of arcs rather than Debye rings (Figure 2.3.4 A) and the relative heavily changed intensities in the EDGE and THROUGH profiles (Figure 2.3.4 B-2.3.4 C) clearly indicate the presence of 020 uniplanar orientation. Moreover the THROUGH pattern, (not reported) showing only Debye rings indicates the absence of axial orientation. This (020) uniplanar orientation characterized by (020) crystallographic planes preferentially parallel to the film plane can be defined as  $b_{\perp}$ , thus indicating that the  $b$  unit-cell axis is preferentially perpendicular to the film surface.

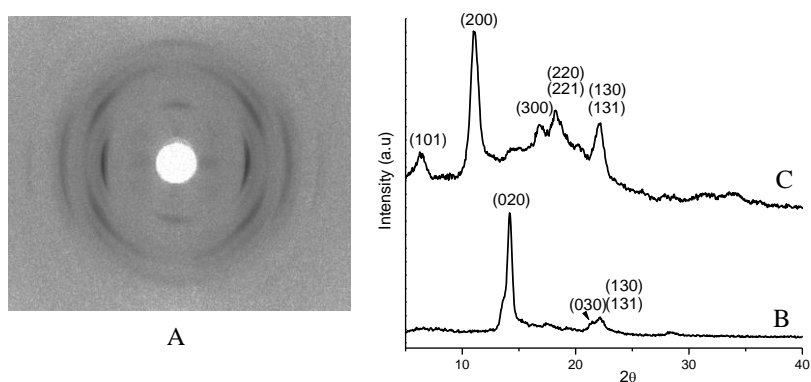


**Fig. 2.3.4.** X-ray diffraction, of  $\epsilon$  PLLA/CPO film presenting (020) uniplanar orientation. (A) Photographic patterns taken with X-ray beam parallel to the film surface (EDGE). (B-C) Diffraction profiles of photographic patterns taken with X-ray beam parallel (EDGE) (B) or perpendicular to the film surface (THROUGH) (C).

The relative intensities of the reflections, as collected by THROUGH and EDGE patterns, of the  $\epsilon$  PLLA/CPO co-crystalline film are reported in Tables 1 (columns 4<sup>th</sup> and 5<sup>th</sup>, respectively) and compared with those of the corresponding co-crystalline powder of Figure 2.3.2 A (column 3<sup>rd</sup>).

Moreover, in the column 6<sup>th</sup> of Table 1, the azimuthal angles ( $\chi_{\text{obs}}$ ) of maximum intensity observed for the different reflections in the X-ray EDGE pattern of Figure 2.3.4 A have been compared with those calculated ( $\chi_{\text{calc}}$ ), (columns 7<sup>th</sup>), in the assumption of complete parallelism of the (020) planes

with respect to the film plane. The good agreement between  $\chi_{\text{obs}}$  and  $\chi_{\text{calc}}$  clearly indicates the occurrence of 020 uniplanar orientations for the  $\epsilon$  PPO/CPO co-crystalline film.

**Table 2.3. 1.** Comparison between the relative intensities of the reflections of the  $\epsilon$  PLLA/CPO co-crystalline form observed in X-ray diffraction patterns of a powder and of amorphous PLLA films crystallized by CPO sorption. The patterns of the films have been collected with beams perpendicular (THROUGH) and parallel (EDGE) to the film plane. As for the EDGE patterns, the observed azimuthal angles ( $\chi_{\text{obs}}$ ) are compared to those calculated ( $\chi_{\text{calc}}$ ) in the assumption of complete parallelism of the (020) plane with respect to the film plane.

| Film crystallized by CPO guest sorption |                         |                         | Film crystallized by CPO guest sorption |                                   |                       |                        |
|---|-------------------------|-------------------------|---|-----------------------------------|-----------------------|------------------------|
| Unoriented samples                      |                         |                         | Oriented samples                        |                                   |                       |                        |
| Proposed unit-cell                      |                         |                         | (020) uniplanar orientation             |                                   |                       |                        |
| a=1,6 nm b=1,25nm<br>c=2,85nm           |                         |                         |   |                                   |                       |                        |
| <i>hkl</i>                              | 2 $\theta_{\text{obs}}$ | <i>I</i> <sub>obs</sub> | <i>I</i> <sub>obs</sub> .<br>THROUGH    | <i>I</i> <sub>obs</sub> .<br>EDGE | $\chi_{\text{obs}}$ . | $\chi_{\text{calc}}$ . |
| 101                                     | 6.2                     | W                       | Mw                                      | -                                 |                       | 90°                    |
| 111                                     | 9.4                     | W                       |   | vw                                | 43°                   | 42°                    |
| 200                                     | 11.0                    | M                       | Vvs                                     | m                                 | 90°                   | 90°                    |
| 020                                     | 14.2                    | Ms                      | Vvw                                     | vs                                | 0                     | 0°                     |
| 120                                     | 15.4                    | W                       |   | w                                 | 20°                   | 21°                    |
| 121                                     |                         |                         |   |                                   | 20°                   | 24°                    |
| 300                                     | 16.7                    | W                       | M                                       | -                                 |                       | 90°                    |

|     |       |    |    |      |     |     |
|-----|-------|----|----|------|-----|-----|
| 220 |       |    |    | s    | 38° | 38° |
| 221 | 18.1  | S  | Ms | s    |     | 39° |
| 310 |       |    |    | ms   | 67° | 67° |
| 223 | 20.25 | M  | W  | m    | 44° | 45° |
| 030 | 21.3  | Mw |    | mw   | 0°  | 0°  |
| 320 | 21.8  | Mw | s  |      |     |     |
| 130 |       |    |    | ms   | 15° | 15° |
| 131 | 22.3  | m  |    | s    |     | 17° |
| 040 | 28.5  | w  |    | vv w | 0°  | 0°  |

The crystal structure of PLLA-CPO clathrate has been examined on the basis of unoriented X-ray powder diffraction patterns (Figure 2.3.5) by dott. O. Tarallo of University of Naples.

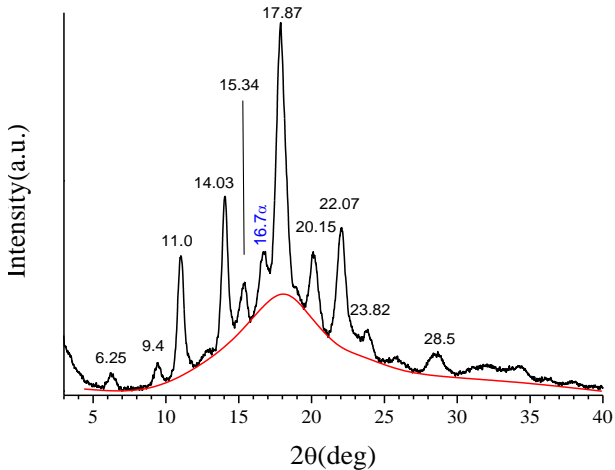


**Fig. 2.3.5.** X-ray powder diffraction pattern of an unoriented sample of PLLA-CPO clathrate form. The presence of a reflection centered at  $2\theta=16.7^\circ$  points out the presence of a minor amount of residual PLLA in  $\alpha$  form. The amorphous and background contributions are indicated by a red line.

As a first working hypothesis, we have considered a crystalline structure analogous to that reported in literature for the clathrate form of PLLA containing DMF<sup>4</sup>. In particular, starting from the structural model of the PLLA/DMF clathrate form proposed by Asai and coworkers, we have modified the proposed unit cell parameters to fit our experimental data and we have arranged CPO guest molecules in the guest locations described in literature by means of molecular mechanic calculations. Surprisingly, for all the structural models investigated, several unacceptable C-C and C-O non bonded distance were present and the calculated structure factors were in complete disagreement with the experimental data.

For these reasons a complete reappraisal of the structure has been carried out.

A schematic representation of the structural model we suggest for the PLLA/CPO clathrate form is reported in Figure 2.3.6. The proposed unit cell is orthorhombic, with cell parameters equal to  $a = 1.61$  nm,  $b = 1.26$  nm,  $c = 2.90$  nm. This cell, for highly oriented PLLA-CPO clathrate samples, is practically identical to that reported in literature by Asai and coworkers.<sup>4</sup>

In this cell, four PLLA chains in 10/7 conformation and 16 CPO guest molecules are packed according the space group  $P2_12_12_1$ .

In this hypothesis the calculated density is  $1.189$  g/cm<sup>3</sup> (the experimental density of PLLA  $\alpha$  form is  $1.26$  g/cm<sup>3</sup> while that of the amorphous phase is  $1.254$  g/cm<sup>3</sup>. No experimental data is currently available for the PLLA-CPO clathrate specimens). Figure 2.3.7 compares the experimental X-ray diffraction pattern of an unoriented sample of the PLLA-CPO clathrate with the calculated pattern obtained from the model reported in Figure 2.3.6. A very good agreement between the experimental and calculated powder patterns is apparent.

It is worth pointing out that the structural model presented in Figure 2.3.6, despite presenting a similar unit cell and the same space group symmetry, is different from that proposed by Asai and co-workers<sup>4</sup> in the case of the clathrate form of

PLLA containing DMF.

In order to validate the structural model proposed in Figure 2.3.6, further structural analysis based on oriented PLLA-CPO clathrate samples are in progress.

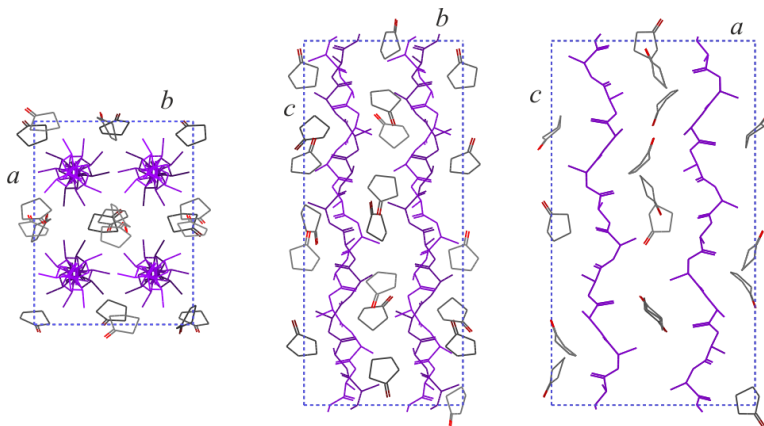


**Fig. 2.3.6.** Schematic representation of the proposed crystalline PLLA-CPO clathrate form in projection along the *c* axis, *a* axis and *b* axis. 10/7 helical chains are reported in magenta. Guest molecules are arranged in isolated elements characterized by a complex shape presenting their main axis parallel to the *c* axis of the unit cell.

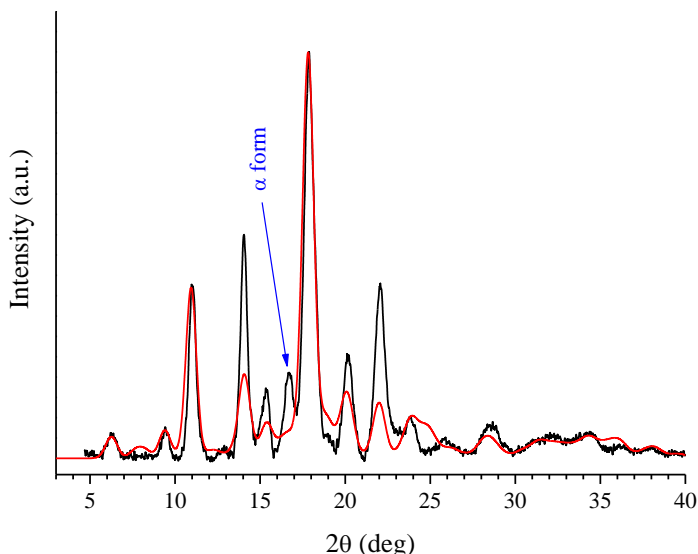


**Fig. 2.3.7** Comparison between experimental (black line) X-ray powder diffraction pattern for the PLLA-CPO clathrate form, after the subtraction of the amorphous contribution, with the calculated one (red line) according to the structural model reported in Figure 2.3.6.

### 2.3.2 Guest exchange in $\epsilon$ PLLA co-crystalline phase

The relevance of crystalline phase orientations in polymer films is also related to their possible stability as a consequence of crystal phase transitions. The uniplanar orientation, as obtained by CPO induced co-crystallization from amorphous PLLA, can be fully maintained as a consequence of guest exchange procedures.

This is shown, for instance, for films exhibiting large  $\epsilon$  PLLA/CPO crystallites with high degree of 020 uniplanar orientation, whose X-ray diffraction patterns is shown in Figures 2.3.8 A.

The X-ray diffraction pattern of this co-crystalline film after exposure to THF vapour at  $-25^{\circ}\text{C}$  for 1 day and complete CPO replacement is shown in Figures 2.3.8 B. (The formation of the PLLA/THF co-crystalline phases, has been evidenced by FTIR measurements)

The (020) diffraction peak, which is the most intense peak of the starting  $\epsilon$  PLLA/CPO co-crystalline film (Figure 2.3.8 A),

remain the most intense peaks of the derived  $\epsilon$  PLLA/THF co-crystalline film (Figure 2.3.8 B). This allows to conclude that 020 uniplanar orientation is retained after guest exchange.

Quantitative evaluations of the degrees of orientation, as obtained on the basis of EDGE patterns, indicate that the degree of orientation remains essentially unaltered as a consequence of guest exchange. For instance, film with high degree of uniplanar orientations ( $f_{020} = 0.89$ ) of the  $\epsilon$  PLLA/CPO co-crystalline phase, after guest exchange leading to the  $\epsilon$  PLLA/THF co-crystalline phase, maintain its high degree of orientation ( $f_{020} = 0.86$ ). It is worth underline that the high degree of uniplanar orientation ( $f_{020} = 0.86$ ) obtained by guest exchange is even higher than that obtained by direct crystallization on amorphous film ( $f_{020} = 0.7$ ) whose pattern is reported in Figure 2.3.3.A.

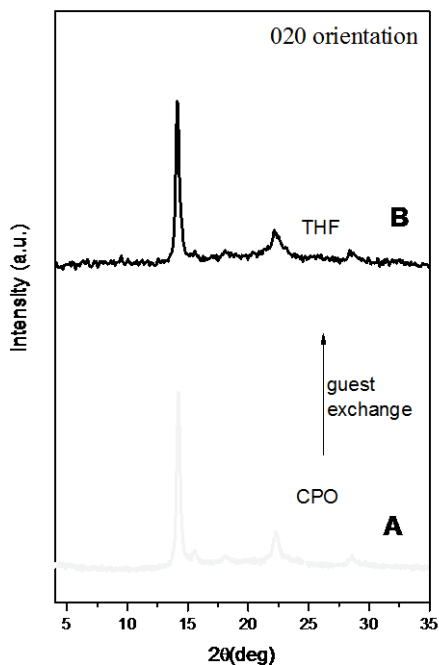


**Fig. 2.3.8** X-ray diffraction patterns of PLLA films: exhibiting (020) uniplanar orientation of the  $\epsilon$  co-crystalline phase including CPO (A) or THF (B).

### 2.3.3 Effects of guest removal from $\epsilon$ form

In Figure 2.3.9 shows the change of X ray diffraction patterns of PLLA with desorption of CPO at room temperature. It appears that guest desorption at room temperature leads to unoriented  $\alpha$  crystalline phase.

After 16 day desorption at room temperature the reflection  $2\theta=16.7$  related to  $\alpha$  form appears. While this reflection increases, the signal  $2\theta=14.2$  and  $2\theta=15.5$  related of  $\epsilon$  form decrease until disappear.

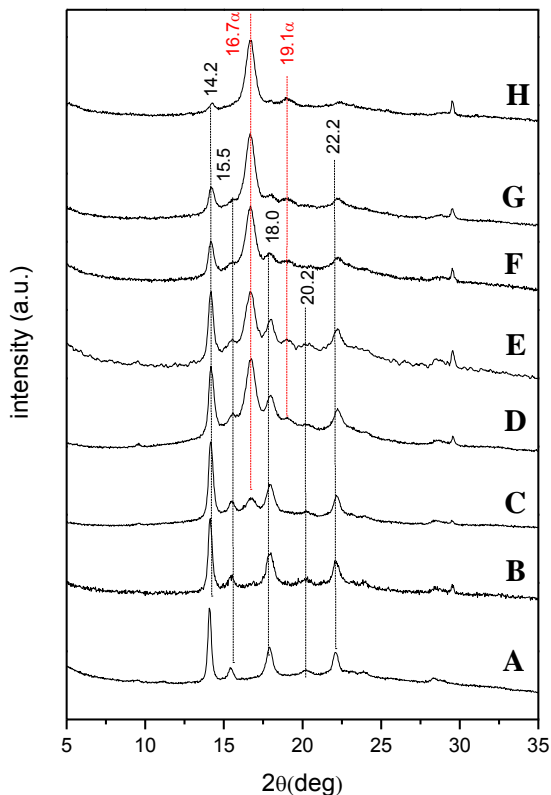


**Fig.2.3.9** Change of X-ray diffraction patterns of  $\epsilon$ - PLLA/CPO films exhibiting (020) uniplanar orientation (A) with solvent desorption after 7days (B), 16days (C), 26 days (D), 30 days (E), 37days (F), 41 days (G), 69 days (H)

Strictly analogous considerations hold for PLLA\DMF and PLLA\THF desorption at room temperature.

After desorption of DMF guest, the appearance of  $\alpha$  form is slow, comparable to CPO desorption. But after 10 minutes of THF desorption, the polymer presents the  $\alpha$  form showing a lower stability of co-crystalline structure than the others

already observed.

After guest removal with supercritical CO<sub>2</sub> leads to oriented  $\alpha$  crystalline phase, as show in figure 2.3.10 B

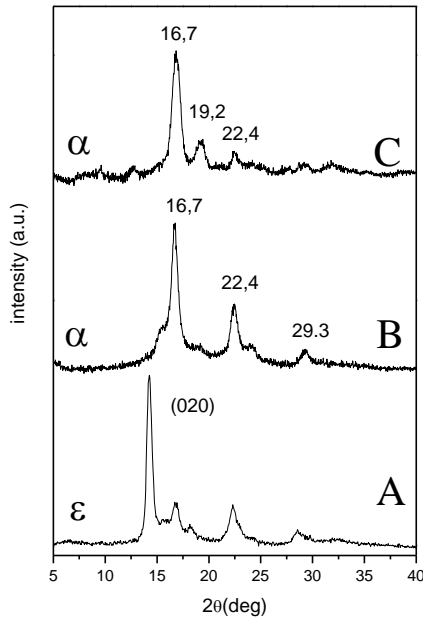


**Fig.2.3.10** X-ray diffraction patterns of PLLA film exhibiting (020) uniplanar orientation of the co-crystalline phase with DMF, before (A) , after extraction with supercritical CO<sub>2</sub> (B), after guest desorption at room temperature (C).

A better understanding of the crystalline phase orientation in these films, can be achieved by X-ray diffraction patterns taken with beam perpendicular (THROUGH) or parallel (EDGE) to the film plane and collected on a photographic cylindrical camera. EDGE pattern as well as EDGE and THROUGH profiles of the film of Figure 2.3.10B are reported in Figure 2.3.11A and 2.3.11B, and 2.3.11C respectively

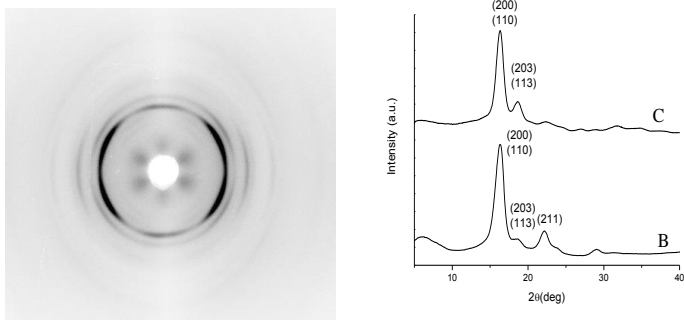


**Fig. 2.3.11.** X-ray diffraction, of  $\alpha$  film presenting uniplanar orientation of the  $\alpha$  crystalline phase. (A) Photographic patterns taken with X-ray beam parallel to the film surface (EDGE pattern). (B-C) Diffraction profiles of photographic patterns taken with X-ray beam parallel (EDGE pattern) (B) or perpendicular to the film surface (THROUGH pattern) (C).

In order to understanding the kind of orientations, the analysis are in progress

### 2.3.4 Conclusion

The guest induced co-crystallization of amorphous PLLA films has been investigated by x-ray diffraction. The occurrence of orientations has been described in terms of X-ray diffraction patterns as collected by standard automatic powder diffractometers, and in terms of thorough analyses of photographic patterns as collected by sending the X-ray beam perpendicular and parallel to the film plane (THROUGH and EDGE patterns). The 020 of uniplanar orientations have been found for PLLA cocrystalline phases with CPO, DMF and THF. In particular, the cocrystalline phases obtained by CPO and DMF treatments of amorphous films present high degrees of uniplanar orientations ( $f_{020} = 0.89$ ). Film with high degree of uniplanar orientations ( $f_{020} = 0.89$ ) of the  $\epsilon$  PLLA/CPO co-crystalline phase, after guest exchange leading to the  $\epsilon$  PLLA/THF co-crystalline phase, maintain its high degree of orientation ( $f_{020} = 0.86$ ). It is worth underline that the high degree of uniplanar orientation ( $f_{020} = 0.86$ ) obtained by guest

exchange is even more higher than that obtained by direct crystallization on amorphous film ( $f_{020} = 0.7$ ).

Moreover, it appears that guest desorption at room temperature leads to unoriented  $\alpha$  crystalline phase. After guest removal with supercritical  $\text{CO}_2$  leads to oriented  $\alpha$  crystalline phase.

Starting from the structural model of the PLLA/DMF clathrate form proposed by Asai and coworkers, we have modified the proposed unit cell parameters to fit our experimental data and we have arranged CPO guest molecules in the guest locations described in literature by means of molecular mechanic calculations. The proposed unit cell is orthorhombic, with cell parameters equal to  $a = 1.61$  nm,  $b = 1.26$  nm,  $c = 2.90$  nm. This cell is practically identical to that reported in literature by Asai and co-workers for highly oriented PLLA-CPO clathrate samples.

In this cell, four PLLA chains in 10/7 conformation and 16 CPO guest molecules are packed according the space group  $P2_12_12_1$ .

### **References**

1. Di Lorenzo M. L., Cocca M., Malinconico M, *Thermochimica Acta* **2011**, 522, 110
2. Zhang J., Tashiro K. *Macromolecules* **2008**, 41, 1352
3. Pan P, Kai W., Zhu B., Dong T., Inoue Y. *Macromolecules* **2007**, 40, 6898
4. Marubayashi H., Asai S., Sumita M., *Macromolecules* **2012**, 45, 1384

## 2.4 Correlation between shrinkage and orientations in sPS films

### 2.4.1 Syndiotactic polystyrene sPS

Syndiotactic polystyrene (sPS) is a high performance thermoplastic semicrystalline material, commercially available, that presents good mechanical properties associated with a high melting temperature (close to 270°C), high chemical stability and high crystallization rate.<sup>1</sup>The thermoplastic nature of sPS allows an easy processing to product suitable for several applications, like films, membranes, and foams, as well as their recycling. As a consequence, a number of applications in the field of chemical separations,<sup>2-5</sup> molecular sensorics,<sup>6-9</sup> and catalysis<sup>10</sup> for these inexpensive and reusable materials have been proposed. As for possible application as films for packaging, of particular economic relevance is the ability of the nanoporous  $\delta$  form to absorb ethylene<sup>11</sup> and carbon dioxide,<sup>12,13</sup> leading to the formation of co-crystalline forms with these gaseous guest molecules. Indeed, it is well known that the postharvest life and quality of many fruits, vegetables, and flowers are negatively affected by the presence of carbon dioxide and seriously shortened by exposure to trace amounts (also few ppb) of ethylene. Films including the  $\delta$ -nanoporous crystalline phase of s-PS present high ethylene solubility associated with negligible water uptake. These features, combined with good chemical and mechanical properties, make polymeric films presenting the  $\delta$ -nanoporous crystalline phase suitable candidates for produce packaging.<sup>11</sup>

Moreover we know that sPS co crystalline film can develop three different kinds of uniplanar orientations, depending on the selected technique (solution crystallization procedures<sup>14</sup> or solvent-induced crystallization in amorphous samples<sup>14</sup>) and on the molecular guest,  $a\perp C//$ ,  $a//C\perp$ ,  $a//C//$ <sup>14</sup> crystalline planes are preferentially oriented parallel to the film plane. The availability of co-crystalline sPS films with three different kinds of uniplanar orientation allows to establish fine structural features: it allows active guest orientation control,

<sup>14d,15</sup> mainly for optical applications (e.g., as fluorescent, photo-reactive, chromophore and magnetic materials); <sup>16</sup> it permits to control guest diffusivity; <sup>14h,15b,17</sup> it has been helpful in the experimental evaluation of the orientation of transition moment vectors of host and guest vibrational modes with respect to the host chain axes. <sup>18</sup> Hence, the study of the development of molecular orientation in sPS films, in order to get different kinds and high degrees of orientation can be particular relevant in order to control the molecular properties also at macroscopic scale.

#### **2.4.2 The Shrinkage**

The shrinkage is a very important mechanical parameter for industrial products, indicating the dimensional stability.

We have investigated on the shrinkage developed in syndiotactic polystyrene (sPS) films after solvent treatments leading to co-crystalline phases, by using X-ray diffraction as well as FTIR measurements. First, sPS films biaxially drawn, presenting “planar” oriented trans-planar  $\alpha$  crystalline phase were exposed to solvent vapours leading to co-crystalline phases. In this sample a high degree of  $a_{//}c_{//}$  “uniplanar” crystalline phase orientation (parallelism of the (010) crystallographic plane to the film surface) has been observed. Then amorphous sPS films were exposed to solvents leading to co-crystalline phases showing different kinds and degrees of crystalline phase orientations. High shrinkage values have been measured on both films. Definitely lower shrinkage values on films with trans-planar mesomorphic or unoriented  $\alpha$  crystalline phases, after their exposure to solvents, have been measured. In this latter case, the transition toward co-crystalline phases can occur without a significant shrinkage.

The influence of the shrinkage behavior was expressed by the measured length variation and it was equal to the ratio of the length variation between the ink marks after shrinkage on the original length.

The shrinkage can be represented as follows:

$$S = \frac{L_0 - L}{L_0} * 100 \quad (1)$$

Where  $L_0$  is the sample length along the measured direction and  $L$  is the sample length after treatment.

### 2.4.3 Oriented $\alpha$ form

In Figure 2.4.1 B X ray diffraction pattern of sPS biaxially drawn films are reported. The peaks at  $2\theta_{\text{CuK}\alpha}$  6.7, 11.7 and 13.6 and at 15.6 correspond to  $\alpha$  trans-planar crystalline phase. By comparing the collected X-ray pattern with the pattern of an unoriented  $\alpha$  crystalline ( Figure 2.4.1 A) <sup>19a</sup> it is evident that the intensity of the layer line reflections (with Miller indexes  $hk1$  and  $hk2$ ) tends to be reduced with respect to all equatorial reflections ( $hk0$ ).

This suggests the occurrence of the so-called “planar” orientation, where the polymer chain axes  $c$  tend to remain nearly parallel to the film plane. <sup>19a, 14i</sup>

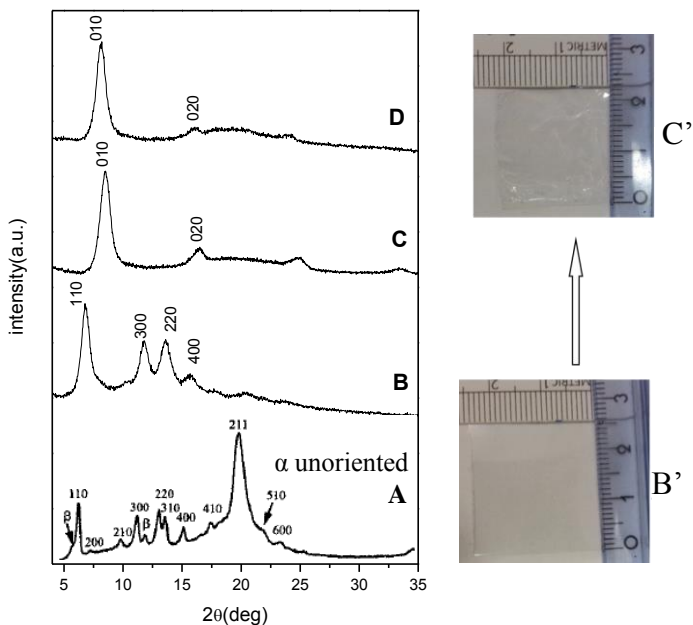


**Fig. 2.4.1** XRD patterns, collected by an automatic powder diffractometer, of biaxially stretched films before showing (B) planar oriented  $\alpha$  crystalline phase, (C)  $a_{\parallel}c_{\parallel}$  uniplanar oriented  $\delta$  co-crystalline phase including DCM, (D)  $a_{\parallel}c_{\parallel}$  uniplanar oriented nanoporous  $\alpha$  crystalline phase. (A) For comparison also unoriented  $\alpha$  crystalline phase spectrum is reported. Photos of biaxially stretched films before (B') and after (C') crystallization procedure

Syndiotactic polystyrene is a polymer able to develop co-crystalline phases by solvent treatments<sup>19a,14</sup> therefore biaxially drawn films presenting planar oriented  $\alpha$  crystalline phase have been first treated to DCM vapours at room temperature leading to  $\delta$  co-crystalline phase including DCM guest molecules (Figure 2.4.1 C) and then guest extraction procedures have been performed leading to nanoporous  $\delta$  crystalline phase (Figure 2.4.1 D).

Substantial variations of the reflection intensities in the XRD

patterns with respect to the unoriented samples clearly point out the occurrence of strong molecular orientation. <sup>19a</sup> In particular, the (010) remains the most intense reflection while the (020), which is not detectable in unoriented samples, becomes second in intensity (Fig. 2.4.1 D). A better understanding of the crystalline orientation present in these films can be achieved using X-ray patterns taken with beams perpendicular and parallel to the film plane on a photographic cylindrical camera (Figure 2.4.2)

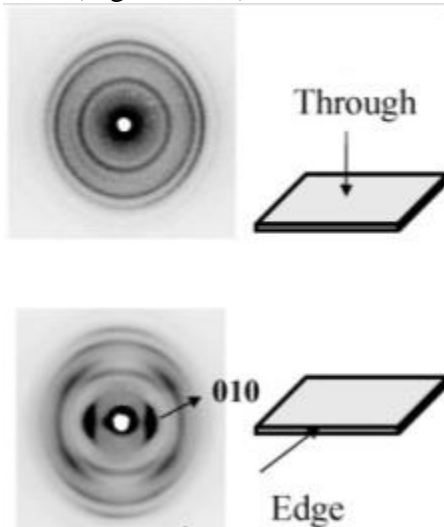


**Fig.2.4.2.** X-ray patterns taken with beams perpendicular (THROUGH) and parallel (EDGE) to the film plane on a photographic cylindrical camera of the  $\delta$  “uniplanar” oriented co-crystalline phase including DCM.

It is worth noting that the XRD patterns collected with beams perpendicular to the film plane show prevailing Debye-Scherrer rings, indicating that there is not any axial orientation in the film plane, whereas the X-ray patterns collected with beams parallel to the film plane show arcs rather than Debye Scherrer rings. In particular, XRD patterns obtained with the beam parallel to the film plane show a very intense reflection due to the (010) crystallographic planes, which disappears in XRD patterns obtained with the beam perpendicular to the film plane.

This indicates that the (010) planes (i.e., the *ac* planes) of the crystallites tend to be parallel to the film plane, i.e., the so called  $a_{//c_{//}}$  “uniplanar” orientation occurs<sup>.19a,14a,f,g</sup>

Hermans’ orientation factors,  $f$ , measured for  $\delta$ -form films presenting  $a_{//c_{//}}$  uniplanar orientation is 0.8.

Shrinkage value measured on sPS  $\delta$  co-crystalline films showing  $a_{//c_{//}}$  uniplanar orientation and including DCM guest molecules is nearly 16% (Photos of biaxially stretched films before (B’) and after (C’) crystallization procedure are reported in fig 2.4.1 B’-C’) whereas negligible shrinkage values have been measured on the same films after guest removal procedures leading to nanoporous  $\delta$  crystalline phase presenting analogous kind and degree of crystalline phase ( $a_{//c_{//}}$  uniplanar orientation).

#### **2.4.4 Amorphous sPS film**

X-ray diffraction patterns of s-PS films, amorphous (A) or presenting different kinds and degrees of oriented  $\delta$  co-crystalline phases are reported in Figure 2.4.3 (B-C).

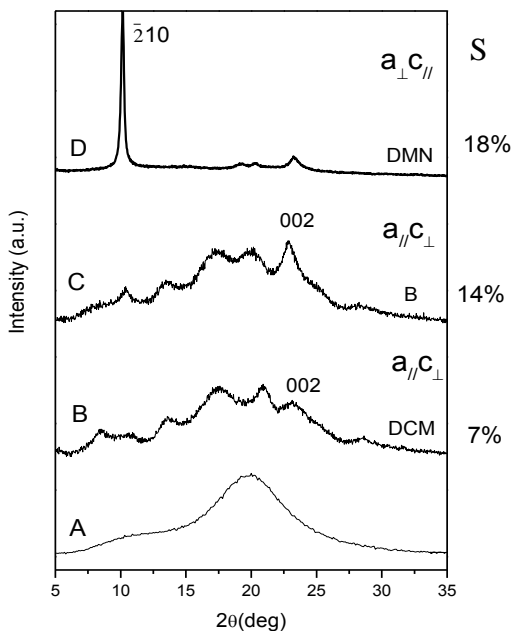


**Fig.2.4.3** X-ray diffraction collected by an automatic powder diffractometer of uniplanar orientation of  $\delta$  *co*-crystalline phases including DCM (B), B(C) and DMNP (D) guest molecules. The orientations can be defined as  $a_{//}c_{\perp}$ , (B-C) and  $a_{\perp}c_{//}$  (D) uniplanar ; for sake of comparison the amorphous is also reported (A) and shrinkage values (S) are also indicated

In particular, the patterns of Figure 2.4.3 B-C refer to films presenting  $\delta$  *co*-crystalline phases including DCM (B) and Benzene (C) guest molecules that showing  $a_{//}c_{\perp}$  crystalline phase orientation; Hermans' orientation factors,  $f$ , measured on these films is close to 0.5 (B) or 0.65 (C) respectively. This kind of orientation can be rationalized by the orientation of the chain axes  $c$  of the crystalline phases preferentially perpendicular to the film plane. The pattern of Figure 2.4.3 D refers to film presenting  $\delta$  *co*-crystalline phases including 1,4 dimethyl- naphthalene (DMN) and showing a different kind of uniplanar orientation named  $a_{\perp}c_{//}$ , with an Hermans'

orientation factors,  $f$ , close to 0.85.

This kind of orientation can be rationalized by the orientation that exhibits the  $a$  axis of the crystallographic  $ac$  plane preferentially perpendicular to the film plane.

The content of the guest molecules in all films was determined by thermogravimetric measurements and it was in the range 9-15%. Shrinkage values measured on sPS cocrystalline films after crystallization by using DCM, benzene and 1,4 dimethylnaphtalene guest molecules are 7%, 14% and 18% respectively.

Negligible shrinkage values have been measured on the same films after guest removal procedures leading to nanoporous  $\delta$  crystalline phase with  $a_{//}c_{\perp}$  or  $a_{\perp}c_{//}$  uniplanar orientations. It is apparent that the higher shrinkage values were observed on polymeric films presenting a more high degree of crystalline phase orientation. In particular the shrinkage seems to be strongly related to the degree of crystalline phase orientation while it seems to be independent or not influenced by the kind of crystalline phase orientation.

In order to minimize or even to erase the shrinkage in sPS cocrystalline films occurs during the co crystallization procedures we have annealed amorphous films at 130°C for different times, leading to mesomorphic trans planar phase, as well as at 220°C leading to unoriented  $\alpha$  crystalline phase.

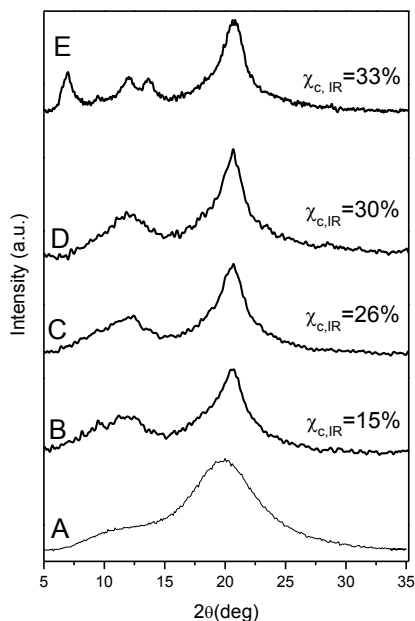


**Fig 2.4.4** X-ray diffraction patterns of s-PS films annealed at different temperatures: (A), mesomorphic trans-planar (B-D) obtained by annealing amorphous films at 130°C for 1h (B), 2h (C), 3h (D), and crystalline  $\alpha$  form films (E), and different crystallinity degree ( $\chi_c$ ) is indicated

X ray diffraction patterns (fig.2.4.4 A-E) as well as FTIR spectra (fig 2.4.5 (A'-E')-(A''-E'')) in the wavenumber range 1130-1260  $\text{cm}^{-1}$  and 925-885  $\text{cm}^{-1}$  are reported.

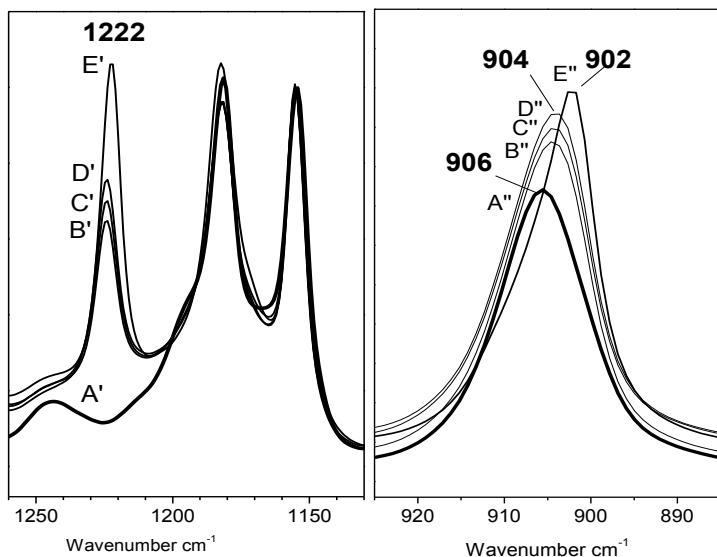


**Fig 2.4.5** FTIR transmission spectra in the wavenumber range 1130-1260  $\text{cm}^{-1}$  of amorphous s-PS film after annealing: (A'), mesomorphic trans-planar (B'-D') obtained by annealing amorphous films at 130°C for 1h (B'), 2h (C'), 3h (D'), and crystalline  $\alpha$  form films (E') and 925-885  $\text{cm}^{-1}$  (A''-E'')

In particular, FTIR spectra show the presence of a peak located at  $1222\text{cm}^{-1}$ , which corresponds to a vibrational mode<sup>20</sup> associated with chains presenting the trans planar conformation; on the other hand, the peak at  $904\text{cm}^{-1}$ , in between the peak at  $906\text{cm}^{-1}$  associated with the amorphous phase and the peak at  $902\text{cm}^{-1}$  associated with the  $\alpha$  trans-planar crystalline phase, clearly confirm the occurrence of a trans planar mesomorphic phase.

The degrees of crystallinity ( $\chi_{c,IR}$ ) of these films were evaluated based on peak at  $1222\text{cm}^{-1}$  by FTIR spectra and they were in the range 15-35%

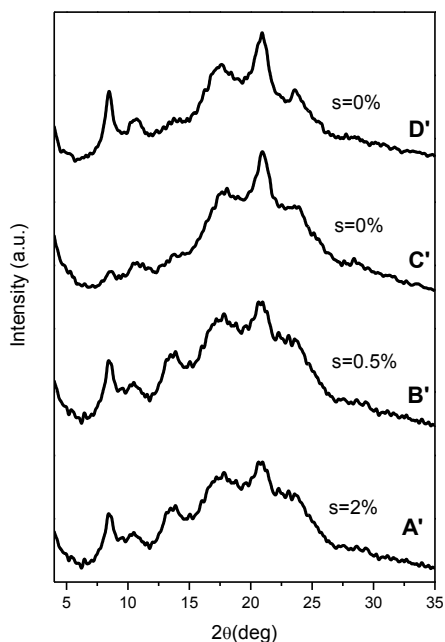


**Fig. 2.4.6** X ray diffraction patterns of mesomorphic trans-planar (A-C), as well as crystalline  $\alpha$  form films (D) after exposition to DCM vapors for 15-30 minutes respectively. Shrinkage values (s) are also reported.

We have exposed mesomorphic trans-planar as well as  $\alpha$  crystalline films to DCM vapors for 15 and 30 minutes respectively and crystallization in  $\delta$  co crystalline phase occurs; the corresponding XRD patterns are shown in Fig. 2.4.6. The degrees of crystallinity of these films evaluated XRD measurements ( $\chi_c$ ) are similar the degrees of crystallinity ( $\chi_{c,IR}$ ) and they are in the range 28-35%.

Shrinkage values measured on these films goes from 2% down to 0% as reported in Fig. 2.4.6.

In particular it is apparent that the degree of crystallinity of the starting films plays a big role.

In fact, by increasing the degree of crystallinity of the starting films the shrinkage values decrease (as show in fig 2.4.7): the shrinkage is close to 2% for starting films presenting a mesomorphic trans-planar phase with  $\chi_{c,IR} \approx 15\%$  but it becomes  $\approx 0\%$  for starting films showing  $\alpha$  or mesomorphic

trans-planar crystalline phases with  $\chi_{c,IR} \geq 30\%$

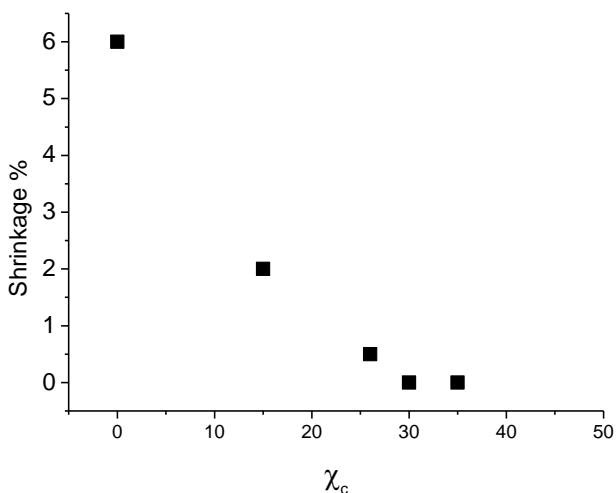


**Fig 2.4.7** The % shrinkage after crystallization procedure versus crystallinity degree  $\chi_{c,IR}$

#### **2.4.5 PP-sPS-PP film multilayer**

Thanks to the patented nanoporous sPS phase, sPS films can be made capable of removing by adsorption some of the gases involved in the production cycle of the plant, such as carbon dioxide and ethylene, responsible of the rapid maceration of vegetable product, thus prolonging 'the storage time ("shelf-life") of foods and reducing post-harvest treatments, resulting in energy savings and reduced environmental impact.<sup>11-13</sup>

The multilayer films with core layer of sPS could be used for packaging. For these applications, it is important to study the shrinkage caused by crystallization process in co-extruded films of polypropylene (PP) and syndiotactic polystyrene (sPS), in particular in PP-sPS-PP film.

In figure 2.4.8 a schematic image of PP-sPS-PP of multilayer is reported

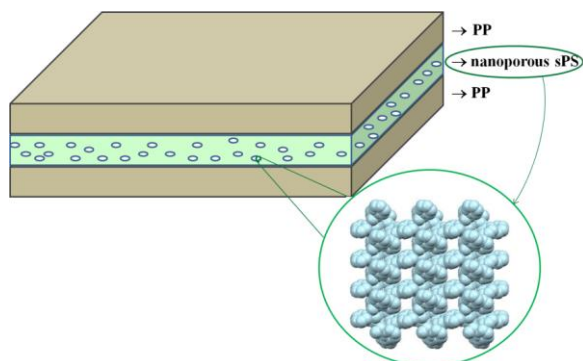


**Fig. 2.4.8** Multilayer film based on the common PP and including a core layer of nanoporous syndiotactic polystyrene (s-PS).

In figure 2.4.9 X-ray diffraction pattern of PP-sPS-PP film before (fig 2.4.9 A) and after (fig.2.4.9 B) crystallization process with eco-friendly solvents are reported (PP signals are indicated with the \*). In figure 2.4.9 B' only the X-ray diffraction pattern of a core layer of sPS, after crystallization process, is reported. Substantial variations of the reflection intensities in the XRD patterns with respect to the unoriented samples (Figure 2.4.9 C) clearly point out the occurrence of strong molecular orientation. In particular, the (010) remains the most intense reflection: it is apparent that this film presents 010 uniplanar orientation.

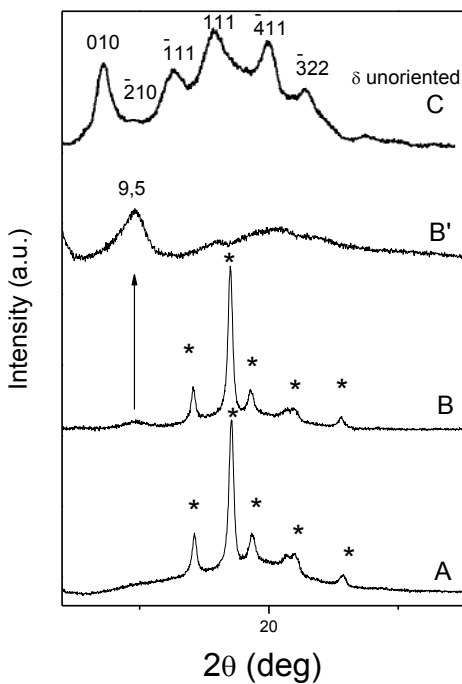


**Fig 2.4.9.** X-ray diffraction of: A) PP-sPS-PP film, B) PP-sPS-PP film after crystallization process (PP signals are indicated with the \*), B') only central sPS film after crystallization process, C) For comparison also unoriented  $\delta$  crystalline phase spectrum is reported

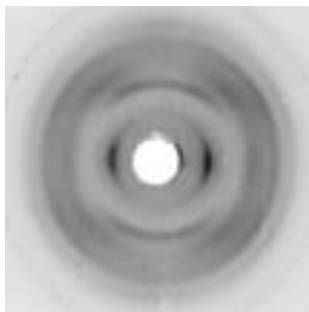


**Fig 2.4.10** X-ray diffraction patterns of s-PS films exhibiting the a//c// uniplanar orientation EDGE

In Fig. 2.4.10 the EDGE photographic X-ray diffraction patterns, i.e. the pattern taken by having the X-ray beam parallel to the film surface (and by placing the film sample parallel to the axis of the cylindrical camera), are reported. The EDGE photographic pattern of the  $\delta$  form film exhibit the  $a_{//}c_{\perp}$  uniplanar orientation.<sup>19a</sup>

In this case, the crystallization can occur without a significant shrinkage because the core sPS film is retained by the external PP films.

Moreover, these PP-sPS-PP films are used for packaging, for shelf life and thermal stress tests of iceberg salad, in Rago's firm.

In figure 2.4.11 the photographic images of three samples are reported:

- 1) PP-sPS-PP film with sPS amorphous film
- 2) PP-sPS-PP film with sPS crystallized with eco-friendly solvent

In each sample there is the same quantity of salad (100 g) and the test is conducted in no controlled atmosphere.



**Fig 2.4.11** Salad iceberg packaging in PP-sPS-PP films: 1) Amorphous 2) crystallized with eco-friendly solvent 3) crystallized with non-eco-friendly solvent. With symbol O maceration is indicated.

After 12 days, it apparent that the salad in sample 2 shows a lower degree of maceration than the salad in sample 1.

In figure 2.4.12 the photographic images of two samples are reported:

- 1) The BOPP (bi oriented polypropylene)
- 2) PP-sPS-PP film with sPS crystallized with eco-friendly solvent.



**Fig 2.4.12** Salad packaging in BOPP film and in PP-sPS-PP crystallized film. With symbol O maceration are indicated

It appantes that, after 12 day, the rotting of vegetable in BOPP film is faster than in PP-sPS-PP crystallized film.

### 2.4.6 Conclusion

We have investigated on the shrinkage behavior developed in syndiotactic polystyrene (sPS) films after co-crystallization procedures leading to co-crystalline phases, as well as after extraction procedures leading to  $\delta$  nanoporous crystalline phase, by using X-ray diffraction as well as FTIR measurements. High shrinkage values have been measured on biaxially drawn films presenting planar oriented  $\alpha$  crystalline phase exposed to solvent vapors; with this procedure  $\delta$  co-crystalline films, that show an high degree of  $a_{//c//}$  uniplanar crystalline phase orientation, have been obtained.

High shrinkage values have been also measured on amorphous sPS films exposed to various solvents; this procedure leads to the formation of  $\delta$  co-crystalline phases showing different kinds and degrees of crystalline phase orientations ( $a_{//c\perp}$  or  $a_{\perp c//}$ ).

Negligible shrinkage values have been measured, instead, on  $\delta$  co-crystalline films after guest removal procedures leading

to nanoporous  $\delta$  crystalline phases presenting both  $a_{//c//}$ ,  $a_{//c\perp}$  or  $a_{\perp c//}$  uniplanar orientations.

From a quantitative point of view this study has evidenced that the higher shrinkage values have been measured on polymeric films presenting a more high degree of crystalline phase orientation; in particular, the shrinkage seems to be strongly related to the degree of crystalline phase orientation while it seems to be independent or not heavily influenced by the kind of crystalline phase orientation.

Definitely lower shrinkage values have been measured on films presenting trans-planar mesomorphic or unoriented  $\alpha$  crystalline phases after their exposure to solvents. In this case, the transition toward  $\delta$  co-crystalline phases can occur without a significant shrinkage. Particularly relevant in this latter case is the degree of crystallinity of the starting films: high degree of crystallinity (close or higher than 30%) leads to negligible shrinkage values. The control of dimensional stability can be particularly relevant, from an industrial standpoint, in order to optimize manufacturing routes leading to industrial production of  $\delta$  nanoporous sPS films.

In the end of chapter we reported the tests of an industrial application of PP-sPS-PP film as films for packaging.

### **References**

1. Guerra G., Alburnia A.R., D'Aniello C. “SYNDIOTACTIC POLYSTYRENE *Synthesis, Characterization, Processing, and Applications*” J.Schellenberg, Eds., John Wiley & Sons, Inc, Hoboken, New Jersey 2009, p.194.
2. Mahesh K. P. O., Sivakumar M., Yamamoto Y., Tsujita Y., Yoshimizu H., Okamoto S., *J. Membr. Sci.* **2005**, 262, 11
3. Daniel C., Alfano D., Venditto V., Cardea S., Reverchon E., Larobina D., Mensitieri G., Guerra G., *Adv. Mater.* **2005**, 17, 1515.
4. Figueroa-Gerstenmaier S., Daniel C., Milano G., Vitillo J. G., Zavorotyńska O., Spoto G., Guerra G., *Macromolecules* **2010**, 43, 8594.
5. Alburnia A. R., Venditto V., Guerra G., *J. Polym. Sci., Part B:*

*Polym. Phys.* **2012**, 50, 1474.

6. Mensitieri G., Venditto V., Guerra G., *Sens. Actuat. B Chem* **2003**, 92, 255.

7. Cusano A., Iadicicco A., Pilla P., Contessa L., Campopiano S., Cutolo A., Giordano M., Guerra G., *J. Lightwave Technol.* **2006**, 24, 1776.

8. Pilla P., Cusano A., Cutolo A., Giordano M., Mensitieri G., Rizzo P., Sanguigno L., Venditto V., Guerra G., *Sensors* **2009**, 9, 9816.

9. Erdogan M., Ozbek Z., Capan R., Yagci Y., *J. Appl. Polym. Sci.* **2012**, 123, 2414.

10. Buonerba A., Cuomo C., Sanchez S. O., Canton P., Grassi A., *Chem. Eur. J.* **2012**, 18, 709.

11. Alburnia A. R., Minucci T., Guerra G., *J. Mater. Chem.* **2008**, 18, 1046.

12. Larobina D., Sanguigno L., Venditto V., Guerra G., Mensitieri G., *Polymer* **2004**, 45, 429.

13. Annunziata L., Alburnia A. R., Venditto V., Guerra G., *Macromolecules* **2006**, 39, 9166.

14. a) P. Rizzo, A.R. Alburnia, G. Milano, V. Venditto, G. Guerra, G. Mensitieri, L. Di Maio *Macromol. Symp.* **2002**, 185, 65; b) P. Rizzo, A. Costabile, G. Guerra *Macromolecules* **2004**, 37, 3071; c) P. Rizzo, S. Della Guardia, G. Guerra *Macromolecules* **2004**, 37, 8043; d) P. Rizzo, A. Spatola, A. De Girolamo Del Mauro, G. Guerra *Macromolecules* **2005**, 38, 10089; e) C. Daniel, A. Avallone, P. Rizzo, Guerra G *Macromolecules* **2006**, 39, 4820; f) A.R. Alburnia, L. Annunziata, G. Guerra *Macromolecules* **2008**, 41, 2683; g) A.R. Alburnia, P. Rizzo, O. Tarallo, V. Petraccone, Guerra G *Macromolecules* **2008**, 41, 8632; h) A.R. Alburnia, P. Rizzo, G. Guerra *Chem. Mater.* **2009**, 21, 3370. i) P. Rizzo, A.R. Alburnia, *Macromolecular Chemistry and Physics* **2011**, 212,1419 j) P. Rizzo, A. R. Alburnia, G. Guerra *Macromolecular Chemistry and Physics* **2012**, 210, 2148

15. a) A.R. Alburnia, A. Grassi, G. Milano, P. Rizzo, V. Venditto, P. Musto , G. Guerra *Macromol. Symp.* **2006**, 234, 102. b) A. R. Alburnia, P. Rizzo, G. Guerra *Polymer* **2013**, 54, 1671

16. a) C. Daniel, A.R. Alburnia, C. D'Aniello, P. Rizzo, V. Venditto, G. Guerra *J.Eur.Opt.Soc.-Rapid Publ.* **2009**, 4, 09037; b) Y. Uda, F. Kaneko, N. Tanigaki, T. Kawaguchi *Adv. Mater.* **2005**, 17, 1846; c) A.R. Alburnia, C. D'Aniello, G. Guerra, D. Gatteschi, M. Mannini, L. Sorace *Chem. Mater.* **2009**, 21, 4750. d) A. R. Alburnia,

- P. Rizzo, M. Coppola, M. De Pascale, G. Guerra *Polymer* **2012**, 53,2727.
- 17.** a) G. Milano, G. Guerra, F. Muller-Plathe *Chem. Mater.* **2002**, 14, 2977; b) V. Venditto, A. De Girolamo Del Mauro, G. Mensitieri, G. Milano, P. Musto, P. Rizzo, G. Guerra *Chem. Mater.* **2006**, 18, 2205; c) L. Annunziata, A.R. Alburnia, V. Venditto, G. Guerra, *Macromolecules* **2006**, 39, 9166; d) A.R. Alburnia, T. Minucci, G. Guerra *J. Mater. Chem.* **2008**, 18, 1046. e) A.R. Albuni, P. Rizzo, G. Ianniello, C. Rufolo, and Gaetano Guerra *Journal of Polymer Science Part B: Polymer Physics* **2014**, 52,657-665
- 18.** a) A.R. Alburnia, P. Rizzo, G. Guerra, F.J. Torres, B. Civalleri, C.M. Zicovich-Wilson *Macromolecules* **2009**, 40, 3895; b) F.J. Torres, B. Civalleri, A. Meyer, P. Musto, A.R. Alburnia, P. Rizzo, G. Guerra *J. Phys. Chem. B* **2009**, 113, 5059.
- 19.** a) P. Rizzo, M. Lamberti, A.R. Alburnia, O. Ruiz de Ballesteros, G. Guerra *Macromolecules* **2002**, 35, 5854; b) A. Immirzi, F. De Candia, P. Iannelli, V. Vittoria, A. Zambelli *Makromol. Chem. Rapid. Commun.* **1988**, 9, 761.
- 20.** G.Schoukens, P.Samyn, S.Maddens, T.an Audenaerde *J. Appl. Polym. Sci.* **2003**, 87, 1462

## Chapter 3

### Chiral optical response of sPS co-crystalline Films

#### 3.1 Introduction

Chiral optical materials are often based on macromolecules, not only due to typical advantages of polymeric materials (e.g., processability, robustness, and durability) but also due to the amplification of chirality associated with the formation of polymer helices with prevalence of one-handedness.<sup>1</sup>

Intense chiral optical responses have been also observed for macromolecular racemic receptors interacting with target nonracemic guests, mainly for polymers in solution<sup>1h-1</sup> and more recently also in the solid state.<sup>2,3</sup> The induction of circular dichroism (CD) in racemic solid polymers is generally associated with the formation of polymer cocrystalline phases,<sup>4</sup> constituted by helical polymer host and nonracemic low molecular-mass guest molecules. It is worth adding that, because regular polymer helical stretches in crystalline phases are generally much longer than in solutions, the chiral amplification phenomena in the solid state are generally much more intense than in solution.

The induction and amplification of chirality in racemic polymers by cocrystallization with nonracemic guest molecules can occur by both molecular and supramolecular mechanisms. For the molecular mechanism,<sup>2</sup> observed for syndiotactic poly(p-methylstyrene)<sup>2a,b</sup> and poly(2,6-dimethyl-1,4-phenylene oxide) (PPO),<sup>2c</sup> a nonracemic guest induces the formation of cocrystals with nonracemic unit cell, where polymer chains exhibit only one-sense of helicity. For the supramolecular mechanism, observed for syndiotactic polystyrene (s-PS),<sup>3</sup> the nonracemic guest induces the formation of nonracemic helical crystallites based on a racemic unit cell (including both right and left-handed polymer helices). Because of its supramolecular nature, the chiral optical response of s-PS remains essentially unaltered not only after the nonracemic guest removal (leading to the nanoporous crystalline  $\delta$  phase<sup>5</sup>) but also after thermal treatments (leading to the dense helical  $\gamma$  phase<sup>6</sup> or to the

trans-planar  $\alpha$  phase<sup>7</sup>) and can be erased only after thermal treatments at temperatures higher than the s-PS melting temperature ( $\approx 270$  °C).

Recently, s-PS-based films with intense chiral optical responses at visible wavelengths have been obtained by exchanging the nonracemic guest with achiral chromophores, provided that (i) the initial crystallization of s-PS has been induced by a nonracemic guest from an amorphous phase and (ii) the chromophore molecules are suitable guest of a s-PS cocrystalline form.<sup>8</sup> s-PS cocrystalline forms exhibit, as a common feature,  $s(2/1)2$  helical polymer conformation (Figure 3.1),<sup>9</sup> while the packing can largely change mainly depending on the molecular structure of the guest molecules,<sup>4</sup> leading to three classes:  $\delta$ -clathrates,<sup>10</sup> intercalates,<sup>11</sup> and  $\epsilon$ -clathrates.<sup>12</sup> In the present paper, we will deal with films exhibiting  $\delta$ -clathrate forms, i.e., cocrystalline forms presenting isolated centrosymmetric guest locations, cooperatively generated by two enantiomorphous helices of two adjacent ac polymer layers (Figure 3.1). In particular, the blue and yellow chiral optical films considered in this paper exhibit the  $\delta$ -clathrate monoclinic and triclinic forms with azulene<sup>8</sup> and 4-nitroaniline (NA)<sup>10e</sup> (Figures 3.1A and 3.1B), respectively.

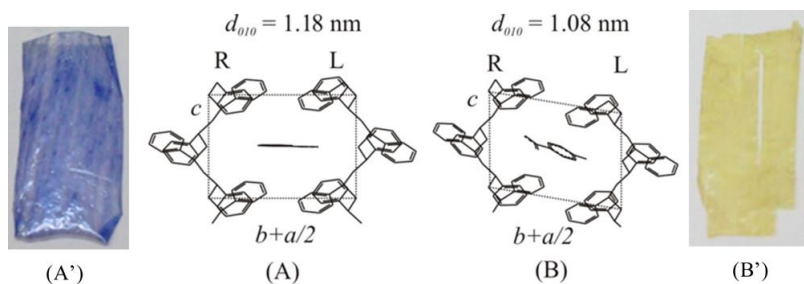


**Fig. 3. 1.** Packing of  $\delta$ -clathrates of s-PS with azulene (A, monoclinic) and NA (B, triclinic). Only a couple of enantiomorphous polymer helices (R = right-handed, L = left-handed) that confine the guest molecule are shown. The NA guest (B) is accommodated by the shifting the ac layers along the chain axis, leading to the triclinic symmetry. Blue (A') and yellow (B') s-

PS films exhibiting the  $\delta$ - clathrate forms with azulene and NA, respectively.

The above-described chiral optical behaviors have been observed not only for thin films as obtained by spin coating (typical thickness of 0.1  $\mu\text{m}$ )<sup>3,8</sup> but also for thick films as obtained by melt extrusion (typical thickness of 20  $\mu\text{m}$ ).<sup>3d,8</sup> In this paper, we compare the chiral optical responses of meltextruded films of different thickness, exhibiting azulene and NA chromophore guests. To better discriminate between the chiral optical response of the polymer host and of the low-molecularmass guests, vibrational circular dichroism (VCD) studies are also reported, with quantitative evaluations of the degree of circular polarization for relevant host and guest peaks

### **3.2 Induction of chirality in melt-extruded s-PS films of different thickness by cocrystallization with a nonracemic guest.**

Fourier transform infrared (FTIR) and VCD spectra of amorphous s-PS films, having a thickness of nearly 20 and 6  $\mu\text{m}$ , after sorption of nonracemic carvone for 1 h at room temperature are shown in Figure 3. 2. In particular, the VCD spectra as obtained after sorption of (R)-(-) carvone and (S)- (+) carvone are shown as red thin and blue thick lines, respectively.

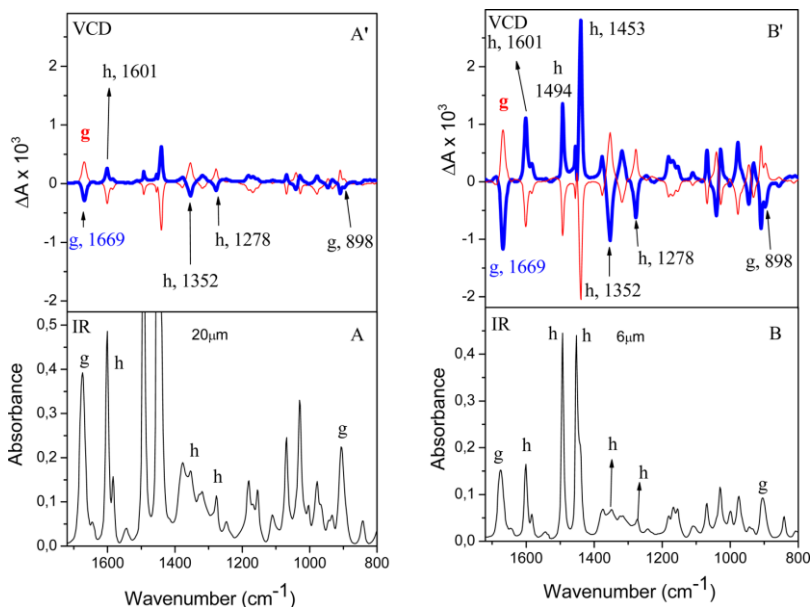


**Fig 3.2.** FTIR (A, B) and VCD spectra (A' , B' ) of amorphous s-PS films, having a thickness of nearly 20  $\mu\text{m}$  (A, A' ) or 6  $\mu\text{m}$  (B, B' ), after crystallization induced by sorption of (R)-(-) carvone (thin red line) or (S)-(+ carvone (thick blue line). The main peaks of the carvone guest are labeled by “g” while some typical peaks of the polymer host are indicated by “h”.

**Table 3. 1.** Degree of circular polarization for some peaks of the carvone guest (gg/carvone), of the polymer host (gh), and of azulene guest (gg/azulene) as evaluated by VCD and CD spectra of sPS films with thickness of 6 and 20  $\mu\text{m}$

| film thickness ( $\mu\text{m}$ ) | gg/carvone                |                           | gh                           |                              | gg/azulene         |                           |                    |
|----------------------------------|---------------------------|---------------------------|------------------------------|------------------------------|--------------------|---------------------------|--------------------|
|                                  | 1669 ( $\text{cm}^{-1}$ ) | 1601 ( $\text{cm}^{-1}$ ) | 1352 ( $\text{cm}^{-1}$ ) cr | 1277 ( $\text{cm}^{-1}$ ) cr | 269 nm             | 1392 ( $\text{cm}^{-1}$ ) | 600 nm             |
| 6                                | $7 \times 10^{-3}$        | $7 \times 10^{-3}$        | $1 \times 10^{-2}$           | $1 \times 10^{-2}$           | $4 \times 10^{-2}$ | $1 \times 10^{-2}$        | $4 \times 10^{-2}$ |
| 20                               | $7 \times 10^{-4}$        | $7 \times 10^{-4}$        | $1 \times 10^{-3}$           | $1 \times 10^{-3}$           | n.a.               | $1 \times 10^{-3}$        | $1 \times 10^{-2}$ |

<sup>a</sup>n.a. = not available, cr = vibrational peak of the s(2/1)2 helices of the crystalline phase.

For both films, according to thermogravimetric analyses, the carvone content is close to 8 wt %.

On inspection of Figure 3.2, it is immediately apparent that the thinner (6  $\mu\text{m}$ ) film presenting lower absorbance peaks (Figure 3.2B) unexpectedly presents much more intense VCD

peaks (Figure 3.2B'). Quantitative evaluations of the degree of circular polarization  $g$  for some host (gh) and guest (gg) peaks, collected in columns 2–5 of Table 3.1, indicate that by reducing the film thickness from 20 to 6  $\mu\text{m}$ , there is an increase of the degree of circular polarization of nearly 1 order of magnitude.

The spectra of Figure 3.2 and the derived data of Table 3.1 also indicate that the degree of circular polarization is higher for the racemic host than for the nonracemic guest, mainly for the crystalline helical peaks (like those at 1352 and 1277  $\text{cm}^{-1}$ , collected in columns 4 and 5 of Table 1) being associated with a single vibrational mode of the s(2/1)2 polymer helix.<sup>9c,d</sup>

UV and CD spectra of melt-extruded s-PS amorphous films, with a thickness of  $\sim 6 \mu\text{m}$ , after crystallization induced by immersion in pure (R)-(-) carvone (red thin line) or (S)-(+)-carvone (blue thick line), are shown in Figures 3.3 A and 3.3 B, respectively. These spectra do not change significantly after complete carvone removal (as, for instance, achieved by treatment with acetonitrile at room temperature for 1 h).

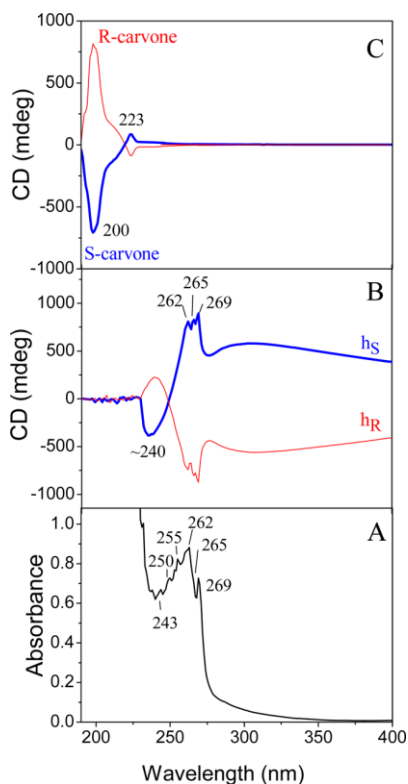


**Fig. 3.3** UV-vis (A) and CD (B) spectra of s-PS amorphous films, with a thickness of  $\sim 6 \mu\text{m}$ , after (R)-(-) carvone (red thin line) or (S)-(+) carvone (blue thick line) induced crystallization. (C) CD spectra of s-PS spin-coated amorphous films, having a thickness of  $\sim 0.3 \mu\text{m}$ , subjected to the same treatments.

The UV spectrum clearly shows typical absorbance peaks of polystyrene,<sup>10</sup> while the CD spectra show intense peaks at 262, 265, and 269 nm and a less intense ill-defined band of opposite sign below 250 nm. These polystyrene CD peaks were not accessible for much thinner spin-coated films ( $0.3 \mu\text{m}$ ), which only show intense peaks located at 200 and 223 nm (Figure 3.3C),<sup>3</sup> neither for thicker films ( $20 \mu\text{m}$ ), which present a too high absorbance in this spectral region.<sup>8a</sup> It is worth adding that the degrees of circular polarization as evaluated for the UV host peaks from the spectra of Figure 3.3 (e.g., for the 269 nm peak  $g = 4 \times 10^{-2}$ , column 6 of Table

3.1) are also higher than those evaluated for the IR helical host peaks ( $g = 1 \times 10^{-2}$ , columns 4 and 5 of Table 1). AFM images of a melt-extruded chiral optical s-PS film, having a thickness of 6  $\mu\text{m}$  like those of Figures 3.2 and 3.3, are presented in Figure 3.4.

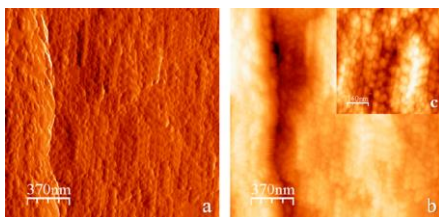


**Fig. 3. 4.** AFM images for a s-PS melt-extruded amorphous film, with a thickness of 6  $\mu\text{m}$ , after carvone-induced crystallization: (a) the real topography of the sample, root-mean-square roughness (rms): 37.2 nm; (b, c) AFM amplitude signal used to highlight changes in surface height, expressed at a scale of 370 nm (b) and 160 nm (c), respectively

The images show closely packed and highly aligned helical crystallites, similar (although much more concentrated) to those reported for spin-coated s-PS chiral optical films with thickness of nearly 0.1  $\mu\text{m}$ <sup>3b</sup>. This morphology remains essentially unchanged after guest removal as well as after thermal treatments above the helix  $\rightarrow$  trans-planar ( $\gamma \rightarrow \alpha$ ) host transition.

It is well-known that, for many different systems,<sup>11</sup> the molecular chirality is expressed at a scale of nanometers and micrometers, giving rise to coiled fiber structures that are observable by microscopic techniques. The same effect is observed here for s-PS film, although the molecular chirality only characterize the temporary cocrystallizing guest.

### 3.3 Chiral optical polymer films with achiral chromophores.

The chiral s-PS films as obtained by cocrystallization with a nonracemic guest have been treated with two different chromophores, whose size is suitable to fit the crystalline cavity of the nanoporous  $\delta$  phase,<sup>5a,b</sup> i.e., azulene and

4-nitroaniline (NA) (Figure 3.1). The reported results have been achieved by direct guest exchange.<sup>12</sup> Similar results are also obtained by chromophore sorption in empty  $\delta$  form films,<sup>5</sup> if their crystallization had occurred from the amorphous phase by cocrystallization with nonracemic carvone, followed by carvone desorption.

FTIR and VCD spectra of s-PS films, having a thickness of nearly 20 and 6  $\mu\text{m}$ , after exchange of nonracemic carvone guests with the achiral azulene guest, with an azulene content close to 14 wt %, are shown in Figure 3.5.

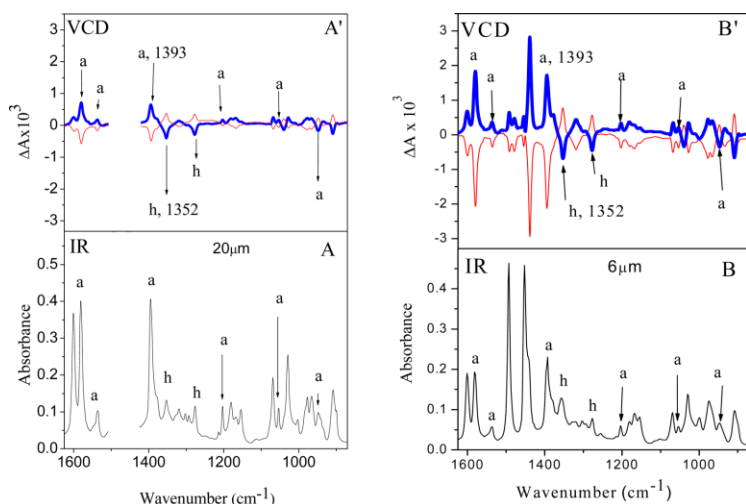


**Fig. 3.5.** FTIR (A, B) and VCD spectra (A', B') of s-PS films, having a thickness of nearly 20  $\mu\text{m}$  (A, A') or 6  $\mu\text{m}$  (B, B'), after crystallization induced by (R)-(-) carvone (thin red line) or (S)-(+)-carvone (thick blue line) and exchange of the nonracemic carvone guest with the achiral azulene guest. The azulene content is close to 14 wt %. The main peaks of the azulene guest molecules are labeled by “a” while some typical polymer host peaks are indicated by “h”.

On inspection of Figure 3.5, it is immediately apparent that again the thinner film presenting lower absorbance peaks (Figure 3.5B) presents much more intense VCD peaks (Figure 3.5 B'), with increases of degree of circular polarization both for host and guest peaks of nearly 1 order of magnitude. In particular, g-values for the azulene peak at 1393  $\text{cm}^{-1}$

(*gg*/azulene, column 7 of Table 3.1) are close to  $1 \times 10^{-3}$  and  $1 \times 10^{-2}$  for the films having thickness of 20 and 6  $\mu\text{m}$ , respectively.

UV and CD spectra of the s-PS films, with a thickness of 20 and 6  $\mu\text{m}$ , after crystallization induced by (R)-(-) carvone (red thin line) or (S)-(+) carvone (blue thick line) and after exchange of the nonracemic carvone guests with the achiral azulene guest, are compared in Figures 3. 6A and 3.6B.

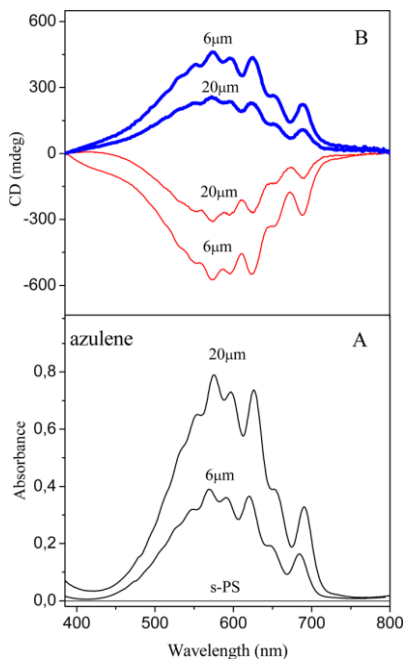


**Fig. 3.6.** Visible (A) and CD (B) spectra, in the range 400–800 nm, of s-PS films, with thickness of 20 and 6  $\mu\text{m}$ , after (R)-(-) carvone (red thin line) or (S)-(+) carvone (blue thick line) induced crystallization and replacement of the nonracemic carvone guests with the achiral azulene guest

The CD spectra present the whole azulene band in the range 450–710 nm,<sup>13</sup> which is negative or positive depending on the S or R chirality of the carvone used to induce the initial crystallization to amorphous s-PS<sup>8a</sup>. The spectra of Figure 3.6 show that, also for the visible region, the thinner film (6  $\mu\text{m}$ )

presents definitely more intense CD bands (Figure 3.6B), although presents a much less intense absorbance band (Figure 3.6A).

Quantitative evaluations of degree of circular polarization for the azulene visible band in the range 450–710 nm, based on the spectra of Figure 3.6A and 3.6B, show  $g$ -values close to  $1 \times 10^{-2}$  and  $4 \times 10^{-2}$ , for sPS films with a thickness of 20 and 6  $\mu\text{m}$ , respectively (column 8 of Table 3.1), thus confirming the higher chiral optical response of the thinner film.

FTIR and VCD spectra of s-PS films exhibiting the  $\delta$  clathrate phase with NA, with a thickness of 6  $\mu\text{m}$  and NA content of 1.7 wt %, are shown in Figures 7A and 7B, respectively. Degrees of polarization of the NA vibrational peaks ( $g_{\text{NA}}$ ) are similar to those observed for the azulene guest and definitely higher than those observed for the nonracemic carvone guest, e.g., for the peak at  $1620\text{ cm}^{-1}$ ,  $g_{\text{NA}} = 1 \times 10^{-2}$ . The  $\text{NH}_2$  deformation region of the FTIR and VCD spectra of Figures 3.7A and B has been enlarged in Figures 3.7B and B', respectively, where the spectra of the same sample not washed with acetonitrile and exhibiting a higher NA content (3.5 wt %) are also added.

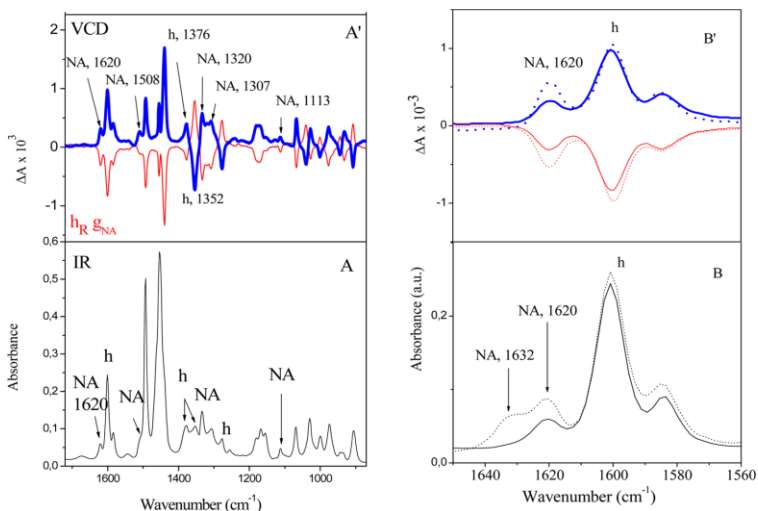


**Fig. 3.7.** FTIR (A, B) and VCD (A', B') spectra of s-PS film, having a thickness of nearly 6  $\mu\text{m}$ , after crystallization induced by (R)-(-) carvone (thin red line) or (S)-(+ carvone (thick blue line) and after exchange of the nonracemic carvone guest with the achiral NA guest. The main peaks of NA guest molecules are labeled by "NA" while some typical peaks of polymer host are indicated by "h". (B, B') Spectral comparison in the 1650–1560  $\text{cm}^{-1}$  region for films with NA content of 3.5 and 1.7 wt %, as obtained without (dotted line) and with (continuous line) washing with acetonitrile, respectively.

The FTIR spectra of Figure 3.7B indicate that there is a fraction of NA (peak at  $1632\text{ cm}^{-1}$ ) which is more easily removed from the s-PS sample and another fraction (peak at  $1620\text{ cm}^{-1}$ ) that is partially retained after the washing procedure. The VCD spectra of Figure 7B' show that only the  $1620\text{ cm}^{-1}$  peak is dichroic while the  $1632\text{ cm}^{-1}$  is completely absent from the VCD spectra.

These results clearly suggest that the nondichroic  $1632\text{ cm}^{-1}$  peak is associated with NA molecules included in the amorphous phase while the dichroic peak located at  $1620\text{ cm}^{-1}$  is associated with NA molecules included in the chiral crystalline phase. This confirms the previous conclusion (based on comparison between VCD data of azulene molecules being guest of chiral s-PS film exhibiting  $\delta$  or  $\alpha$  crystalline forms)<sup>8a</sup> that the chiral optical response of achiral

guest chromophores only occurs when such molecules are included as guest in the nanoporous crystalline phase, rather than simply dissolved in the amorphous phase.

The UV-vis and CD spectra of s-PS 6  $\mu\text{m}$  films, exhibiting the  $\delta$  clathrate form with NA, with a NA content close to 1.7 wt %, whose FTIR and VCD spectra are shown in Figure 3.7 are shown in Figure 3.8.

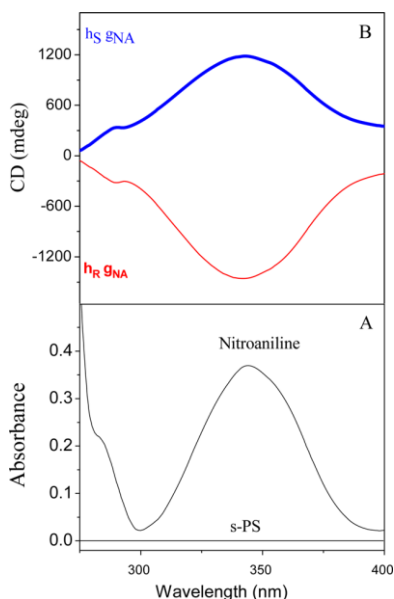


**Fig. 3.8.** UV-vis (A) and CD (B) spectra, in the range 275–400 nm, of s-PS 6  $\mu\text{m}$  films, exhibiting the  $\delta$  clathrate phase with NA, with NA content close to 1.7 wt %. Thin red line and thick blue line correspond to films first crystallized by sorption of (R)-(–) carvone or (S)-(+ carvone, respectively.

As usual, thin red lines and thick blue lines correspond to films first crystallized by sorption of (R)-(–) carvone or (S)-(+ carvone, respectively. The UV-vis spectrum shows the broad band of NA, in the range 300–400 nm,<sup>12</sup> as well as a minor broad band (present as a shoulder) in the range 275–290 nm. In the corresponding CD spectra, both bands are negative or positive depending on the R or S chirality of the carvone used to induce crystallization in amorphous s-PS. The

degree of circular polarization of the band centered at 343 nm is particularly high ( $g = 1 \times 10^{-1}$ ). This high  $g$ -value is possibly due to the inclusion of most chromophore molecules in the chiral crystalline phase, as clearly proved by the  $\text{NH}_2$  deformation region of the FTIR and VCD spectra of Figure 3.7

### **3.4 Considerations relative to $g$ -value variations with film thickness.**

As for the dependence of the degree of circular polarization on the thickness of chiral optical films, two different behaviors are generally observed. For some types of polymer films,  $g$ -value is independent of the thickness of the film and, as a consequence, can be considered an intensive property,<sup>14</sup> as generally occurs for  $g$  of dilute solutions of nonracemic molecules. In contrast, for other polymer films,  $g$  value is an extensive property and increases with the thickness of the film, and the origin of the chiral optical effect is extrinsic to the site of photon absorption.<sup>14c,15</sup> As for the chiral optical behavior of melt-extruded s-PS films, as induced by cocrystallization with nonracemic guest molecules, we presently show an unusual strong increase of  $g$  with decreasing the thickness from 20 to 6  $\mu\text{m}$ . This thickness dependence of  $g$ , because the chiral optical effect is due to the chiral morphology of s-PS crystallites,<sup>3,8</sup> can be rationalized by a more efficient formation of chiral crystallites close to the film surfaces (possibly due to higher carvone concentration).

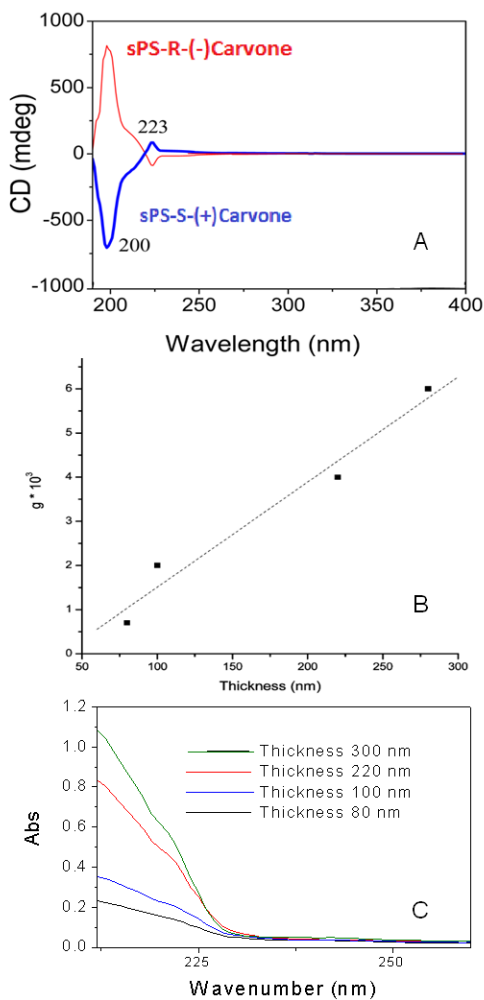
Also relevant is a comparison with the degree of circular polarization of host and guest peaks of thin spin-coated sPS films. In particular, for a spin-coated film with thickness of 0.1  $\mu\text{m}$ ,  $g$ -values for UV peaks of polymer host ( $g_h$ ) and of azulene guest ( $g_g/\text{azulene}$ ), as evaluated by the spectra of ref 8a, are reported in Table 2. A comparison of the data of Table 2 with those of the third row of Table 1 shows that the  $g$ -values of the 0.1  $\mu\text{m}$  film are roughly of 1 order of magnitude lower than those of 6  $\mu\text{m}$  films. In fact, all measured  $g$  for the 6  $\mu\text{m}$  film are in the range  $7 \times 10^{-3-4} \times 10^{-2}$  (third row of

Table 3.1) while for 0.1  $\mu\text{m}$  film are in the range  $1 \times 10^{-3-4} \times 10^{-3}$  (Table 3.2).

**Table 3.2.** Degree of circular polarization for a host peak ( $g_h$ ) and of two azulene guest peaks ( $g_{g/\text{azulene}}$ ) as evaluated by UV and CD Spectra on chiral sPS films with thickness of 0.1  $\mu\text{m}$ <sup>8b</sup>

| film thickness ( $\mu\text{m}$ ) | $g_h$              | $g_{g/\text{azulene}}$ |                    |
|----------------------------------|--------------------|------------------------|--------------------|
|                                  | 223 nm             | 280 nm                 | 340 nm             |
| 0.1                              | $2 \times 10^{-3}$ | $4 \times 10^{-3}$     | $1 \times 10^{-3}$ |

This suggests an extensive nature of  $g$  for s-PS chiral optical films, which well agrees with the chirality being extrinsic to the site of photon absorption. In order to better investigate on the dependence of the degree of circular polarization on the thickness of s-PS chiral optical films, films from chloroform solutions have been prepared by spin-coating procedures. These films, having thickness in the range 0.08–0.3  $\mu\text{m}$ , have been exposed to nonracemic carvone for 1 h at room temperature and their degrees of circular polarization have been reported in Figure 3.9. In figure 3.9 A CD spectra are reported, in particular the CD spectra of polystyrene show intense peaks located at 200 and 223 nm, the degrees of circular polarization are evaluated on the band at 223 nm. The absorbance spectra of the respective films with varying thickness are shown in Figure 3.9 C. From the CD and the absorption spectrum,  $g_{\text{aps}}$  can be calculated by equation reported in experimental section (Chapter 5 section 5.2.2 equation 6), it is apparent that this  $g$ -value linearly depends on film thickness (fig 3.9 B) and reach a value of  $6 \times 10^{-3}$  for the  $\sim 0.3 \mu\text{m}$  thick films, in this case  $g_{\text{abs}}$  is not an intensive property of the material.



**Fig. 3. 9.** (A) CD spectra of film (thickness 300 nm), after (R)-(-) carvone (red thin line) or (S)-(+)-carvone (blue thick line) induced crystallization; (B) Degree of circular polarization as a function of film thickness for sPS spin-coated films; (C) UV Absorbance spectra of sPS spin-coated films.

This result definitively confirms the extensive nature of  $g$  for *s*-PS chiral optical films.

### 3.5 Conclusion

The chirality induced on melt-extruded *s*-PS films of different thickness, by cocrystallization with a nonracemic guest (carvone), has been studied. The intense VCD and CD phenomena, already observed for 20  $\mu\text{m}$  films, are markedly increased for 6  $\mu\text{m}$  films. In particular, the degree of circular polarization relative to VCD peaks, both for polymer host and for low-molecular-mass nonracemic as well as achiral (azulene and NA) guests, increases of roughly 1 order of magnitude. This phenomenon is possibly rationalized by a more efficient formation of chiral crystallites close to the film surfaces. AFM images of melt-extruded chiral optical *s*-PS films show closely packed and aligned helical crystallites, whose morphology remains substantially unchanged after guest removal as well as after thermal treatments above the helix  $\rightarrow$  trans planar ( $\gamma \rightarrow \alpha$ ) host transition.

The use of chiral films with a thickness of  $\sim 6 \mu\text{m}$  has also allowed to identify intense CD peaks at 262, 265, and 269 nm of polystyrene, which were not accessible for much thinner spin-coated films (0.3  $\mu\text{m}$ ) and for thicker films (20  $\mu\text{m}$ ), which exhibit in this spectral region too low CD signals and too high UV absorbance, respectively.

Surprisingly, for all the considered thicknesses and spectral ranges, the chiral optical responses of the considered achiral guests (azulene and 4-nitroaniline) are definitely higher than for the chirality-inducing nonracemic guest (carvone). This indicates that the origin of the chiral optical response is extrinsic to the site of photon absorption. Moreover, the extensive nature of the chiral optical response of *s*-PS films is clearly indicated by the large increases of  $g$  values (of both host and guest peaks) going from thin spincoated films (with thickness in the range 0.08 to 0.3  $\mu\text{m}$ ) to thick melt-extruded films (6  $\mu\text{m}$ ). This extrinsic and extensive nature of the chiral optical response of *s*-PS films well agrees with the hypothesis

that it is associated with the nonracemic helical morphology of crystallites, as induced by the chirality of the cocrystallizing nonracemic guest.

The use of a low cost, commercially available, robust, and thermoplastic polymer which can be processed by standard industrial processes (like melt extrusion), followed by simple liquid bath treatments, and the possibility to get chiral optical responses at wavelengths of achiral chromophores suggest that s-PS-based chiral optical materials and devices can be easily designed and produced.

### **References**

1. a) Hirschberg, J. H. K. K.; Brunsveld, L.; Ramzi, A.; Vekemans, J. A. J. M.; Sijbesma, R. P.; Meijer, E. W. *Nature* **2000**, 407, 167. b) Cornelissen, J. J. L. M.; Rowan, A. E.; Nolte, R. J. M.; Sommerdijk, N. A. J. M. *Chem. Rev.* **2001**, 101, 4039. c) Nakano, T.; Okamoto, Y. *Synthetic Chem. Rev.* **2001**, 101, 4013. d) Angiolini, L.; Bozio, R.; Giorgini, L.; Pedron, D.; Turco, G.; Dauru, A. *Chem. Eur. J.* **2002**, 8, 4241. e) Pijper, D.; Jongejan, M. G. M.; Meetsma, A.; Feringa, B. L. J. *Am. Chem. Soc.* **2008**, 130, 4541. f) Shiraki, T.; Dawn, A.; Tsuchiya, Y.; Shinkai, S. J. *Am. Chem. Soc.* **2010**, 132, 13928. g) Castiglioni, E.; Abbate, S.; Lebon, F.; Longhi, G. *Chirality* **2012**, 24, 725. h) Green, M. M.; Khatri, C.; Peterson, J. *Am. Chem. Soc.* **1993**, 115, 4941. i) Yashima, E.; Maeda, K.; Okamoto, Y. *Nature* **1999**, 399, 449. j) Green, M. M.; Park, J. W.; Sato, T.; Teramoto, A.; Lifson, S.; Selinger, R. L. B.; Selinger, J. V. *Angew. Chem., Int. Ed.* **1999**, 38, 3138. k) Yashima, E.; Maeda, K. *Macromolecules* **2008**, 41, 3. l) Goto, H.; Yokochi, Y.; Yashima, E. *Chem. Commun.* **2012**, 48, 3291.
2. a) La Camera, D.; Petraccone, V.; Artimagnella, S.; Ruiz de Ballesteros, O. **2001**, 34, 7762–66. b) Esposito, G.; Tarallo, O.; Petraccone, V. *Eur. Polym. J.* **2007**, 43, 1278. c) Tarallo, O.; Petraccone, V.; Daniel, C.; Fasano, G.; Rizzo, P.; Guerra, G. J. *Mater. Chem.* **2012**, 22, 11672.
3. a) Buono, A. M.; Immediata, I.; Rizzo, P.; Guerra, G. *J. Am. Chem. Soc.* **2007**, 129, 10992. b) Guadagno, L.; Raimondo, M.; Silvestre, C.; Immediata, I.; Rizzo, P.; Guerra, G. *J. Mater. Chem.* **2008**, 18, 567. c) Rizzo, P.; Beltrani, M.; Guerra, G. *Chirality*

- 2010**, 22, E67– E73. d) Rizzo, P.; Daniel, C.; Guerra, G. *Macromolecules* **2010**, 43, 1882–87.
- 4.** Guerra, G.; Daniel, C.; Rizzo, P.; Tarallo, O. *J. Polym. Sci., Polym. Phys. Ed.* **2012**, 50, 305.
- 5.** a) De Rosa, C.; Guerra, G.; Petraccone, V.; Pirozzi, B. *Macromolecules* **1997**, 30, 4147–52. b) Milano, G.; Venditto, V.; Guerra, G.; Cavallo, L.; Ciambelli, P.; Sannino, D. *Chem. Mater.* **2001**, 13, 1506. c) Gowd, E. B.; Shibayama, N.; Tashiro, K. *Macromolecules* **2006**, 39, 8412.
- 6.** a) Immirzi, A.; De Candia, F.; Iannelli, P.; Vittoria, V.; Zambelli, A. *Chem., Rapid Commun.* **1988**, 9, 761. b) Rizzo, P.; Lamberti, M.; Alburnia, A. R.; Ruiz de Ballesteros, O.; Guerra, G. *Macromolecules* **2002**, 35, 5854.
- 7.** a) De Rosa, C.; Guerra, G.; Petraccone, V.; Corradini, P. *Polym. J.* **1991**, 23, 1435. b) Cartier, L.; Okihara, T.; Lotz, B. *Macromolecules* **1998**, 31, 3303.
- 8.** a) Rizzo, P.; Montefusco, T.; Guerra, G. *J. Am. Chem. Soc.* **2011**, 133, 9872. b) Guerra, G.; Rizzo, P. *Rendiconti* **2013**, 24, 217–226.
- 9.** a) Kobayashi, M.; Nakaoki, T.; Ishihara, N. *Macromolecules* **1989**, 22, 4377. b) Grassi, A.; Longo, P.; Guerra, G. *Makromol. Chem., Rapid Commun.* **1989**, 10, 687. c) Alburnia, A. A.; Musto, P.; Guerra, G. *Polymer* **2006**, 47, 234. d) Torres, F. J.; Civalieri, B.; Meyer, A.; Musto, P.; Alburnia, A. R.; Rizzo, P.; Guerra, G. *J. Phys. Chem. B* **2009**, 113, 5059.
- 10.** a) Gupta, M. C.; Gupta, A.; Horwitz, J.; Kliger, D. *Macromolecules* **1982**, 15, 1372. b) Wandelt, B. *Polymer* **1991**, 32, 2707. c) Grana, E.; Katsigiaannopoulos, D.; Karantzalis, A. E.; Baikousi, M.; Avgeropoulos, *Eur. Polym. J.* **2013**, 49, 1089. d) Guillet, J. *Polymer Photophysics and Photochemistry*; Cambridge University Press: Cambridge, **1985**; Chapter 7.
- 11.** Brizard, A.; Oda, R.; Hic, I. *Top. Curr. Chem.* **2005**, 256, 167.
- 12.** a) Chatani, Y.; Shimane, Y.; Inoue, Y.; Inagaki, T.; Ishioka, T.; Ijitsu, T.; Yukinari, T. *Polymer* **1993**, 33, 488. b) Yoshioka, A.; Tashiro, K. *Macromolecules* **2003**, 36, 3593. c) Uda, Y.; Kaneko, F.; Kawaguchi, T. *Polymer* **2004**, 45, 2221. d) Rizzo, P.; Della Guardia, S.; Guerra, G. *Macromolecules* **2004**, 37, 8043–49. e) Uda, Y.; Kaneko, F.; Kawaguchi, T. *Makromol. Rapid Commun.* **2004**, 25, 1900. f) Kaneko, F.; Tsuchida, T. *Polymer* **2013**, 54, 760.
- 13.** Shevyakov, S. V.; Li, H. R.; Muthyala, R.; Asato, A. E.; Croney, J. C.; Jameson, D. M.; Liu, R. S. H. *J. Phys. Chem. A* **2003**, 107, 3295.

- 14.** a) Lakhwani, G.; Koeckelberghs, G.; Meskers, S. C. J.; Janssen, R. A. *J. Phys. Lett.* **2007**, 437, 193. b) Vandeleene, S.; Van den Bergh, K.; Verbiest, T.; Koeckelberghs, G. *Macromolecules* **2008**, 41, 5123.
- c) Lakhwani, G.; Gielen, J.; Kemerink, M.; Chhristianen, P. C. M.; Jansenn, R. A. J.; Meskers, S. C. J. *J. Phys. Chem. B* **2009**, 113, 14047–51.
- 15.** a) Saeva, F. D.; Olin, G. R. *J. Am. Chem. Soc.* **1976**, 98, 2709. b) Craig, M. R.; Jonkheijm, P.; Meskers, S. C. J.; Schenning, A. P. H. J.; Meijer, E. W. *Adv. Mater.* **2003**, 15, 1435–38.

# Chapter 4

## Photonic Crystals (PhC)

### 4.1 Introduction

Photonic crystals, are attractive optical materials for controlling and manipulating the flow of light: they can be used as reflective coatings on lenses, color pigments in paints and inks, waveguides for directing the propagation of light along a specific path, highly reflective mirrors in laser cavities, and many other optical components<sup>1</sup>. The photonic effect can also be used as a mechanism to develop chemical and biological sensors for detecting target analytes by outputting optical signals. These types of crystals may also find great use as active color units in the fabrication of flexible display media, including both active video displays and rewritable paper that can be reused many times<sup>1</sup>.

Photonic crystal (PhC) structures are characterized by a periodic modulation of the dielectric function on a scale comparable to the wavelength of interest<sup>2</sup>. The simplest example of a partially photonic structure is that of a dielectric multilayer stack, often called a Bragg mirror. This is made up of a series of alternating layers of different refractive indices importantly it can be designed to reflect any particular optical wavelength.<sup>3</sup>

However this cannot deliver a truly photonic material. In a true photonic device the reflected wavelength is a photonic stopband, where the wavelengths of light in the stopband are unable to propagate in the structure, similar to the unallowed states seen in semiconductors band diagrams (Brioullin zones). The wavelength of light diffracted from the PhCs is given by the Bragg-Snell equation:

$$m\lambda_{\text{Bragg}} = 2D\sqrt{n_{\text{eff}}^2 - \sin^2\theta} \quad (1)$$

where  $m$  is the diffraction order,  $D$  is the interplanar spacing in the direction which is perpendicular to the surface,  $\theta$  is the incidence angle measured off from the normal, and  $n_{\text{eff}}$  is the effective refractive index<sup>4</sup>.

However in the partial photonic Bragg reflector, the reflected wavelength depends upon the optical thickness ( $n_1d_1+n_2d_2$ ) and refractive index of each layer ( $n_1, n_2$ ). Additionally, the width of the wavelength distribution or angular distribution depends on the total number of layers ( $N$ ). For inorganic materials such as metals it is possible to produce a large difference in refractive index ( $\Delta n$ ), consequently good quality Bragg mirrors require only a small number of alternating layers.<sup>3</sup>

PhC can be prepared with different dimensionality, in particular 1D, 2D or 3D dimensions.

A crystal 1-D is obtained by alternating layers of materials having different refractive index for a periodic structure. A 2-D structure is obtained in a generic substrate "holes" in thickness and depth determined in an appropriate manner, for a two-dimensional periodic structure. The 3-D crystals are more complex because of their isotropic structures: among the techniques adopted the so-called "stacking" which consists of the "construction" Crystal "layer by layer"<sup>5</sup> or some other serial deposition technique using a layer-by-layer approach, (most likely under high vacuum conditions) making the total production costs high.

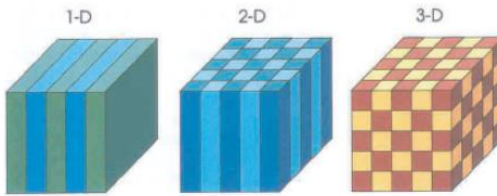


**Fig 4.1.1** 1D, 2D or 3D dimensions

This periodic modulation of the refractive index gives to the photonic crystal optical properties which are similar to the electrical conduction properties of crystals (hence the name crystal). In particular, the photonic crystals may have a band gap for light similar to that of semiconductors. An example of such a serial technique to create a photonic structure, by using polymers, was the use of spin coating of alternating layers of

poly(styrene) and poly(vinylpyrrolidone) to create a Distributed Bragg Reflector (DBR).<sup>3</sup>

We focus the attention in 1D PhC photonic crystals, the simplest types of PhC, composed of two materials, in particular polymeric materials, with different refractive indexes, arranged in alternate layers.

#### 4.2 Results: Cellulose Acetate (CA) and Poly(2,6-dimethyl-1,4-phenylene ether) (PPO) Photonic Crystals (PhC)

The 1D PhC photonic crystals are fabricated with a spin-coating method. The spin-coating techniques are instead very powerful to obtain polymer Distributed Bragg Reflector (DBR) structures because they require only the use of macromolecules or colloids possessing a significant dielectric contrast, which could be dissolved in orthogonal solvents<sup>2</sup>.

The 1D photonic crystal (fig 4.2.1 b-c), prepared by Professor Comoretto et al. at University of Genova, is a multilayer of CA layers alternates with PPO layers. These materials are chosen because:

- they have different solubility in different solvents (an important feature to create a multilayer with spin coating technique)
- they have different refractive index: CA has a 1.47 refractive index and PPO has a 1.57 refractive index<sup>6</sup>

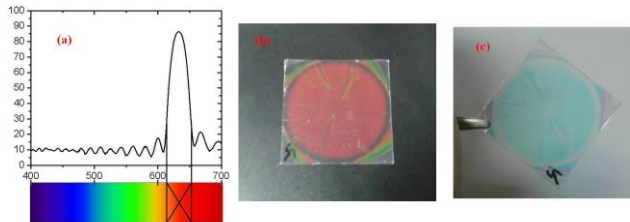


**Fig.4.2.1** The part of the visible spectrum that does not propagate in the structure (a), photographs of the same sample on the black surface (b) and white (c)

In the figure 4.2.1 (a) is shown the visible spectral range and the corresponding red wavelength unable to propagate in the structure (a photonic *gap*): this gap gives to the structure a particular color, as shown in Fig 4.2.1 (b) and (c). For the

sample placed on a black surface (fig 4.2.1 b), red is the reflected color unable to propagate in the structure for a normal incidence of light but if incidence angle of light changes, the color of PhC changes, as observed in figure 4.2.1 c <sup>6</sup>

In figure 4.2.2 FTIR spectra of amorphous (fig. 4.2.2 A) and co-crystalline phase (fig. 4.2.2 B-C) of PPO layers, in PhC, will be described.

PPO layers of PhC were crystallized by treatment of benzene vapors.

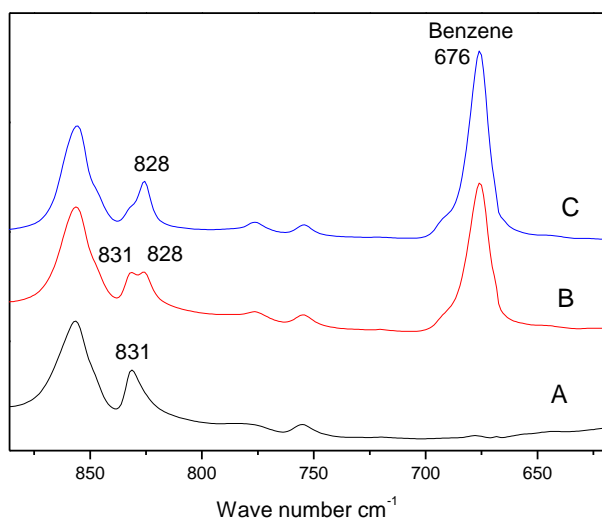


**Fig 4.2.2** FTIR spectra of PhC (or CA/PPO multilayers). A) Amorphous PPO, B) PhC vapours benzene for 15min at 50°C treatment, C) PhC vapours benzene for 30 min at 50°C treatment.

The peak of PPO amorphous phase is located at 831 cm<sup>-1</sup> as shown in fig 4.2.2 A.<sup>7</sup> The spectra of PhC after exposition to benzene vapors, for 15 min at 50°C (fig. 4.2.2.B) and for 30min at 50°C (fig. 4.2.2 C), are reported. In fig 4.2.2 B, PPO layers are partially crystallized, in fact the peaks 831 cm<sup>-1</sup>, associated to amorphous phase, and 828 cm<sup>-1</sup>,

associated to crystalline phase, appear. In fig. 4.2.2 C the only  $828\text{ cm}^{-1}$  peak, associated to crystalline phase, appears, so all PPO layers are crystalline. The peak located at  $676\text{ cm}^{-1}$ (fig. 4.2.2 B-C), due to benzene molecules, is also apparent.

The UV spectrum of amorphous film (whose IR spectrum is shown in fig 4.2.2.A) is reported in fig 4.2.3 A and the UV spectrum of crystalline film (whose IR spectrum is shown in fig 4.2.2.C) is reported in fig 4.2.3. B

In PhC's UV spectrum (fig. 4.2.3 A), the reflectivity signals at 632 nm, associated at the first reflection order, and at 331 nm, at the second one, appear. The peak at 299 nm is related to PPO signal.

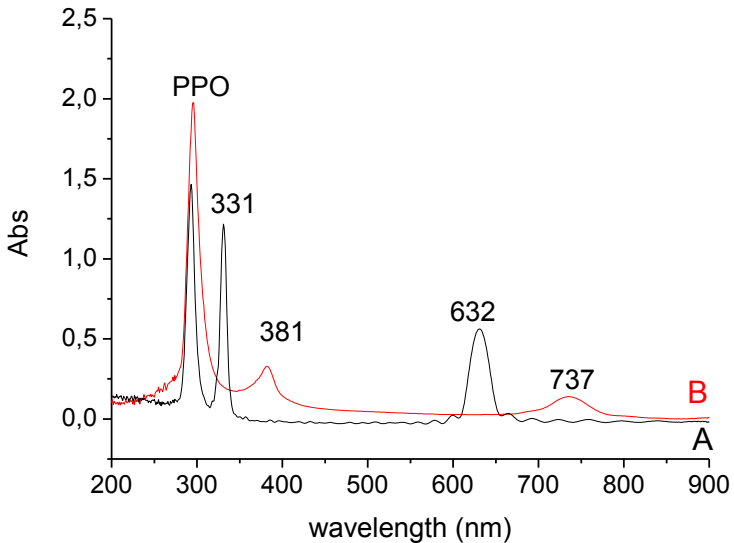


**Fig 4.2.3** UV spectra of PhC with amorphous PPO layers (A)(black line), PhC with crystalline PPO layers (B) (red line)

After crystallization, in PhC's UV spectrum (fig 4.2.3 B) a reduction of intensity and a red shift of the 633 and 331 reflections occurs. The shift of photonic band gap ( $633\text{nm} \rightarrow 737\text{nm}$ ) and ( $331\text{nm} \rightarrow 381\text{nm}$ ) suggests an increase of

PPO thickness after crystallization procedure. However the presence of second-order photonic band gap suggests that the order of multilayer structure is substantially retained.

The effect's evaluation of the benzene guest in PhC's co-crystalline phase is another investigated aspect.

FT-IR spectra and the corresponded UV spectra of co-crystalline PPO/benzene ( fig 4.2.4 b and 4.2.5 b) and empty PPO crystalline layers (fig 4.2.4 c and 4.2.5 c) are reported in fig. 4.2.4 and in fig. 4.2.5 respectively.

It is apparent that the signal at 735 nm, associated to the photonic gap (fig. 4.2.5) does not show significant variation by removing benzene molecules. It means that this guest does not influence the PhC's optical response.

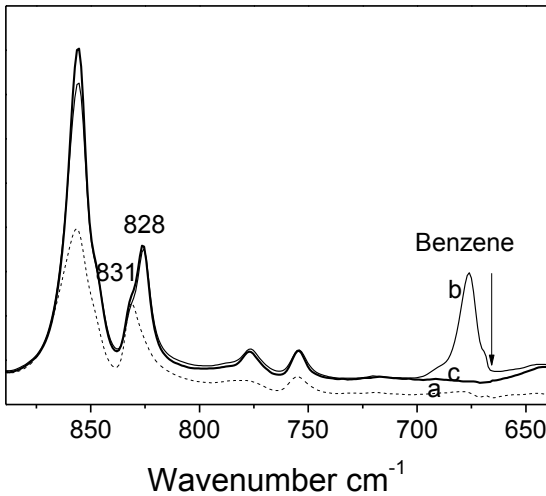


**Fig 4.2.4** FTIR transmission spectra in the wavenumber range 900-650  $\text{cm}^{-1}$  of PPO in PhC has collected (a) amorphous PPO (dot line); (b) co-PPO/benzene crystal (thin line); (c) extracted by  $\text{CO}_2$  (thick line)

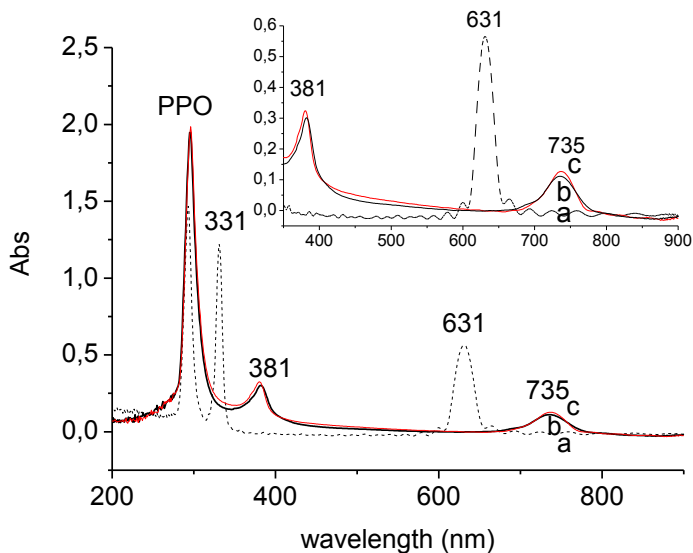


**Fig 4.2.5** UV spectra (a) amorphous PPO (dot line); (b) co-PPO\benzene crystal (black line); (c) extracted by CO<sub>2</sub> (red line)

### 4.3 Thin films

In order to realize a photonic crystal, by using thin layers of PPO presenting nanoporous crystalline phase, it has been necessary to characterize amorphous as well as crystalline phases of PPO thin films.

#### 4.3.1 FT-IR and IRRAS analysis of PPO thin films

Thin polymeric films have helped in the development of nanostructures and nanomaterials for new and emerging technologies.<sup>8</sup>

Thin polymer layers on a substrate are prepared by spin-coating, this technique has specific limitations: spin coating and patterned substrates require a solvent during processing, which can limit the choice of polymer. The process itself also produces a small amount of material that contains a free surface, which is known to affect the properties of the polymer thin layer.<sup>9</sup>

The thickness of the films can be controlled by setting conditions such as the speed of rotation and the concentration

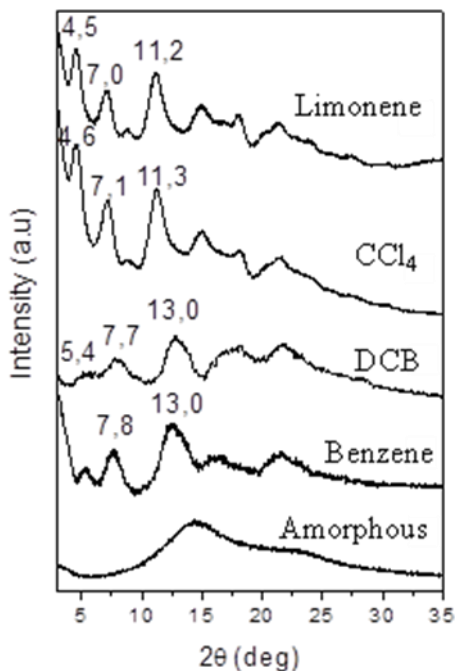
of the deposited solutions. Often very thin polymer films with a thickness  $> 1 \mu\text{m}$  can be successfully characterized with FT-IR (*Fourier Transform Infrared Spectroscopy*) spectroscopy. While thin polymer films with a thickness  $< 1 \mu\text{m}$ , deposited on a metal reflective substrate, can be successfully characterized with IRRAS (*Infra-red reflection absorption spectroscopy*). The two polarization states, of the incident electric field, are the  $I_s$  (parallel to the film plane) and  $I_p$  (perpendicular to the film plane) components. Unlike conventional experiments, where the  $I_p$  and  $I_s$  components of the transmitted intensity are approximately equal, the IRRAS intensities of the two reflected components are dramatically different.<sup>10</sup> The perpendicular component  $I_p$  is visible in the IRRAS analysis. This vibrational spectroscopic technique is required for acquire structural information, such as orientation in polymer films.

In this section we reported the FT-IR and IRRAS spectra of thin films, obtained by spin coating, of amorphous and semicrystalline PPO films obtained by treating amorphous PPO with 1,2-dichlorobenzene (DCB), carbon tetrachloride ( $\text{CCl}_4$ ) and limonene. These solvents are able to form PPO co-crystals and are able to form the two limit nanoporous crystalline modifications after solvent removal, as shown in fig 4.3.1.

It is known, from literature, that PPO samples show a continuum of nanoporous modifications between two limit ones, exhibiting diffraction peaks located at different diffraction angles. A limit nanoporous modification by benzene exhibits diffraction peaks at  $2\theta$  values 7.8-13.0 and a second limit nanoporous modification by  $\text{CCl}_4$  show diffraction peaks at  $2\theta$  values 7.1-11.3.<sup>11</sup>

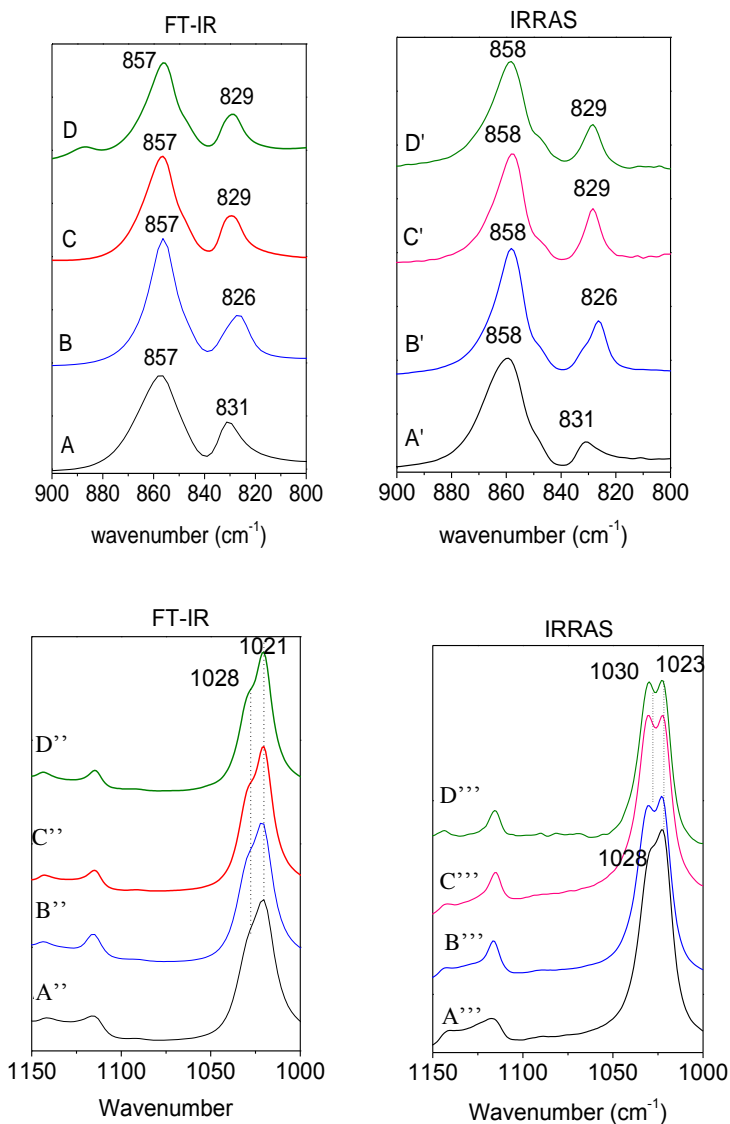
It appears that 1,2-dichloro-benzene (DCB) and limonene exhibit nanoporous crystalline modifications; i.e. 1,2-dichloro-benzene (DCB) shows nanoporous phase similar to nanoporous phase from benzene and limonene shows nanoporous phase similar to nanoporous phase from  $\text{CCl}_4$ , as

shown in fig 4.3.1.



**Fig. 4.3.1** X-ray diffraction, collected by an automatic powder diffractometer. Trend of different nanoporous crystalline phase of PPO obtained by CO<sub>2</sub> extraction of benzene; DCB (1,2-dichlorobenzene); CCl<sub>4</sub>; limonene. For comparison also the PPO Amorphous spectrum is reported.

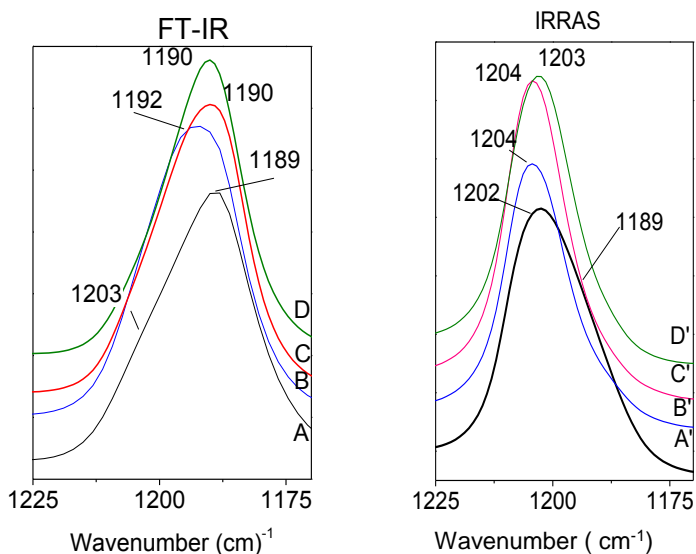
Thin films with thickness  $> 1 \mu\text{m}$ , obtained from 8%wt in chloroform solution, at a spin rate of 1000 rpm, are characterized by FT-IR. Whereas thin films with thickness  $< 1 \mu\text{m}$  obtained from 3%wt in toluene solution, at a spin rate of 5000 rpm, are characterized by IRRAS.



**Fig 4.3.2** FT- IR (A-D) and IRRAS (A'-D') spectra in the 900-800 cm<sup>-1</sup> wavenumber range, FT- IR (A''-D'') and IRRAS (A'''-D''') spectra in the 1150-1000 cm<sup>-1</sup> wavenumber range. Trend of different nanoporous crystalline phase of PPO: (A) Amorphous; (B) 1,2-dichlorobenzene; (C) CCl<sub>4</sub>; (D) limonene.

FT-IR and IRRAS spectra in the 900-800  $\text{cm}^{-1}$  wavenumber range of amorphous and semicrystalline PPO films, reported in figure 4.3.2 (A-D) and (A'-D'), are very similar. FT-IR spectra (fig. 4.3.2 (A-D)) show a peak at 831  $\text{cm}^{-1}$  that corresponds at PPO amorphous phase and peak at 826  $\text{cm}^{-1}$  and 829  $\text{cm}^{-1}$  that correspond at two different nanoporous modifications respectively<sup>11</sup>. IRRAS spectra in fig 4.3.2 (A'-D') show the same peaks of two different nanoporous modifications.

In the 1150-1000  $\text{cm}^{-1}$  spectra range some differences in FT-IR (fig. 4.3.2 (A''-D'')) and IRRAS (fig. 4.3.2 (A'''-D''')) spectra appear. In particular, FT-IR spectra of amorphous (A'') and semicrystalline PPO (B''-D'') present a peak at 1021  $\text{cm}^{-1}$  and a shoulder at 1028  $\text{cm}^{-1}$  that in IRRAS spectra, of semicrystalline PPO films (curve B'''-D'''), becomes a narrow peak located at 1030  $\text{cm}^{-1}$  assigned to *the methyl rocking vibrations*.<sup>12-13</sup>



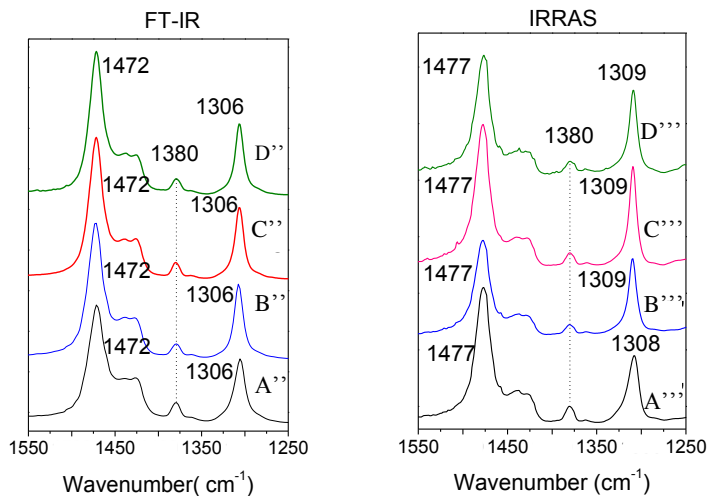


**Fig. 4.3.3** FT- IR (A-D) and IRRAS (A'-D') spectra in the 1225-1170  $\text{cm}^{-1}$  wavenumber range, FT- IR (A''-D'') and IRRAS (A'''-D''') spectra in the 1550-1250  $\text{cm}^{-1}$  wavenumber range. Trend of different nanoporous crystalline phase of PPO: (A) Amorphous; (B) 1,2-dichlorobenzene; (C)  $\text{CCl}_4$ ; (D) limonene.

Great differences appear in the 1225  $\text{cm}^{-1}$  -1170  $\text{cm}^{-1}$  wavenumber range of the FT-IR ( fig. 4.3.4 A-D) and IRRAS ( fig. 4.3.4 A'-D') spectra. In particular: FT-IR spectra of amorphous (fig.4.3.4 A) and semicrystalline PPO film (fig. 4.3.4 B-D) present an asymmetric band at 1189-1192  $\text{cm}^{-1}$  with a shoulder at  $\approx 1203 \text{ cm}^{-1}$

Definitely different appear the IRRAS spectra (fig 4.3.4 A'-D'). In particular, IRRAS spectrum of amorphous PPO (A') show a band at 1202  $\text{cm}^{-1}$  and a shoulder at 1189  $\text{cm}^{-1}$ . This band becomes narrow in the semicrystalline films and preferentially centered at 1204  $\text{cm}^{-1}$  (B'-D')

It's apparent that FT-IR and IRRAS spectra show a shift of the band at  $\approx 1200 \text{ cm}^{-1}$ , assigned at the *asymmetric ether stretching* mode<sup>12</sup>, about 10  $\text{cm}^{-1}$ .

Other differences in the 1550-1250  $\text{cm}^{-1}$  wavenumber range are evident. It apparent that the peak at 1472  $\text{cm}^{-1}$ , 1306  $\text{cm}^{-1}$  in the FT-IR spectra (fig. 4.3.4 A''-D'') are located at 1477

$\text{cm}^{-1}$  and  $1309 \text{ cm}^{-1}$  (fig. 4.3.4 A''''-D'''')) in the IRRAS spectra. It's evident that these peaks, assigned at the *ring stretching* mode,<sup>12</sup> show a shift about of  $5 \text{ cm}^{-1}$  and  $3 \text{ cm}^{-1}$  respectively. Whereas the position of the peak at  $1380 \text{ cm}^{-1}$ , assigned at the *CH<sub>3</sub> symmetric deformation* mode<sup>12</sup>, does not change.

The spectroscopic analysis shows that IRRAS spectra exhibit significant variation respect to FT-IR spectra:

- the narrow peaks located at  $1030 \text{ cm}^{-1}$  assigned to the *in plain CH deformation* mode.
- the big shift of peak located at  $1204 \text{ cm}^{-1}$  assigned to the *asymmetric ether stretching* mode of PPO.
- the shift of peak located at  $1477 \text{ cm}^{-1}$  and at  $1309 \text{ cm}^{-1}$  assigned at the *ring stretching* mode.

For better understanding of this phenomenon we compare our data with the results of VCD measurements of co-crystals of PPO \ (1R) - (+)  $\alpha$ -pinene and PPO \ (1S) - (-)  $\alpha$ -pinene whose the structure and helix conformation  $4_1$  (fig. 4.3.4) is known.

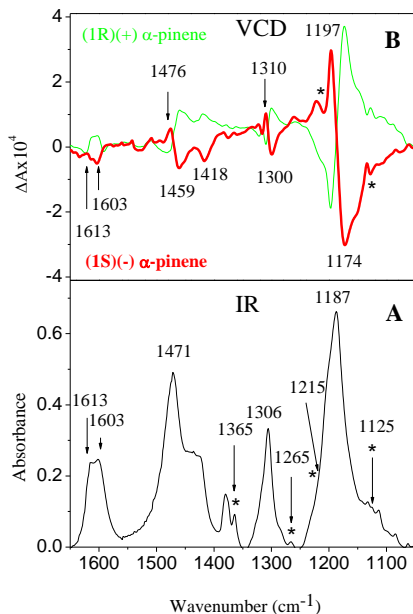


**Fig. 4.3.4** FT-IR (A) and VCD (B) of PPO powders, exhibiting co-crystalline phase with (1R)-(+) $\alpha$ -pinene (thin green line) and (1S)-(-)  $\alpha$ -pinene (thick red line) and an  $\alpha$ -pinene content close 30%. The  $\alpha$ -pinene peaks are indicated by a star (\*)<sup>15</sup>

In particular we observe that the FT-IR intense absorption band centered at  $1187\text{ cm}^{-1}$  give rise in the VCD spectrum two intense peaks at  $1197\text{ cm}^{-1}$  and  $1174\text{ cm}^{-1}$ . Analogously, FT-IR absorption band centered at  $1306\text{ cm}^{-1}$  and  $1471\text{ cm}^{-1}$  give rise to two intense VCD peaks at  $1310\text{ cm}^{-1}$  and  $1300\text{ cm}^{-1}$ , and  $1476\text{ cm}^{-1}$  and  $1459\text{ cm}^{-1}$  presenting opposite Cotton signals.

Probably the  $1187\text{ cm}^{-1}$ ,  $1306\text{ cm}^{-1}$  and  $1471\text{ cm}^{-1}$  FT-IR bands are made to multiple components and in particular the signals  $1477\text{ cm}^{-1}$ ,  $1310\text{ cm}^{-1}$  and  $1197\text{ cm}^{-1}$ , which have the same sign in the VCD spectra, could have the variation of transition moment perpendicular to the film plane because they appear the most intense in the IRRAS spectra.

### 4.3.2 Desorption of CCl<sub>4</sub> in PPO thin films

It is known that semicrystalline films are characterized by a gas solubility and diffusivity which are much larger than in the case of totally amorphous PPO.<sup>7</sup>

The non-negligible sorption capacity of the crystalline domains, against what is commonly observed in semicrystalline polymers is further supported by the fact that the density of amorphous PPO is slightly higher than that of semicrystalline samples. Because of its peculiar mass transport properties, semicrystalline PPO could be a potential candidate for membrane based gas separation processes<sup>7</sup>

In this section the desorption of CCl<sub>4</sub> in amorphous and in crystalline PPO thin films have been investigated.

IRRAS spectra of amorphous PPO film before and after CCl<sub>4</sub> vapours treatment, at room temperature, for 5 minute (fig. 4.3.5 A) and 30 minute (fig. 4.3.5 B), are reported in figure 4.3.5.

It appears that after exposition to CCl<sub>4</sub> for 5 minutes the film does not crystalline, as shown from the peak at 831 cm<sup>-1</sup> in fig. 4.3.5 A, whereas after exposition for 30 minutes the film crystallize, as shown from the peak at 829 cm<sup>-1</sup> in fig. 4.3.5 B. In fig 4.3.5 we can see that CCl<sub>4</sub> signal (786 cm<sup>-1</sup>) decreases over time, in particular desorbed after 36h in PPO amorphous film (A) and after 40min in PPO crystalline film (B).

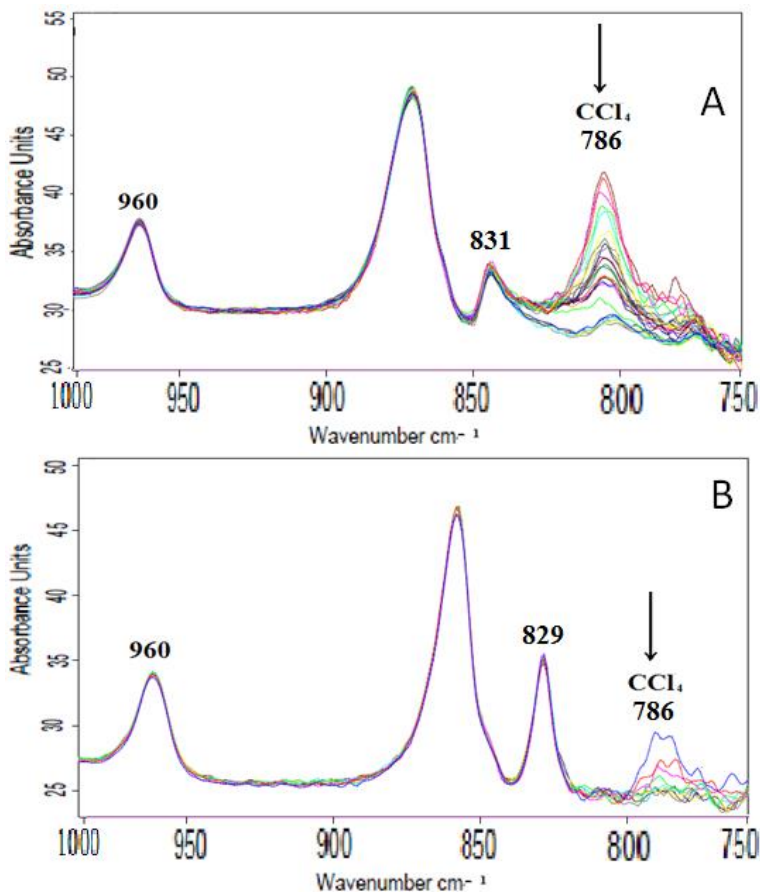


**Fig 4.3.5** FTIR transmission spectra in the wavenumber range 1000–750  $\text{cm}^{-1}$  of amorphous PPO/ $\text{CCl}_4$  film (A) at 36h; and crystalline PPO/ $\text{CCl}_4$  film (B) at 40 min.

The evaluation of the guest desorption at room temperature, in amorphous and crystalline samples of PPO shown in Figure 4.3.5A-B, has been reported in fig. 4.3.6. The absorbance reduction for  $\text{CCl}_4$  vibrational peak ( $A_t = 786 \text{ cm}^{-1}$ ) has been normalized respect to a PPO reference peak  $960 \text{ cm}^{-1}$  ( $A_o$ ).  $A_t/A_o$  are reported versus the desorption time.

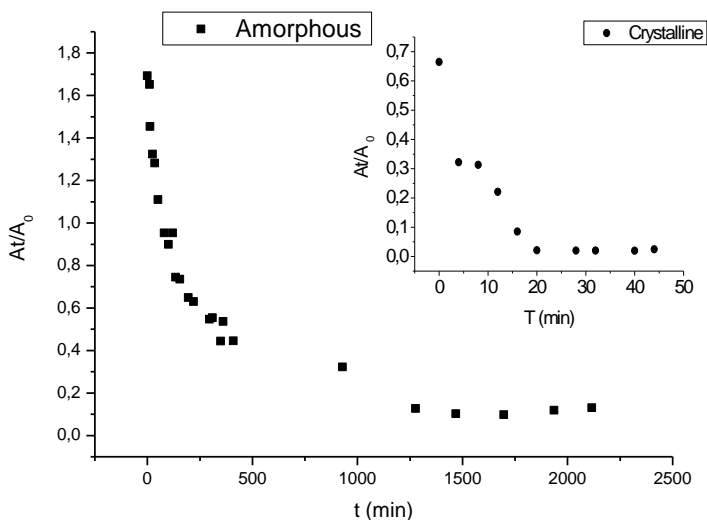


**Fig. 4.3.6** Desorption at room temperature, in amorphous (■) and crystalline (●) samples of PPO \(\text{CCl}\_4\). ( $A_t=786 \text{ cm}^{-1}$ ) is a  $\text{CCl}_4$  vibrational peak normalized respect to a PPO reference peak  $960 \text{ cm}^{-1}$  ( $A_0$ ).  $A_t/A_0$  are reported versus the desorption time.

The results of Figure 4.3.6 are also reported as classical Fick's plots in Figure 4.3.7, with  $(A_0-A_t)/A_0$  versus the square root of desorption time divided by film thickness ( $\sqrt{t(\text{sec})}/L(\text{cm})$ ).

The curves of Figure 4.3.7 confirm that a slower  $\text{CCl}_4$  desorption occurs from the amorphous phase ( $D_{\text{am}} = 1.41 \times 10^{-15} \text{ cm}^2 \text{ s}^{-1}$ ), while a faster desorption occurs for the crystalline phase ( $D_{\text{cr}} = 2.30 \times 10^{-14} \text{ cm}^2 \text{ s}^{-1}$ ), about one order of magnitude bigger.

This result is consistent with the literature data; in fact, it was found that the samples (PPO powders and areogels) semicrystalline have greater capacity for gas absorption and diffusivity compared to those amorphous: This behavior has been attributed mainly to the nanoporous nature of the crystalline phases induced by treatment with solvents.<sup>16</sup>

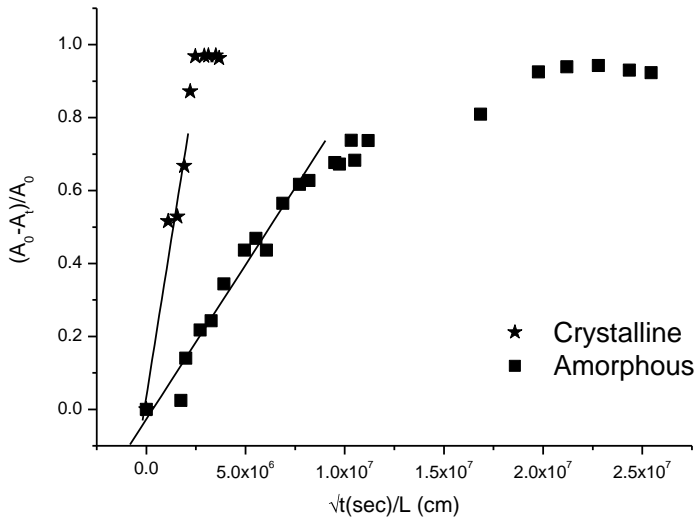


**Fig. 4.3.7**  $\text{CCl}_4$  desorption isotherms, presenting the FTIR absorbance variations  $(A_0 - A_t)/A_0$  versus the square root of desorption time divided by film thickness ( $\sqrt{t}/L$ ). For comparison,  $\text{CCl}_4$  desorption from amorphous phase and from crystalline phase of PPO, is reported.

Generally, crystallites do not contribute to the sorption and diffusion processes, acting like a constraint for the amorphous phase and as a geometrical obstacle to diffusion. In the present case the picture is rather different, because the crystalline phase evidently takes part to the sorption and transport processes, as a consequence of its nanoporous structure, with mass transport rates even higher than those proper of the amorphous domains.<sup>16</sup>

### 4.3.3 Refractive Index

Optical properties of these films were evaluated, in particular, the refractive index of amorphous and nanoporous crystalline thin films were measured.

The refractive index,  $n$ , depends on the density of the material, the temperature and the wavelength of the incident light.

Ellipsometry is an optical technique that allows to detect the

variation of the polarization state of a polarized light beam produced by the interaction with a linear optical element. This technique allows to characterize thin films, in particular: the refractive index  $n$ , the extinction coefficient  $k$  and the thickness  $t$  can be evaluated.<sup>17</sup>

Generally, the refractive index is a function of the light frequency  $n = n(\nu)$  or the wavelength  $n = n(\lambda)$ .<sup>17</sup> The dependence of the refractive index by wavelength is usually identified by empirical equation, such as the Cauchy equation:

$$\begin{cases} n(\lambda) = A + \frac{10^4 \cdot B}{\lambda^2} + \frac{10^9 \cdot C}{\lambda^4} \\ k(\lambda) = 0 \end{cases} \quad (2)$$

The coefficient  $A$  is the refractive index for  $\lambda \rightarrow \infty$

Refractive indexes and the thickness of PPO amorphous and crystalline films, obtained from 3%wt in toluene solution, at a spin rate of 5000 rpm, were measured with ellipsometry. Ellipsometric measurements to evaluate the refractive index were performed by Ing. Mario Iodice and Ing. Antonella Ferrara of CNR, Naples.

The film thickness evaluated is about 140 nm.

The measurement of amorphous PPO refractive index versus wavelength is reported in figure 4.3.8.

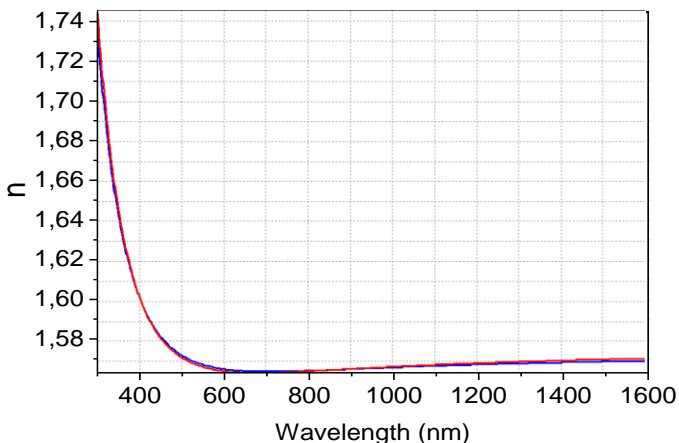


**Fig.4.3.8** Refractive index  $n$  of amorphous PPO thin film versus wavelength

The  $n$  value of amorphous films, at 600nm, is 1.57 (blue curve). The red curve indicates the  $n$  measurement after 12 days and it appears that the  $n$  value is constant.

Amorphous PPO films have been crystallized with benzene and  $\text{CCl}_4$  vapors, and IRRAS spectra in figure 4.3.9 B' and in figure 4.3.10 B'' are reported.

The refractive index of these films with nanoporous crystalline structures has been evaluated. As shown in figure 4.3.9 and 4.3.10 the amorphous curve is always higher than the crystalline curve. In particular the refractive index, at 600 nm, of amorphous PPO (black curve (4.3.9 A and 4.3.10 A)) is 1.56 and 1.57 respectively, the  $n$  value of PPO crystalline films, at 600 nm, becomes 1.49 and 1.52 respectively.

It's apparent that the nanoporous crystalline structure has a lower refractive index of the amorphous structure, which confirms that the nanoporous phase is less dense than the amorphous phase.

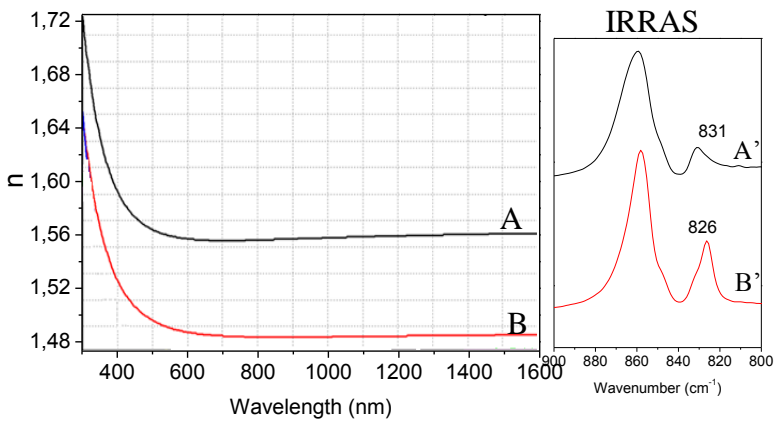


**Fig. 4.3.9** Refractive index  $n$  of PPO thin film versus wavelength: A) Amorphous PPO ( black line); B) PPO nanoporous crystalline structure by benzene (red line). The respective IRRAS spectra (A'-B') are reported.

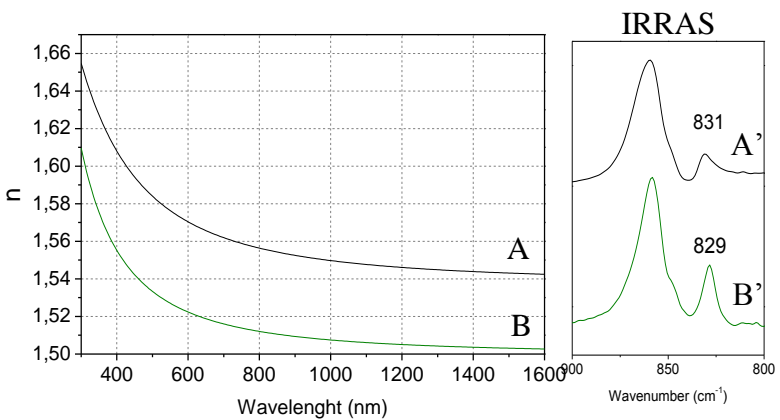


**Fig. 4.3.10** Refractive index  $n$  of PPO thin film versus wavelength: A) Amorphous PPO ( black line); B) PPO nanoporous crystalline structure by  $\text{CCl}_4$  (green line). The respective IRRAS spectra (A'-B') are reported

## 4.4 Conclusion

In this chapter it has been reported the possibility of realize PhC by using polymeric materials like PPO able to form nanoporous crystalline structure.

We reported the FTIR and UV spectra of Photonic Crystal (PhC) before and after crystallization process of PPO layers, with benzene vapors. The comparison of UV spectra of PhC with amorphous and crystalline PPO layers shows a variation in the optical properties of PhC. This phenomenon could depend on the variation of thickness and the reflective index of PPO layers after crystallization.

Thin polymer layers on a substrate are prepared by spin-coating. These thin films are characterized by FTIR and IRRAS spectroscopy. The spectroscopic analysis shows that IRRAS spectra exhibit significant variation respect to FT-IR spectra:

- the narrow peaks located at  $1030\text{ cm}^{-1}$  assigned to the *in plain CH deformation* mode.
- the big shift of peak located at  $\sim 1200\text{ cm}^{-1}$  assigned to the *asymmetric ether stretching* mode of PPO.
- the little shift of peak located at  $1477\text{ cm}^{-1}$  assigned at the *ring stretching* mode.

For a better understanding this phenomenon we compare the results VCD spectra of co-crystals of PPO \ (1R) - (+)  $\alpha$ -pinene and PPO \ (1S) - (-)  $\alpha$ -pinene. Probably the  $1187\text{ cm}^{-1}$ ,  $1306\text{ cm}^{-1}$  and  $1471\text{ cm}^{-1}$  FT-IR bands are made to multiple components and in particular the signals  $1477\text{ cm}^{-1}$ ,  $1310\text{ cm}^{-1}$  and  $1197\text{ cm}^{-1}$ , which have the same sign in the VCD spectra, could have the variation of transition moment perpendicular to the film plane because they appear the most intense in the IRRAS spectra.

The guest desorption at room temperature, in amorphous and crystalline samples of PPO is evaluated. A slower  $\text{CCl}_4$  desorption occurs from the amorphous phase ( $D_{\text{am}} = 1.41 \times 10^{-15}\text{ cm}^2\text{ s}^{-1}$ ) while a faster desorption occurs from the

crystalline phase ( $D_{cr} = 2.30 \times 10^{-14} \text{ cm}^2 \text{ s}^{-1}$ ). To PPO peculiar mass transport properties, semicrystalline PPO could be a potential candidate for membrane based gas separation processes.<sup>7</sup>

In the end also the refractive index of amorphous and crystalline PPO thin films are measured. The refractive index of crystalline PPO films has a lower value than amorphous PPO and it is evidence that the nanoporous crystalline phase of PPO is less dense of amorphous phase of PPO.

### References

1. Ge J., Yin Angew Y., *Chem. Int. Ed.* **2011**, 50, 1492 .
2. Frezza L., Patrini M., Liscidini M., Comoretto D., *J. Phys. Chem. C* **2011**, 115, 19939.
3. Parnell A.J. and Fairclough J.P.A. *Self-assembling Polymer Photonics* 1-29
4. Morandi V., Marabelli F., Amendola V., Meneghetti M., Comoretto D., *Adv. Funct. Mater.* **2007**, 17, 2779.
5. <http://fisica.unipv.it/CILSOMAF/OldSite/files/activities/student%20seminars/mascoli.pdf>.
6. Bozzoni E., Comoretto D. “*Preparazione e Caratterizzazione Ottica di Multistrati polimerici*” tesi 2012/2013.
7. Galizia M., Daniel C., Fasano G., Guerra G., Mensitieri G., *Macromolecules* **2012**, 45, 3604.
8. Joel.M. C., Langhe S. D., Michael T. P., Hiltner A., Bear E. J. *Mater. Res*, **2012**, 27, 1327.
9. Wang Y., Chan C.M., Ng K.M., Li L. *Macromolecules* **2008**, 41, 2548.
10. Mendelsohn R., Flach R.C: *Infrared Reflection–Absorption Spectrometry of Monolayer Films at the Air–Water Interface* **2002**, vol2 pag 1028.
11. Daniel, C.; Longo, S.; Fasano, G.; Vitillo, J.; Guerra, G. *Chem. Mater.* **2011**, 23, 3195.
12. Kenichi N., Yanzhi R., Toshikatsu N., Nobutaka T., Isao N., Yukihiro O. *J. Phys. Chem. B* **1999**, 103, 6704.
13. Benedetti E., Moscatelli D., Vergamini P., *Macromol. Chem. Phys.* **2002**, 203, 1497.
14. Wellinghoff, S. T.; Koenig, J. L.; Baer, E. *J. Polym. Sci., Polym. Phys.* **1977**, 15, 1913.

15. Tarallo, O.; Petraccone, V.; Daniel, C.; Fasano, G.; Rizzo, P.; Guerra, G. *J. Mater. Chem.* **2012**, *22*, 11672.
16. M. Galizia; C. Daniel; G. Guerra, G. Mensitieri; *Journal of Membrane Science*, **2013**, 443, 100.
17. G. Stracci, F. De Matteis, *Libello Di Ellissometria e Spettrofotometria*

## Summary

My PhD thesis focused on the study and the characterization of polymer films with co-crystalline and nanoporous crystalline phases.

In this work I have studied the procedure to obtain disordered nanoporous crystalline phases in sPS films and their possible application (chapter 1); the possible molecular orientations that may be induced by solvents during co-crystallization process in polymeric films, (chapter 2); the development of chiro optical response, after co-crystallization with temporary chiral guest (chapter 3) and the possibility to realize photonic crystals by using polymers able to form nanoporous crystalline forms (chapter 4).

In *chapter 1* a novel procedure to obtain disordered nanoporous crystalline phases in sPS films and their possible application are reported. The results show that the sorption behavior of the disordered crystalline phase is high and comparable to the nanoporous  $\delta$  phase, rather than being negligible as for the dense  $\gamma$  phase. As a consequence, these disordered crystalline forms of s-PS can be considered as nanoporous-crystalline forms.

The sPS polymeric films, presenting the  $\delta$ -nanoporous crystalline phase able to absorb ethylene and carbon dioxide, are suitable candidates for produce packaging. This active packaging by nanoporous-crystalline films could be complemented by the slow-release of antimicrobial molecules, which could be included as guest of the film crystalline cavities. Therefore a co-crystalline form of s-PS with carvacrol (a relevant natural antimicrobial molecule) has been prepared by carvacrol sorption, from solutions in suitable carrier solvents, in films exhibiting the nanoporous-crystalline  $\delta$  phase. We have described the preparation of s-PS films with antimicrobial molecules, being prevalingly placed as guest of the crystalline phase, it assures slow antimicrobial release and hence long-term antimicrobial properties. These s-PS films, mainly for low guest content (possibly <1 wt %), can be useful for packaging of fruits and vegetables, due to

the combination of ethylene and carbon dioxide removal from the empty cavities of the  $\delta$  nanoporous crystalline phase and the slow release of a scented natural antimicrobial guest from the filled cavities of the same crystalline phase.

In *chapter 2*, the study of the possible molecular orientations, that can be developed in polymeric films able to form co-crystalline phases, are reported. In particular, polymers such as poly (2, 6-dimethyl-1, 4-phenylene oxide) (PPO) and poly (L-lactide) (PLLA), thank to their abilities to form co-crystalline structures can develop orientations during the co-crystallization process with solvents. The guest induced co-crystallization of amorphous PPO films has been investigated by x-ray diffraction and FT-IR spectroscopy. In particular, two different kinds of uniplanar orientations have been found for the PPO cocrystalline phase with  $\alpha$ -pinene. Analogous high degrees of 110 uniplanar orientations are obtained by cocrystallization of amorphous films as induced by decalin or tetralin sorption.

Another different uniplanar orientation (00 $\ell$ ) has been found for PPO\limonene co-crystal. In this case the Edge profile is similar to a "tilted" fiber spectrum: this data is important because the fiber spectrum of PPO is absent. Moreover, it is worth noting that due to the absence of fiber spectra, the development of uniplanar orientations in PPO films could be useful to solve crystal structures of both crystalline and nanoporous-crystalline modifications. In fact it has been proposed a preliminary model of PPO nanoporous structure.

Also poly (L-lactide) (PLLA) is able to form co-crystalline phases and (020) uniplanar orientations have been found for PLLA co-crystalline phase with CPO, DMF and THF guests. In particular, our experimental data have been useful to refine model of the PLLA/DMF clathrate form proposed by Asai: we have modified the proposed unit cell parameters to fit our experimental data and we have arranged CPO guest molecules in the guest locations described in literature by means of molecular mechanic calculations.

We have also investigated on the shrinkage behaviour

developed in syndiotactic polystyrene (sPS) films after co-crystallization procedures leading to co-crystalline phases. First, biaxial drawn sPS films, presenting “planar” oriented  $\alpha$  crystalline phase, were exposed to solvent vapours leading to  $\delta$  co-crystalline phase showing of  $a_{//c_{//}}$  “uniplanar” crystalline phase orientation (parallelism of the (010) crystallographic plane to the film surface). High shrinkage values have been measured on these films. Then, amorphous sPS films were exposed to different solvents leading to  $\delta$  co-crystalline phases showing various kinds and degrees of crystalline phase orientations (named  $a_{\perp c_{//}}$  or  $a_{//c_{\perp}}$ ); also in this case high shrinkage values have been measured. Definitively lower shrinkage values have been measured on films with trans-planar mesomorphic or unoriented  $\delta$  crystalline phases after their exposure to solvents. In this last case, the transition toward  $\delta$  co-crystalline phases can occur without a significant shrinkage.

Another aspect of my thesis focused on the study of chiro optical response of crystalline films with a temporary chiral guest, is reported in *chapter 3*. The degree of circular polarization (g-value) of infrared and UV–VIS bands of melt-extruded syndiotactic polystyrene (s-PS) films of different thickness ~~has~~ induced by cocrystallization with a nonracemic guest ((R)-(–) or (S)-(+)) carvone, and their nonracemic and achiral guests has been studied. The induced circular dichroism (CD) phenomena, both for polymer host and for chromophore guests, are maximized for films with thickness of few micrometers. Surprisingly, for all examined thicknesses, the response of achiral guest (azulene and 4-nitroaniline) is higher than the non-racemic guest (carvone). It indicates that the origin of the optical response is extrinsic to photons absorption site. In addition the dependence of the circular polarization degree by the film thickness of sPS, obtained with the technique of spin coating, has been evaluated; it was observed that the value of circular polarization increases with the thickness increase (up to a thickness of up to 300 nm), showing that the nature of the

response is extensive. These studies confirm that the intense chiral responses of s-PS films are associated with a nonracemic helical morphology of crystallites, as induced by the nonracemic guest.

Finally, in *chapter 4*, the possibility to realize PhC by using PPO layers, polymer able to form nanoporous crystalline structures, alternates to CA layers, has been reported. In order to obtain a photonic crystal, with nanoporous crystalline phases PPO layers it has been necessary to characterize amorphous and crystalline PPO thin films. Therefore, techniques such as IRRAS and ellipsometry, have been used. Thin polymer layers on a substrate are prepared by spin-coating. These thin films are characterized by FTIR and IRRAS spectroscopy. The spectroscopic analysis shows that IRRAS spectra exhibit significant variation respect to FT-IR spectra in the range  $1190\text{ cm}^{-1}$ - $1480\text{ cm}^{-1}$ . By a comparison of IRRAS data with VCD measurements of co-crystals of PPO \ (1R) - (+)  $\alpha$ -pinene and PPO \ (1S) - (-)  $\alpha$ -pinene we can conclude that probably the  $1187\text{ cm}^{-1}$ ,  $1306\text{ cm}^{-1}$  and  $1471\text{ cm}^{-1}$  FT-IR bands are made to multiple components and in particular the signals  $1477\text{ cm}^{-1}$ ,  $1310\text{ cm}^{-1}$  and  $1197\text{ cm}^{-1}$ , which have the same sign in the VCD spectra, could have the variation of transition moment perpendicular to the film plane because they appear as the most intense in the IRRAS spectra.

Thickness and refractive index of amorphous and crystalline PPO thin films are measured by ellipsometric techniques. In particular the nanoporous crystalline structure has shown a lower refractive index with respect to the amorphous confirming that the nanoporous phase is less dense than the amorphous phase.

## Chapter 5

### Experimental Section

#### 5.1 Materials and Sample preparation

All the solvents used in this study were purchased from Sigma Aldrich and used without further purification.

##### 5.1.1 Syndiotactic polystyrene (sPS)

s-PS was manufactured by Dow Chemical Company under the trademark Questra 101. The  $^{13}\text{C}$  nuclear magnetic resonance characterization showed that the content of syndiotactic triads was over 98%. The weight-average molar mass obtained by gel permeation chromatography (GPC) in trichlorobenzene at 135 °C was found to be  $M_w = 3.2 \times 10^5$  with the polydispersity index,  $M_w/M_n = 3.9$ . Amorphous unoriented s-PS films of different thickness were obtained by melt extrusion at 300 °C with an extrusion head of 200 mm x 0.5 mm.

Axially oriented s-PS films, having a thickness of 100 - 150  $\mu\text{m}$ , have been prepared by uniaxial stretching of amorphous films with a dynamometer INSTRON 4301 in the temperature range 105°C–110 °C, at a strain rate of  $0.16 \text{ s}^{-1}$ , and at a draw ratio of  $\lambda$  (final length/initial length)  $\sim 3.3$ . Axially oriented films, 30–80  $\mu\text{m}$  thick, were also obtained by immersing trans-planar mesomorphic films in liquid DCM for 30 min and by subsequent immersion in a saturated solution of DBF in acetone for 24 h; complete guest removal was obtained by immersion in liquid acetonitrile for 24 h. The acetonitrile was removed in air at 50 °C for 1 h

Unoriented co-crystalline samples were obtained by immersion of amorphous films in liquid guests Nanoporous-crystalline  $\delta$ -form films (exhibiting axial and uniplanar axial orientations or unoriented form) were obtained from the prepared co-crystalline films, after guest removal by immersion in acetonitrile or after complete guest removal with a SFX 200 supercritical carbon dioxide extractor (ISCO Inc., using the following conditions:  $t = 40 \text{ }^\circ\text{C}$ ,  $p = 200 \text{ bar}$ , extraction time  $t = 120 \text{ min}$ )

Unoriented  $\lambda$  form samples were obtained by annealing  $\delta$  form samples at 130 °C for 30 min.

s-PS films showing *a//c//* uniplanar orientation were obtained by casting from 1 wt% solution in chloroform<sup>1</sup>.

By immersion of these films in pure guest at room temperature for 24 h, films presenting the *a//c//* uniplanar orientation of the corresponding intercalate phases were obtained. Guests removal was conducted by immersing intercalate films in liquid acetonitrile .

Amorphous s-PS films, having thickness in the range 0.08–0.3  $\mu\text{m}$ , were obtained by spin-coating of sPS solutions in chloroform (0.125, 0.25, 0.5, and 0.75 wt %) onto quartz surfaces at a spin rate of 1600 rpm.

Sorption experiments of various guests from dilute solutions at different concentration (ppm or % wt) on sPS films were conducted at 25°C.

The residual guest content in the samples, was evaluated by thermogravimetric measurements (TGA)

### **5.1.2 Poly(2,6-dimethyl-1,4-phenylene ether) (PPO)**

The PPO used in this study was purchased by Sigma-Aldrich and presents weight-averaged and number-averaged molecular masses  $M_w = 58500$  and  $M_n = 17000$ , respectively. Amorphous PPO films, having a thickness of 200–400  $\mu\text{m}$ , were obtained by compression molding, after melting at 235 °C. The crystallization of these amorphous films has been induced by vapor sorption procedures at different temperatures for 24h. The solvent was removed from the crystallized films by treating these films with a SFX 200 supercritical carbon dioxide extractor (ISCO Inc.) using the following conditions:  $T = 40^\circ\text{C}$ ,  $P = 250$  bar, extraction time  $t = 300$  min

PPO gel samples were prepared in hermetically sealed test tubes by heating the mixtures above the boiling point of the solvent until complete dissolution of the polymer and the appearance of a transparent and homogeneous solution had occurred. Then the hot solution was cooled down to room

temperature where gelation occurred.

PPO powders including guest were obtained by solvent desorption at room temperature. PPO empty powders were obtained by the above described extraction procedure with supercritical carbon dioxide

Amorphous PPO films, having thickness in the range  $<1 \mu\text{m}$ , were obtained by spin-coating of sPS solutions in Toluene 3% wt onto glass or metalized glass, with gold, surfaces at a spin rate of 5000 rpm and 1500rpm\ sec

### **5.1.3 Poly (L-lactide) (PLLA)**

The PLLA used in this study was purchased by Sigma-Aldrich and presents weight-averaged and number-averaged molecular masses  $M_w = 152000$  e  $M_n = 99000$  respectively. Amorphous PLLA films, having a thickness of 70–200  $\mu\text{m}$ , were obtained by compression molding, after melting at 200 °C. The crystallization of these amorphous films has been induced by vapor sorption procedures or immersion at different temperatures for 1-3 day. PLLA powders including guest in cocrystalline phases were prepared by gels after 1day solvent desorption at room temperature.

## **5.2 Techniques**

### **5.2.1 X-ray diffraction analysis**

Wide-angle X-ray diffraction patterns with nickel-filtered Cu  $K\alpha$  radiation were obtained, in reflection, by an automatic Bruker diffractometer.

The degree of crystallinity of powders and films was obtained from the X-ray diffraction data, by applying the standard procedure of resolving the diffraction pattern into two areas corresponding to the contributions of the crystalline and amorphous fractions (in particularly for PPO in the  $2\theta$  range  $4^\circ$ - $35^\circ$ ). Wide-angle X-ray diffraction patterns were also obtained, in transmission, by using a Philips diffractometer with a cylindrical camera (radius =57.3 mm). In the latter case the patterns were recorded on a BAS-MS imaging plate (FUJIFILM) and processed with a digital imaging reader (FUJIBAS 1800). In particular, photographic X-ray

diffraction patterns were taken by having the X-ray beam parallel (EDGE) and perpendicular (THROUGH) to the film surface and by placing the film sample parallel to the axis of the cylindrical camera. The degree of uniplanar orientation of a crystal plane exhibiting  $hkl$  Miller indexes ( $f_{hkl}$ ), with respect to the film plane, has been formalized on a quantitative numerical basis using Hermans' orientation function:

$$f_{hkl} = \frac{\overline{\cos^2 \chi_{hkl}} - 1}{2} \quad (1)$$

by assuming  $\overline{\cos^2 \chi_{hkl}}$  as the average cosine squared values of the angle,  $\chi_{hkl}$ , between the normal to the film surface and the normal to the ( $hkl$ ) crystallographic plane.

If the direction normal to the  $hkl$  plane is unique (i.e., there are no other equivalent directions in the crystal),<sup>2</sup>  $f_{hkl}$  is equal to +1 or -0.5 when the ( $hkl$ ) crystallographic planes of all crystallites are perfectly parallel or perpendicular to the film plane, respectively. For the case of random orientation  $f_{hkl}$  is equal to zero.

The quantity  $\overline{\cos^2 \chi_{hkl}}$  has been experimentally evaluated, by the above-described EDGE X-ray diffraction patterns, as:

$$\overline{\cos^2 \chi_{hkl}} = \overline{\cos^2 \chi_{hkl}} = \frac{\int_0^{\pi/2} I(\chi_{hkl}) \cos^2 \chi_{hkl} \sin \chi_{hkl} d\chi_{hkl}}{\int_0^{\pi/2} I(\chi_{hkl}) \sin \chi_{hkl} d\chi_{hkl}} \quad (2)$$

where  $I(\chi_{hkl})$  is the intensity distribution of a ( $hkl$ ) diffraction on the Debye ring and  $\chi_{hkl}$  are the azimuthal angles measured from the horizontal line of the EDGE patterns.

The crystallinity index was evaluated by X-ray diffraction patterns on powders or powdered films; in particular it was obtained by resolving the X-ray diffraction patterns into the diffraction area relative to crystalline peaks ( $I_c$ ) and amorphous halo ( $I_a$ ) according to the following equation:

$$X_{c,R} = \frac{Ic}{(Ic + Ia)} \quad (3)$$

### 5.2.2 FT-IR Infrared spectra

Fourier Transform Infrared (FTIR) spectra were obtained at a resolution of  $2.0 \text{ cm}^{-1}$  with a Vertex 70 Bruker spectrometer equipped with deuterated triglycine sulfate (DTGS) detector and a Ge/KBr beam splitter. The frequency scale was internally calibrated to  $0.01 \text{ cm}^{-1}$  using a He-Ne laser. 32 scans were signal averaged to reduce the noise. Polarized infrared spectra were obtained using a KRS-5 polarizer from Specac. As far as infrared spectroscopy is concerned, the axial orientation function is given by:

$$f_{c,IR} = \frac{(R - 1)(2\cot^2 \alpha + 2)}{(R + 2)(2\cot^2 \alpha - 1)} \quad (4)$$

where  $R = A_{//}/A_{\perp}$  is the dichroic ratio,  $A_{//}$  and  $A_{\perp}$  being the measured absorbance for electric vectors parallel and perpendicular to the draw direction respectively, and  $\alpha$  is the angle between the chain axis and the transition moment vector of the vibrational mode. For evaluation of the  $\alpha$  angle relative to transition moment vectors of guest vibrational modes, the orientation factor relative to the helical chains of the host polymer phase ( $f_{c,IR}$ ) was evaluated by the dichroic ratio of the  $572 \text{ cm}^{-1}$  infrared band<sup>3</sup>. As usual, an order parameter  $S$  is defined as the ratio:

$$S = (R-1)/(R+2) \quad (5)$$

The degree of crystallinity was evaluated by FTIR spectra,<sup>4</sup> expressed as weight fraction  $\chi_c$ , according to  $k = l/l'(1 - \chi_c)$ , where  $k$  is the subtraction coefficient,  $l$  and  $l'$  are the thickness of the sample and of an amorphous reference film. The  $l/l'$  ratio is estimated from the absorbance ratio of a conformationally insensitive peak (at  $1601 \text{ cm}^{-1}$  for sPS and  $906 \text{ cm}^{-1}$  for PPO).

CD spectra were measured using a Jasco J-715 spectropolarimeter.

All measurements were performed using the following parameters: single scan, continuous scanning mode (350–190 nm range), 200 nm/min scanning speed, 2 nm SBW (constant bandpass mode), 0.2 nm data interval, vertical scale in autoranging mode, no baseline correction. The CD data have been expressed as the ellipticity (1 mdeg equals 0.001 deg).

IR and VCD measurements were recorded using a commercial Bruker Tensor 27 FT-IR spectrometer coupled to a PMA50 external module (needed to double modulate the infrared radiation) using a linear KRS5 polarizer, a ZnSe 50 kHz photoelastic modulator (PEM, by HINDS) with a proper antireflecting coating, an optical filter (transmitting below 2000  $\text{cm}^{-1}$ ), and a narrow band MCT (mercury cadmium telluride) detector. All VCD spectra were recorded for 5 min of data collection time, at 4  $\text{cm}^{-1}$  resolution. According to experimental procedures described in the literature,<sup>5</sup> films were tested for satisfactory VCD characteristics by comparison of the VCD obtained with the film rotated by  $\pm 45^\circ$  around the light beam axis. In separate measurements with 1 h data collection time, we have also tested  $\pm 90^\circ$  rotation of the film; VCD bands were found to be unaffected by changing collection time as well as by changing the rotation of the film.

For CD and VCD spectra the degree of circular polarization or dissymmetry ratio (*g*-value) is, as usual, defined as

$$g = \frac{\Delta A}{A} = \frac{A_L - A_R}{\frac{1}{2}(A_L + A_R)} \quad (6)$$

where  $A_L$  and  $A_R$  denote the absorbance for left and right circular polarized light. Quantitative evaluations of the degree of circular polarization based on the UV–vis and CD spectra were effected by using the relationship between ellipticity ( $\Theta$ ) and  $\Delta A$ :

$$\Delta A = 4\pi\Theta \text{ (deg)}/180 \ln 10 = \Theta \text{ (mdeg)}/32980 \quad (7)$$

Images are acquired using a commercial atomic force microscope (Nanoscope IIIa, Bruker) in Tapping mode in air.

The levers (Bruker) used for this investigation have a nominal spring constant of 5 N/m and resonance frequency around 130 kHz; the nominal tip radius of curvature is 10 nm.

Infra-red reflection absorption spectroscopy, IRRAS measurements, were recorded using a commercial Bruker Tensor 27 FT-IR spectrometer coupled to a PMA50 external module (needed to double modulate the infrared radiation) using a linear KRS5 polarizer, a ZnSe 50 kHz photoelastic modulator (PEM, by HINDS) with a proper antireflecting coating, an optical filter (transmitting below  $2000\text{ cm}^{-1}$ ), and D313/Q MCT detector. All measurements were performed in  $720\text{ cm}^{-1} - 3860\text{ cm}^{-1}$  frequency range with a  $2\text{ cm}^{-1}$  resolution and 100, 200 or 600 scans, the measurements were performed by setting the incidence angle at  $85^\circ$ . When the incident radiation is reflected from a metal surface, the electric field vector changes phase, which depends on the incidence angle and the polarization of light. The two polarization states are:  $I_s$  (perpendicular to the reflection plane or parallel to the film plane) and  $I_p$  (parallel to the reflection plane or perpendicular to the film plane). For  $I_s$  polarization state the incident vector and reflected vector, in the point of contact, are annulled and the s component is nothing.

In the case of oblique incidence of radiation, for  $I_p$  polarization state, two electric field vectors (incident and reflected) do not cancel in the point of contact and their resultant vector is perpendicular to the metal surface

The polarization of the incident electric field is rapidly modulated between the  $I_s$  and  $I_p$  components of the transmitted intensity. The reflected beam signal is electronically filtered and demodulated with an amplifier (lock-in SR 830). The absorbance of surface-confined species in the PEM-IRRAS spectra is given by Equation

$$\Delta R/R = J_2(\phi_0) * (I_p - I_s) / (I_p + I_s) \quad (8)$$

$J_2$  is a function's Bessel  $\phi_0$  is a PEM parameter in order to have the maximum of the function  $J_2$  in the spectral region.

the polymer is deposited on a glass substrate (2x4 cm<sup>2</sup>) on which is deposited a thin layer of gold<sup>6</sup>

The gold depositions were made with a metalizer (EMITECH-K500X) in Helium atmosphere. The conditions for the deposition are:

- deposition time: 3 min
- intensity: 50 mA ,

Two depositions were performed on each substrate.

### 5.2.3 TGA measurements

The content of the guest molecules in the films was determined by the intensity of FTIR guest peaks, as calibrated by thermogravimetric measurements. Thermogravimetric measurements (TGA) were performed with a TG 209 F1 equipment from Netzsch.

### References

1. Rizzo, P., Lamberti, M., Albunia, A.R., Ruiz de Ballesteros, O., Guerra, G. *Macromolecules* **2002**, 35, 5854.
2. Alexander, L. E. In X-Ray Diffraction Methods in Polymer Science; Krieger, R. E., Ed.; Huntington: New York, **1979**; Chapter 4, p 210.
3. Albunia, A.R., Di Masi, S., Rizzo, P., Milano, G., Musto, P., Guerra, G. *Macromolecules* **2003**,36, 8695.
4. a) Guerra, G.; Manfredi, C.; Musto, P.; Tavone, S. *Macromolecules* **1998**, 31, 1329  
b) Musto, P.; Mensitieri, G.; Cotugno, S.; Guerra, G., Venditto, V. *Macromolecules* **2002**, 35, 2296 .  
c) Albunia, A. R.; Musto, P.; Guerra, G. *Polymer* **2006**, 47, 234.  
d) Li, M.; Wu, H.; Huang, Y.; Su, Z. *Macromolecules* **2012**, 45, 5196.
5. a) Shanmugam, G.; Polavarapu, P. L. *Vibrational J. Am. Chem. Soc.* **2004**, 126, 10292.  
b) Petrovic, A. G.; Polavarapu, P. L. *J. Phys.Chem. B* **2006**, 110, 22826.
6. Lardone M., Daniel C., Guerra G.,tesi **2008/2009**